ACS Catalysis

pubs.acs.org/acscatalysis Account

A Career in Catalysis: Enrique Iglesia

David G. Barton, Aditya Bhan, Prashant Deshlahra, Rajamani Gounder,* David Hibbitts, Beata A. Kilos,* Gina Noh, Justin M. Notestein, Michele L. Sarazen, and Stuart L. Soled

Cite This: *ACS Catal.* 2024, 14, 10583−10613 Read Online

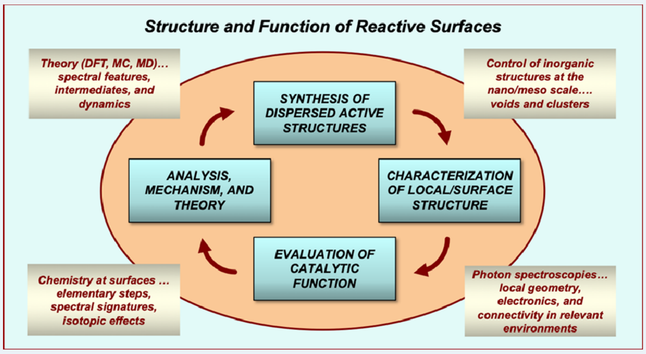

ABSTRACT: Enrique Iglesia is an internationally recognized leader in the field of heterogeneous catalysis. His trademark approach places a premium on kinetic and mechanistic descriptions of catalytic sequences, complemented by synthetic methods to prepare catalytic centers uniform in composition and by computational chemistry methods to adjudicate among competing hypotheses, with the aim of describing the function of catalytic active sites at the level of elementary steps in reaction mechanisms. Enrique began his independent career in industry, spending 11 years at the Exxon Corporate Research Laboratories. In 1993, he moved to academia to become a full professor in the Department of Chemical and Biomolecular Engineering at the University of California, Berkeley where he founded the Berkeley incarnation of the Laboratory for the Science and Applications of Catalysis (LSAC). In that time, he has coauthored >350 publications (with an h-index of >120) and >50 patents and has advised ∼30 Ph.D. students and ∼100 postdoctoral and visiting scholars, more than 30 of whom continue his legacy of teaching and scholarship in their own academic appointments around the world. Enrique is a member of the National Academy of Engineering, the American Academy of Arts and Sciences, the National Academy of Inventors, and the Spanish Royal Academy of Sciences, and has received numerous awards from the American Chemical Society, the American Institute of Chemical Engineers, and the Catalysis Societies of North America and Europe. In this Account, we discuss major research themes that have underpinned Enrique's career, using examples that illustrate how his research has led to significant conceptual advances in our understanding of reactions facilitated by metals and metal oxides, of the consequences of acid strength and confinement in microporous solids, of the relevance of describing surfaces under realistic coverages for catalysis, and in disentangling the chemistry of active sites that mediate catalysis from the specific influences of the environments within which reactions proceed. These insights have allowed for the development of more precise and unifying descriptions of chemical reactivity and selectivity, including field-defining mechanistic interpretations and practical developments in the conversion of C_1 molecules, acid−base and redox catalysis, hydrocarbon and oxygenate chain growth chemistries, NO_x abatement, and Fischer−Tropsch synthesis across supported metals, carbides, and oxides. His work unifies some of the most enduring concepts in physical, organic, solid-state, and theoretical chemistry into surface catalysis, through deep knowledge about the fundamentals of catalysis and their translation into practical solutions. His research group chooses to study catalytic systems that are technologically relevant and often occur in complex environments, irrespective of whether such topics are in vogue at the time of inquiry, guided by an approach that seeks fundamental knowledge that can be recycled, one day, to develop solutions to problems that we cannot yet envision from our current vantage point. This constancy of purpose, intense focus, and dedication has allowed Enrique to become a leader in science and of scientists, including those who once trained under his guidance and continue to learn alongside him and to receive mentorship, in work and in life, well beyond their time in LSAC.

KEYWORDS: *heterogeneous catalysis, active sites, reaction kinetics, reaction mechanisms, surface catalysis*

1. INTRODUCTION

Enrique Iglesia graduated with a B.S. (1977) in Chemical Engineering from Princeton University, and then completed his M.S. (1979) and Ph.D. (1982) from Stanford University under the guidance of Professor Michel Boudart. He then spent the next 11 years of his career at the Exxon Corporate Research Laboratories, quickly rising through the ranks to become the Head of Catalysis Science, leading one of the most influential industrial research groups of the modern era. While

Received: April 29, 2024
Revised: June 3, 2024
Accepted: June 5, 2024
Published: June 28, 2024

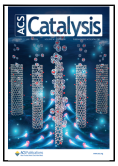

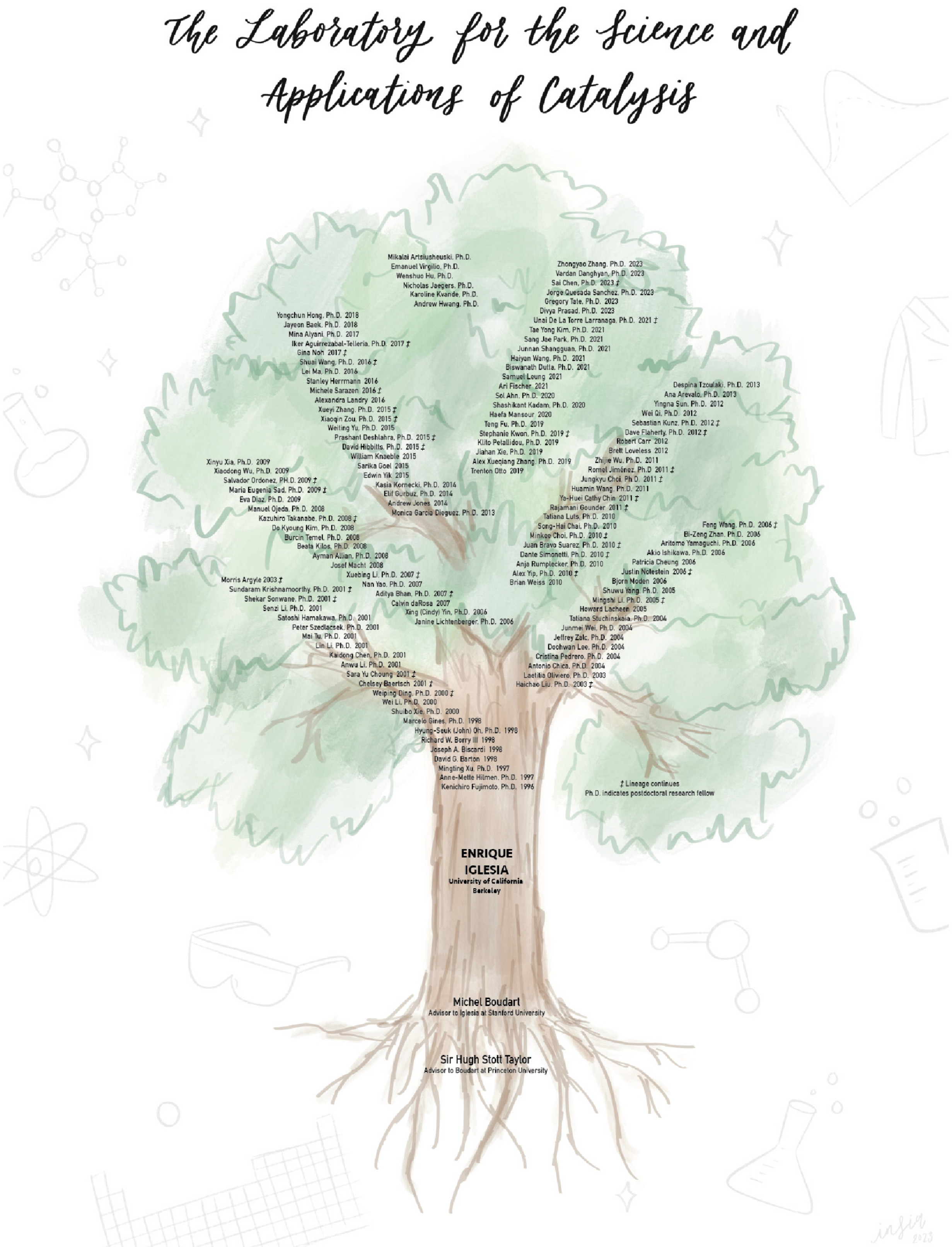

Figure 1. Enrique Iglesia's academic family tree (as of March 2024). (Figure credit: Letters by Insia).

serving as Section Head, he continued to direct his own research programs, which provided some of the enabling knowledge for Exxon's gas-to-liquids technology. In 1992, Enrique received the Golden Tiger Award, the annual Exxon Award recognizing "Inspirational Leadership and Outstanding Contributions in Catalytic Science and Technology". In 1993, Enrique started his academic career as a full professor in the Chemical Engineering Department at the University of California, Berkeley, where he founded the Laboratory for the Science and Applications of Catalysis (LSAC). He again quickly rose through the ranks at UC Berkeley, holding the titles of Chancellor Professor and the Theodore Vermeulen Chair in Chemical Engineering, ultimately becoming a Distinguished Professor of Chemical Engineering in 2019, before retiring and becoming a Distinguished Professor of the Graduate School in 2022. During his tenure at UC Berkeley, Enrique also served as a Faculty Senior Scientist at the Lawrence Berkeley National Laboratory (LBNL, 1993−2019) and a Laboratory Fellow at the Pacific Northwest National Laboratory (PNNL, 2019−2023), and Founder and Director of the Berkeley Catalysis Center (2006−2016). In 2023, he became the Michel Boudart Distinguished Professor in the Davidson School of Chemical Engineering and the Presidential Fellow for Energy Transitions at Purdue University.

Enrique's scientific and practical achievements and his leadership have been recognized with election to the National Academy of Engineering, the American Academy of Arts and Sciences, the National Academy of Inventors, and the Spanish Royal Academy of Sciences. Enrique is recognized for the eloquence and clarity of his lectures, which have led to 30+ named lectures at academic institutions (since 2016), three international lectureships (Burwell, Gault, Cross-Canada), and 30+ plenary lectures as well as prestigious awards from the American Chemical Society, the American Institute of Chemical Engineers, and the Catalysis Societies of North America and Europe. He is a dedicated mentor and teacher, recognized with the highest teaching awards at Berkeley, including the Donald Sterling Noyce Prize for Excellence in Undergraduate Teaching (2005). His groundbreaking contributions to acid catalysis led to his selection as the inaugural Tanabe Prize recipient and those in C_1 chemistry to the ENI Prize and to the Natural Gas Conversion Prize. His 350+ publications have a mean citation rate >85 (h-index >120), and his 50+ patents (some of which have led to commercial implementation) reflect his unique talent for balancing concepts in catalysis with their applications in practice.

Enrique has made an indelible impact on the vitality and growth of the catalysis community by dedicating himself selflessly and tirelessly to its stewardship. Most notably, he served as Editor-in-Chief of the *Journal of Catalysis* (1997−2010) with the encouragement and mentorship of Nick Delgass and Roel Prins,[1] and as President of the North American Catalysis Society (2009−2017) and the International Association of Catalysis Societies (2020−2022). At the time of writing this article, Enrique graduated 29 Ph.D. students and mentored 103 postdoctoral and visiting scholars. As shown in his academic tree (Figure 1), 32 of his mentees have chosen to pursue their own academic careers, continuing his storied lineage in the field of catalysis.

Enrique's unique blend of technical excellence and statesmanship has made him an international leader in the chemistry of surface catalysis. His work combines fundamental concepts in surface reactivity with practical breakthroughs that impact a broad portfolio of catalytic processes. He is a quintessential proponent of fundamental science as the enabler of practical applications with significant societal impact. His work shows how uncovering knowledge of enduring value requires rigorous mechanistic analysis at relevant conditions on catalysts designed and created with well-defined atomic architectures. In this Account, we review significant practical and conceptual advances in Enrique's publications that have now become the recognized trademark of the Iglesia group, a trait inherited by the >130 mentees who practice at leading academic and industrial institutions around the world.

2. EARLY YEARS AND EDUCATION

A complete oral history of Enrique Iglesia's life and career was recorded in an interview conducted by the Chemical Heritage Foundation in 2014; the audio recording and written transcript are now preserved and archived as a digital exhibit at the Science History Institute.[2]

Born in Havana, Cuba in 1954, to parents of Spanish immigrants, Enrique immigrated to the United States in 1969. A precocious student who had skipped two years of primary school in Cuba, Enrique had at this point also overcome an intervening turbulent six month period when he was the sole financial provider for his family. High school proved to be instrumental as Enrique first met Teresa (Terry), who would eventually become his wife and lifelong influence, and he received encouragement from his math teacher to apply to Princeton. He was accepted and graduated summa cum laude from the School of Engineering and Applied Science in 1977 with a B.S. in Chemical Engineering. Undergraduate research on diffusion of hydrogen isotopes through stainless steel as part of his senior thesis at Princeton inspired an interest in surface chemistry and encouragement from Princeton faculty. A chance encounter with Michel Boudart, a PhD graduate and once faculty member at Princeton, during his visit to give the Wilhelm Lectures influenced Enrique to attend Stanford for graduate school.

His PhD thesis, titled "Formic acid decomposition on copper, nickel, and copper−nickel alloys", concerned the catalytic dehydration and dehydrogenation of formic acid on nickel and copper−nickel powders and sought to reconcile surface science ultrahigh-vacuum (UHV) descriptions of this chemistry with what transpired on catalytic surfaces at relevant conditions.[3−8] Enrique's thesis involved the use of temperature-programmed surface reaction studies and isotopic reagents for careful kinetic assessments and quantitative descriptions of turnover rates. It also gave Enrique his first look at what he describes as "real catalytic surfaces under steady-state, relevant conditions", interrogated using a method of inquiry that has endured throughout his career, as described in this perspective.

3. CAREER AT EXXON

Enrique started his career at the Exxon Corporate Research Laboratories in Clinton, NJ toward the end of 1982. His research philosophy became influenced by several close collaborators at Exxon including Stu Soled, Sebastian Reyes, John Sinfelt, Gary McVicker, Joe Baumgartner, Sal Miseo, and Ross Madon. In 1983, a decision had been made that Exxon would start exploring synfuels made by Fischer−Tropsch synthesis (FTS), prompted by the fact that the company had abundant methane reserves but dwindling liquid inventory, among the backdrop of "peak oil". A large on-site symposium was organized in 1984 on all aspects of FTS, with many renowned faculty coming to the Exxon facility, including Michel Boudart, Keith Hall, Kamil Klier, and many others. Following that symposium, many researchers within Exxon were recruited into projects in the area, including Stu Soled focusing on catalyst discovery and Enrique focusing on kinetics and modeling.

Enrique probed the effects of metal dispersion, alloying elements, supports, and reaction conditions on the chemical and transport features that determine FTS rates and selectivity, as well as the design criteria for optimal reactor types to maximize liquid product yields.[9−12] He coauthored some of the enabling patents and knowledge for catalysts and bubble column reactors for Exxon's AGC-21 Gas-to-Liquid technology.[13−17] He worked with Sebastian Reyes and Ross Madon to develop quantitative models for product distribution and selectivity, particularly focusing on how differences in molecular diffusivities influence the readsorption of olefins and lead to decreasing olefin-to-paraffin product ratios with increasing chain length, and on how the relatively small selectivity to C_2 products driven by readsorption and reincorporation of C_2 olefins into growing chains (Figure 2).[11,12,18,19] In studying bimetallic systems, particularly those with Co−Ru and Co−Re, he showed that Re increases the number of active sites of similar reactivity, whereas Ru increases the rate without influencing metal dispersion because it attenuated active site poisoning. He also investigated the use of $MgCr_2O_4$ spinel as a support to provide epitaxial control over Co_3O_4, described how Co eggshells on millimeter-sized particles would behave and developed simple ways of preparing rimmed eggshell catalysts.[20] Together with Reyes, he developed models of eggshell formation as well as a detailed reaction transport model to guide the *a priori* design of large particle FTS catalysts.[21] He became interested in the unexplained strong effects of water on FTS rates and chain length and started to explore this topic,[22] an area of interest which continued for many years in academia,[23] as discussed later in this perspective (Section 9).

Enrique's early contributions in FTS spanned the design of Co and Fe catalysts[24] and the development of accurate descriptions of the relevant chemistry and hydrodynamics. His later contributions elucidated the role of hydrogen and water assistance in kinetically relevant CO activation.[25,26] The quantification of metal crystallite size effects in supported Co and Co-alloy catalysts and the development of reaction-transport models that, for the first time, explained the relationship between transport and selectivity have provided a paradigm for the evolving generation of FTS catalysts with improved reactivity, selectivity, and stability. The methods developed allowed separation of primary and secondary reaction pathways during FTS synthesis, measurement of their absolute and relative rates, and simulation of their role in determining product selectivities.

Enrique's work provides a strong foundation for renewed interest in producing clean and high performing diesel fuel and lubricants from renewable feedstocks, natural gas, and carbon dioxide. While at Exxon, he did not limit himself to just Fischer−Tropsch chemistry. With Reyes, he helped advance the ideas of percolation theory in catalysis[27] and explained the mechanistic details of C_6 aromatization reactions on Pt-KL zeolite catalysts and why Pt was more beneficial for this reaction than Ir and Rh. He also studied the role of bifunctional catalysis on tungsten carbides with surface oxygen.[28] In other work with Reyes, he developed Monte Carlo simulations of structural properties of packed beds and reaction networks for oxidative coupling of methane.[29] He also started investigating reactions on solid acid catalysts with early studies providing mechanistic details of active site formation on sulfated and tungstated zirconias, an area he expanded upon after moving to Berkeley,[30−34] as discussed in a later section in this perspective (Section 7).

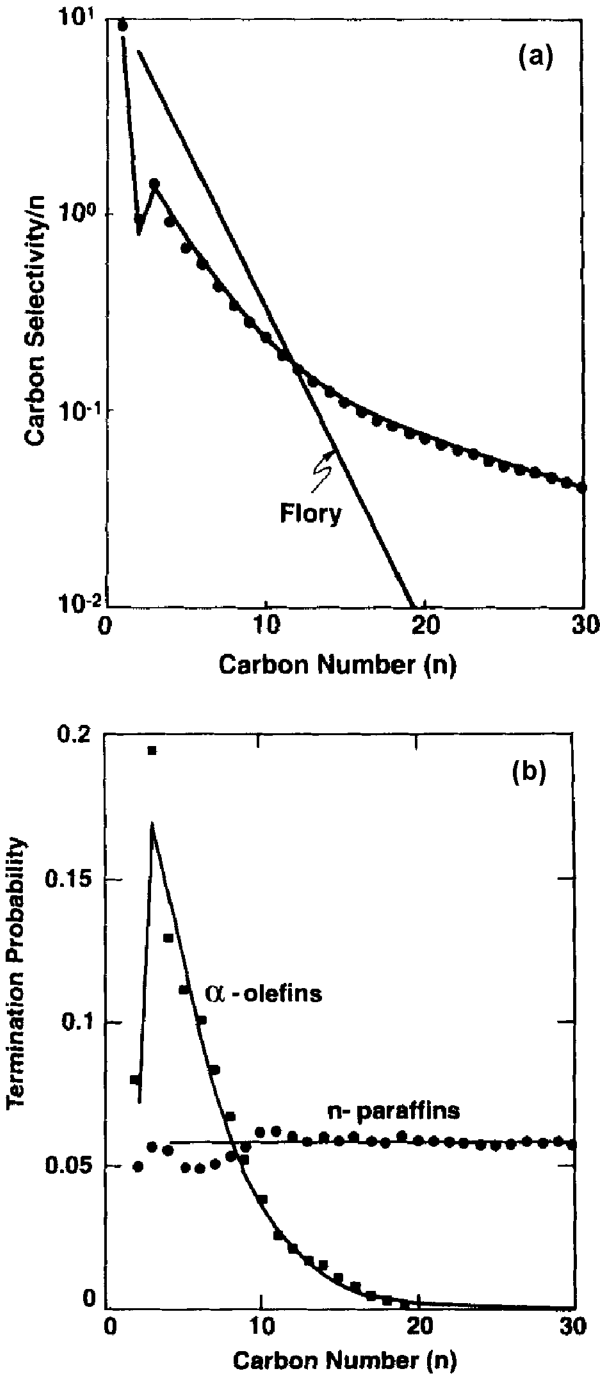

Figure 2. Diffusion-enhanced olefin readsorption model to predict the (a) carbon selectivity and (b) olefin and paraffin chain termination probability as a function of carbon number (experimental data: 11.7% Co/TiO_2, 473 K, 2000 kPa, < 2 s residence time, 9.5% CO conversion). Reproduced with permission from Iglesia et al.[11] Copyright 1993 Elsevier.

In 1986, Exxon experienced a major disruption in its research organization, during which time Enrique assumed the role of group and then section head (additional details provided by Stu Soled in the Supporting Information). He encouraged researchers across the entire Clinton site to become active participants and contributors to the scientific community, including presenting at the North American

Catalysis Society meetings. While he was the section head of a very large group, Enrique kept two technicians working in his lab (Joe Baumgartner and Rich Ernst), allowing him in 1993 to publish four long articles in the *Journal of Catalysis* and four book chapters. Enrique's interactions with Michel Boudart and Stanford proved fateful during this time. Enrique had the opportunity over a three year period to serve as a consulting professor at Stanford where he would spend a few weeks every year visiting Michel's group, giving seminars, and teaching a short course.[2] These stints at Stanford gave him a glimpse of what it may be like to run his own academic lab. With some help from Michel, he began interviewing and received offers from top chemical engineering departments across the country. He accepted the offer from the University of California, Berkeley, where he established the Berkeley incarnation of the Laboratory for Science and Application of Catalysis (LSAC), which has been a vibrant research group for 30+ years. Those who knew him well at Exxon realized that it was Enrique's fate to be a professor, in the footsteps of his professional idol, Professor Michel Boudart. In making the transition from industry to academia, Enrique could influence more lives than he could by staying in industrial research and could also establish his own academic legacy.

That being said, even once at Berkeley, his learnings and ideas have continued to impact industrial research and the practice of catalysis through several strong collaborations. These include collaborations with BP (under the leadership of Theo Fleisch and George Huff), Chevron (under the leadership of Alex Kuperman, Stacey Zones, Bi-Zeng Zhan, and Trenton Otto), ExxonMobil (under the leadership of Stu Soled and Sara Yacob), and BASF (under the leadership of Carlos Lizandara Pueyo, Joe Dellamorte, and Andrey Karpov) on a broad range of chemistries, including acid−base, C_1, and alkane activation catalysis. These collaborations affirm the wide-ranging relevance of Enrique's work and of the methods and approaches his research group has developed.

4. METHANE AND ALKANE CONVERSION

The chemistry of organic C_1 species, typified by methane, has been a research focus throughout the history of LSAC. Enrique's work on methane activation spans reforming, combustion, partial oxidation, oxidative coupling, and dehydroaromatization chemistry on metals, metal carbides, and metal oxides. A quintessential context to examine his work on methane activation catalysis is its underpinnings in concepts of chemical kinetics and thermodynamics, enabled by a seamless combination of kinetic, chemical transient, isotopic, spectroscopic, and theoretical methods. It is this foundation in the fundamentals of mechanistic understanding, reaction rates and reversibility, and reaction-transport formalisms that gives this body of work its enduring clarity and edifying characteristic.

4.1. Methane Dehydroaromatization. Following a 1993 report by Wang et al.[35] in which ZSM-5 (MFI) zeolites modified by contact with aqueous Mo^{6+} salts (Mo/H-ZSM-5) alleviated kinetic barriers to methane pyrolysis and catalyzed methane dehydroaromatization (DHA) with high benzene ($\gtrsim$70%) and aromatic ($\gtrsim$95%) selectivity, Borry and Kim initiated an effort in Enrique's newly established lab at Berkeley to determine the identity of Mo-based catalytic centers and the species and pathways involved in the reaction. Their work established that air treatment of physical mixtures of MoO_3 and H-ZSM-5 resulted in catalytic formulations that behaved similarly to impregnated Mo/H-ZSM-5 formulations, indicating that solid-state ion exchange is the only route by which isolated MoO_x species migrate into zeolite channels, given that large aqueous molybdate ions cannot enter the small (∼0.55 nm diameter) channels of ZSM-5.[36,37] A careful analysis of the stoichiometry of Mo ion exchange for samples of varying Mo loading (1.0−6.3 wt % Mo; Mo/Al = 0.11−0.68) using chemical transient protocols to assess the loss of O atoms upon exposure to methane and H/D isotopic exchange to count residual H^+ sites showed two important findings in DHA catalysis. First, ion exchange of Mo at low loadings (Mo/Al < 0.5) results in each Mo species displacing one proton, and this ion exchange reaction requires proximal Al centers to form $(Mo_2O_5)^{2+}$ species that serve as precursors to the carbidic Mo species that are active for DHA. Second, higher loadings of Mo result in extraction of Al from the framework to form inactive $Al_2(MoO_4)_3$ species. MoC_x species are formed via carburization of the catalyst upon exposure to methane, regenerating protons on framework Al centers, and these carbidic Mo moieties are devoid of all oxygen, as 2.5 O atoms per Mo are removed as CO_x and H_2O during an initial induction period during DHA catalysis prior to observed maximum rates of hydrocarbon production. This early work also showed that conversion-selectivity trends overlap when conversion is varied by changing the residence time or the number of active sites via deactivation (Figure 3), illustrating that deactivation removes active sites from the catalyst without altering any properties of the remaining active sites.

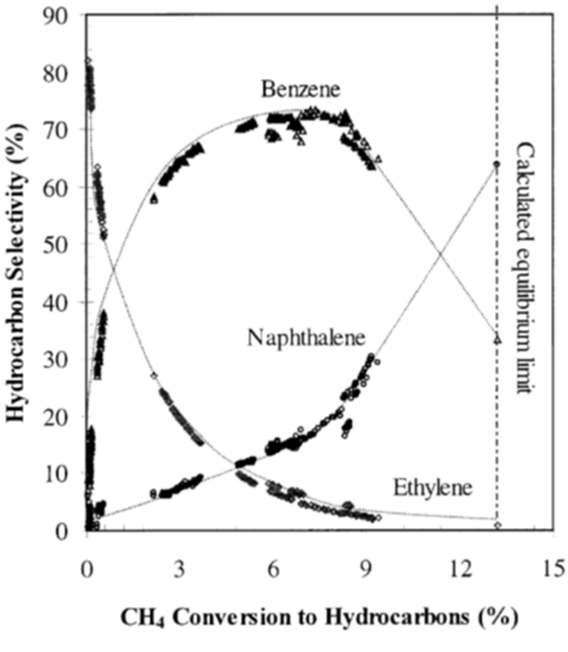

Figure 3. CH_4 conversion into C_2−C_{10} hydrocarbons versus product selectivity, excluding CO_x and solid carbon (950 K, 0.5−1.0 g 4% Mo/H-ZSM-5, 5−50 cm^3/min 1:1 CH_4:Ar, 0−96 h reaction time. Reproduced with permission from Kim et al.[37] Copyright 2000 Elsevier.

Research in LSAC followed carburization dynamics using X-ray absorption[38−40] and transient online mass spectrometric measurements to note the stoichiometric loss of oxygen and deposition of superfluous carbon, which could be mitigated to some extent by cofeeding oxygenates like CO_2 but could also result in the loss of active MoC_x species. Through these

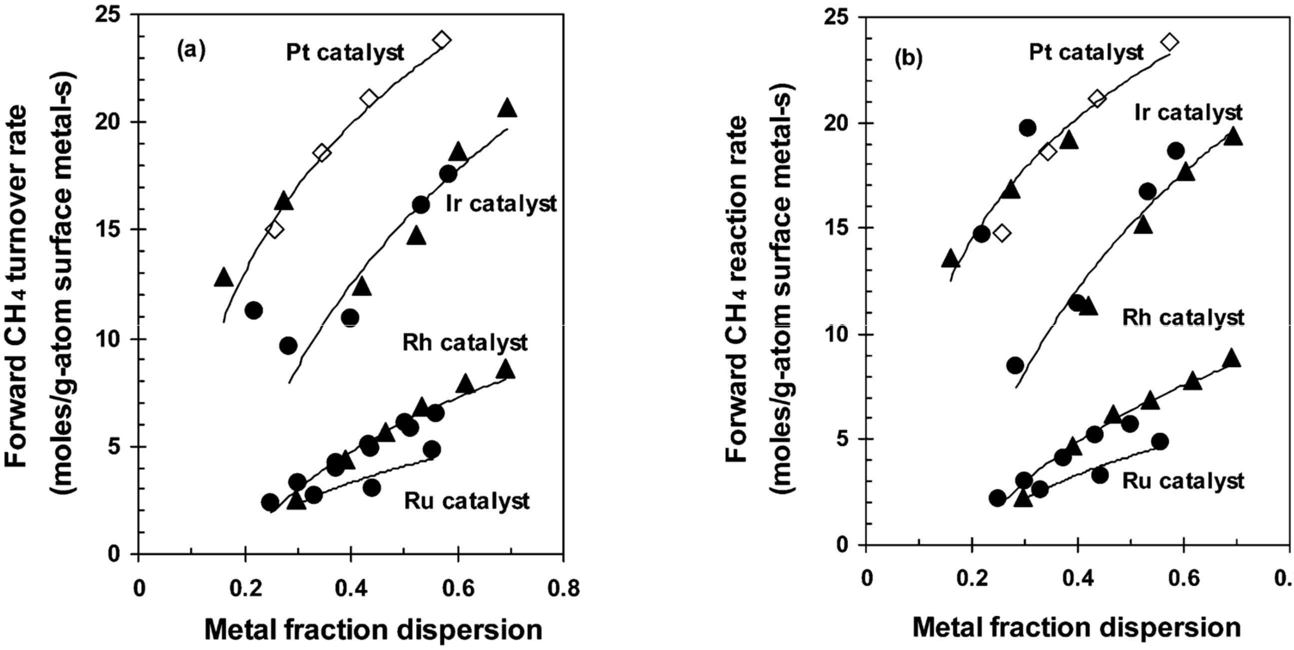

Figure 4. Forward CH_4 turnover rates for CO_2 (a) and H_2O (b) reforming of CH_4 on different metal clusters as a function of metal dispersion on various supports (873 K, 20 kPa CH_4, (filled triangle) ZrO_2, (filled circle) γ-Al_2O_3, (open diamond) ZrO_2−CeO_2 as support, (open circle) MgO-A, (closed diamond) MgO-B. Reproduced from Wei et al.[50] Copyright 2004 American Chemical Society.

reports, his group was the first to scrutinize the effects of reversibility on observed space time yields in DHA catalysis, which appear to decline with higher contact times. Superimposed on this interplay between kinetic and thermodynamic barriers to CH_4 conversion is deactivation of the catalyst with time-on-stream. Lacheen and Iglesia isolated the kinetic and thermodynamic effects of H_2 and CO_2 cofeeds to show that CO_2 cofeeds reversibly oxidize MoC_x species to result in loss of catalytic centers that create shorter catalytic beds, which can be described as staged beds, one catalyzing reforming upstream on MoO_x moieties and the other catalyzing pyrolysis on MoC_x moieties.[41,42] This work on CH_4 pyrolysis has provided broad and pervasive insights into how high valent cations can be deposited in zeolite micropores,[43,44] how spectroscopy can be used to monitor the on-stream formation and deactivation of active sites in Mo-exchanged ZSM-5, and how carbon chains grow sequentially $C_1 \rightarrow C_2 \rightarrow C_6$. These insights provide a clear and simple explanation for why many research groups across the world report very similar time-on-stream characteristics in the induction period and conversion-selectivity trends in their DHA catalytic data for Mo/H-ZSM-5.

4.2. Methane Reforming, Partial Oxidation and Combustion. The body of work perhaps most emblematic of Enrique's group at Berkeley, at least in the first 15 years of its existence, is on methane reforming. At the time, only a handful of studies[45] had directly compared CO_2 and H_2O reforming reactions on supported metal catalysts, using undiluted catalyst pellets and beds that invariably led to case-specific descriptions of rate and various attributions to role of oxide supports in activating the H_2O or CO_2 oxidant. In a tour-deforce series of six papers,[46−51] all published in 2004, Wei and Iglesia brought these seemingly disparate chemistries into a common mechanistic framework using dilution within packed beds and catalytic pellets to exclude heat and mass transport artifacts, isotopic methods to probe the reversibility of C−H activation and O−H bond formation steps, and reversibility considerations to assess whether concurrent water gas shift pathways are kinetically relevant. Rate measurements using either CH_4/CO_2 and CH_4/H_2O feeds, when examined under these conditions of strict kinetic control over Ni, Pt, Pd, Ir, and Rh catalysts supported on metal oxides, appear indistinguishable from one another, controlled simply by the rate of activating C−H bonds in CH_4 and described by a first-order rate constant that varies only slightly with changes in particle size (Figure 4). The absence of $CH_{4-x}D_x$ isotopologues from CH_4−CD_4 reactant mixtures and the magnitude of the CH_4/CD_4 kinetic isotope effect on all metals, when using either H_2O or CO_2 co-reactants, showed that irreversible C−H bond cleavage steps were kinetically relevant. CD_4-H_2O and CD_4-D_2O rates were identical, and complete equilibration of H/D ratios in water and dihydrogen when using $CH_4/CO_2/D_2$ mixtures was observed, suggesting that H_2O has no kinetic role and that all steps forming water and dihydrogen are quasi-equilibrated. Isotopic equilibration of CO and CO_2 in the effluent when using $^{12}CH_4/^{12}CO_2/^{13}CO$ reactant mixtures at chemical conversions of methane far from equilibrium suggested that water−gas-shift reactions would also be at equilibrium during CO_2 and H_2O reactions, as was indeed found under all reaction conditions. CO oxidation was used as a structure-insensitive probe reaction before and after reforming reactions to show that metal surfaces were bare at catalytic conditions and did not redisperse during the course of reaction.

A unified and simple mechanistic picture of reforming reactions on Group VIII metals under the challenging conditions of industrial practice emerged from these studies—that of irreversible C−H bond activation being the only kinetically relevant step under all conditions free of transport artifacts. Today, it represents the "modern standard" against which the reforming community benchmarks new findings and mechanistic proposals. Even within LSAC, steeped in thinking about mechanisms and kinetics of catalytic systems, these six papers from Wei and Iglesia acquired a lore about how seemingly "simple" chemistries are quite complex but can be dissected into their simplest and most essential components. Purportedly, it also led to a philosophical question that became a hallmark of Enrique's, one that often featured in his discussions with students and in many of his (and their) talks: "What do you measure when you measure a rate?"

The common mechanistic description of rate-limiting C−H activation steps coupled with reactions of CH_x fragments with O-adatoms derived from CO_2 and H_2O in methane reforming led Chin and Iglesia[52−56] to probe reactions of CH_4−O_2 mixtures and examine if the sequence of elementary steps in methane combustion share these characteristics. CH_4−O_2 reactions also offered a paradox, given that the catalytic partial oxidation of methane (CPOX) could seemingly be accomplished to directly form CO and H_2 at temperatures of 1000−1200 K, incongruous with the much more facile combustion of H_2 and CO than CH_4 in the presence of O_2. Concurrent studies of CH_4 and CO oxidation using mixtures of ^{13}CO−$^{12}CH_4$ under strict kinetic control readily showed that $^{13}CO_2$ was formed much faster than ^{12}CO, so that any possibility of direct partial oxidation at the scale of methane reforming turnovers could be ruled out. No detectable CO is observed in reactions of CH_4−O_2 over Pt, Ru, and Rh nanoparticles so long as residual O_2 is present. These two observations demonstrate clearly that H_2 and CO do not directly form in CPOX reactions because any CO that desorbs would scavenge O-adatoms downstream in the catalytic bed to form CO_2 at all residence times required to achieve discernible CH_4 conversions. Partial oxidation products observed in the effluent merely represent the stoichiometry of sequential total combustion and reforming reactions at aggregate reactor scales but do not transpire in catalytic turnover events.

The mechanistic connections between reforming and (partial) combustion emerged in the work of Chin and Iglesia in that the rates of combustion are also exclusively determined by C−H activation in CH_4. Rates of combustion, however, were noted to be much larger than those for reforming even though these chemistries share a common sole rate-determining step. These observations were reconciled in an elaborate series of kinetic studies done as part of a strong intellectual collaboration with Matthew Neurock's group (then at the University of Virginia), a collaboration that persisted for more than a decade and showcased synergy between experiment and theory that became essential to the Iglesia group in the years that followed. The distinction among combustion and reforming mechanisms arises from the prevalence of vacant site pairs (*-*) when weak oxidants such as H_2O and CO_2 are used, resulting in bare metal clusters that activate C−H bonds via apparent first-order kinetics. Surface coverages of O-adatoms are considerably higher when O_2 is used as an oxidant, and C−H bond activation is still the sole kinetically relevant step but occurs on different active sites, which evolve from oxygen−oxygen pairs (O*-O*) to oxygen-vacancy pairs (O*-*) and to vacancy−vacancy (*-*) pairs as O* coverages decrease. Measured rates of CH_4 combustion are different among the O*-O*, O*-*, and *-* site pairs. DFT calculations illustrate that radical-like activated complexes are formed on O*-O* via homolytic abstraction, which results in methane combustion rates being first-order in CH_4 pressure but independent of the O_2 pressure. O*-* pairs become prevalent when vacancies become available on O*-covered surfaces, and instead accomplish C−H activation via concerted oxidative addition and H-abstraction steps akin to organometallic complexes. In this regime, O_2 activation is irreversible since the O-adatoms formed are scavenged by CH_4; thus, the coverage of O* species and O*-* pairs is determined by the O_2/CH_4 ratio. Depletion of O* at high CH_4/O_2 ratios results in the prevalence of *-* pairs, which exhibit no CD_4/CH_4 kinetic isotope effect; in this regime, turnover rates are proportional to the O_2 pressures and independent of the CH_4 pressures. O*-* pairs catalyze C−H activation with the highest rates among the three cataloged regimes. The essential role of oxygen coverage and of the reactivity of chemisorbed oxygen in CH_4 combustion explains the observed effects of metal particle size, wherein smaller particles that bind O* more strongly show decreased reactivity for H-abstraction. Stronger O* binding on Pd than on Pt atoms of the same coordination leads to less effective C−H bond activation on O*-O* pairs on Pd. This catalog of different kinetic regimes (Figure 5), and the essential role of oxygen coverage and reactivity of chemisorbed oxygen in determining these regimes, were delineated in great detail in this body of work and were found to apply in the same context of the availability of either O* or oxygen vacancies for NO oxidation on Pt and Pd.[57,58]

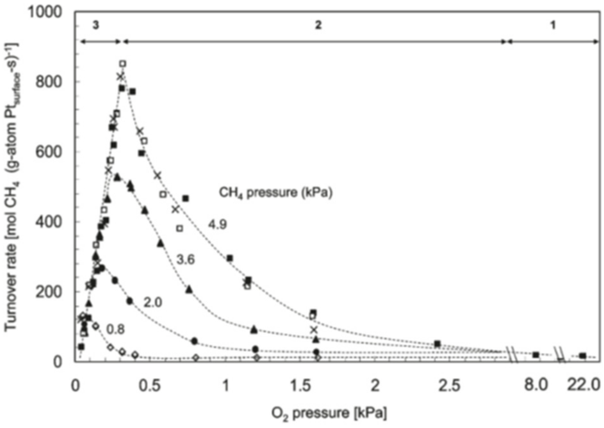

Figure 5. CH_4 turnover rates (873 K) during CH_4−O_2 reactions with 0.8 kPa (open diamond), 2.0 kPa (closed circle), 3.6 kPa (closed triangle), or 4.9 kPa (closed square) CH_4 and during $^{13}CH_4$−O_2-CO_2 (x) and CH_4−O_2-CO_2 (open square) reactions with either 5 kPa of CO_2 or 5 kPa of H_2O on Pt clusters (8.5 nm average cluster size) as a function of the O_2 pressure. Kinetic regimes 1−3 are labeled **1**−**3**, respectively. (0.15 mg 0.2% wt. Pt/Al_2O_3, 200 SiO_2/catalyst intraparticle (λ) and 4700 quartz/catalyst interparticle (χ) dilution ratios, 2.08 cm^3 (STP) s^{-1}; **1:** $O_2/CH_4 > 2$; **2:** $0.08 < O_2/CH_4 < 2$; **3:** $0 < O_2/CH_4 < 0.08$). Reproduced from Chin et al.[52] Copyright 2011 American Chemical Society.

4.3. Oxidative Coupling of Methane.

Another illustrative example of the use of isotopic and kinetic studies, dilution within beds and pellets to eliminate nonchemical effects of heat and mass transport, and mechanistic descriptions of surface-mediated steps at the level of elementary rate constants is the work of Takanabe and Iglesia[59,60] for the oxidative coupling of methane (OCM) on $Mn/Na_2WO_4/SiO_2$ catalysts. OCM involves coupled heterogeneous−homogeneous reactions, in which C−H abstraction from CH_4 leads to $CH_3^\bullet$ species that couple in the gas phase to form C_2H_6. Subsequent reactions of C_2H_6, which possesses weaker C−H bonds than CH_4 and occurs via C−H abstraction steps similar to those for CH_4, leading to the formation of C_2H_4 and CO_x. Consequently, the favored OCM reactions are only favored at CH_4-rich conditions that limit CO_x formation. While descriptions based on C−H abstraction in CH_4, C_2H_6, and C_2H_4 were readily available in the OCM literature, Takanabe and Iglesia showed that autocatalytic pathways in OCM are initiated by H_2O formed as a byproduct of combustion reactions. The presence of H_2O results in the generation of $OH^•$, and homogeneous pathways of C−H bond abstraction mediated by $OH^•$ result in higher C_2 yields as the reaction proceeds. Isotopic tracer studies of mixtures of $^{13}CH_4/O_2$ with $^{12}C_2H_6$ or $^{12}C_2H_4$ in the presence or absence of H_2O showed that H_2O increases the rate of H-abstraction for all hydrocarbons, but to varying extents such that selectivity for secondary overoxidation steps is diminished. $OH^•$ is a better H-abstractor than oxygen-derived species because H-abstraction steps involving $OH^•$ are more exothermic and occur via earlier transition states along the reaction coordinate in which C−H bonds are less fully cleaved, which renders them less selective for weaker C−H bonds. Consequently, higher C_{2+} selectivity is attained at all conversions when H_2O is cofed in the reactant stream (Figure 6).[60] These $OH^•$ mediated routes account for nearly 30% of C_2 yields currently attainable in OCM catalysis.

4.4. Alkane Hydrogenolysis. Other studies into alkane activation on metals includes the work of Flaherty, Hibbitts, and Iglesia[61−66] in alkane hydrogenolysis, which is now finding applications not only in petrochemical upgrading but also in waste plastics upcycling. This work also highlights the evolution in the context and type of work that the Iglesia group undertook from 2008 onward—an emphasis on the role of entropy in discussing kinetics, explicit formulation of thermochemical cycles, and a prominent role for DFT calculations coupled with experiments.

C_2−C_4 alkane hydrogenolysis on metals, a prototypical structure-sensitive reaction, and one studied extensively in the literature, lacked unifying concepts that attributed reactivity to specific molecular attributes until the aforementioned studies from the Iglesia group. The key to the experimental effort spanning acyclic and cyclic alkanes ranging from C_2−C_{10} on Pt, Rh, Ru, and Ir clusters of different sizes and to a unifying mechanistic and kinetic interpretation is the judicious choice of reaction conditions that lead to H* species reaching saturation coverages and becoming the predominant surface-bound adsorbate (most abundant intermediate; MASI). In this scenario, a mechanistic sequence which involves H_2 dissociation, molecular adsorption of alkanes (C_nH_{2n+2}) and their dehydrogenation to form a quasi-equilibrated pool of unsaturated intermediates (C_nH_{2n+2-y}; where y is the number of H atoms removed from the alkane) that undergoes C-C bond cleavage was derived. Measured rates of hydrogenolysis represent the combined rates of C−C bond cleavage at all positions with this quasi-equilibrated pool of reactive surface intermediates (termed the "zoo"), with C−C bond cleavage being the sole kinetically relevant step (Figure 7). Then, using a combination of detailed kinetic studies, statistical mechanics, and DFT calculations, rates, and selectivity for cyclic and acyclic alkane hydrogenolysis could be attributed to molecular characteristics.

Activation enthalpies and entropies and the number of $H_2(g)$ formed with transition states were noted to be larger for C−C activations at branch points (i.e., ^3C-^xC bonds) than for C−C activations of unbranched ^2C−^2C or ^2C−^1C bonds. Reactions at branches occurred in more deeply dehydrogenated intermediates and thus were more inhibited by H_2 pressure, allowing H_2 pressure to tune hydrogenolysis selectivity. This could be attributed to molecular configurations that exist in surface-bound hydrocarbon fragments that immediately precede the rate-limiting C−C bond cleavage step. Transition states for ^3C-^xC cleavage have three or more points of attachment to catalytic surfaces and cleave through α,β,γ- or $\alpha,\beta,\gamma,\delta$-bound transition states, whereas less-substituted bounds involve α,β-bound species. These data and their mechanistic interpretation explain the observed effects of H_2 pressure and relative rates of hydrogenolysis of

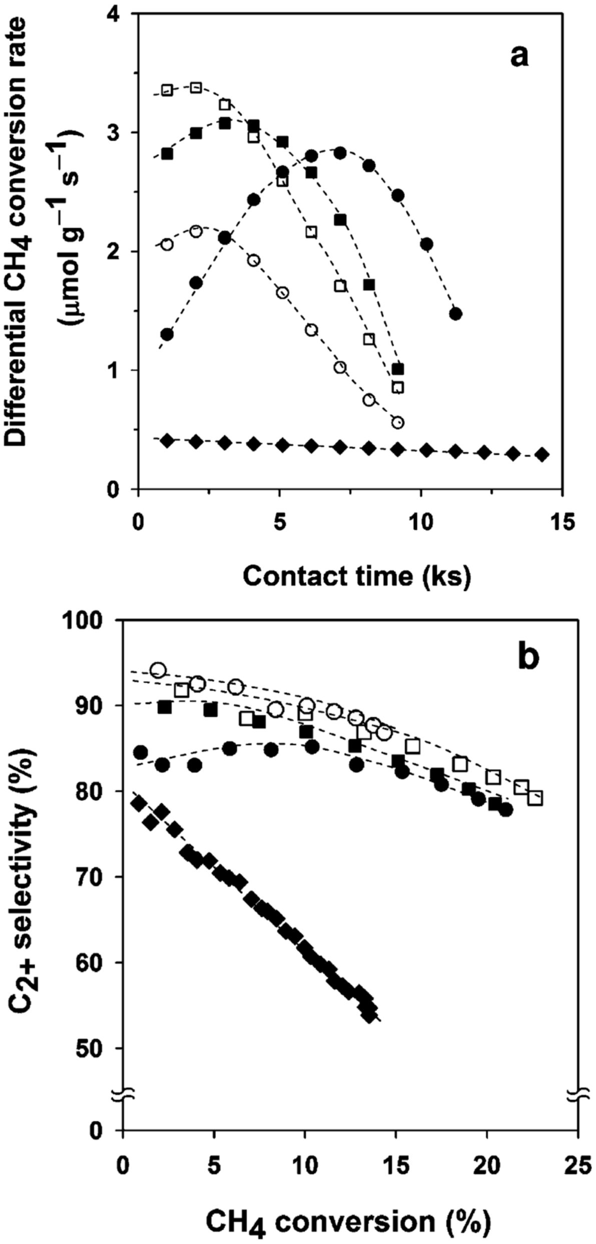

Figure 6. Differential CH_4 conversion rate as a function of contact time (a) and C_{2+} selectivity as a function of CH_4 conversion (b) measured in a recirculating reactor (0.02 g, 1073 K, volume: 275−650 cm^3, 10.7 kPa CH_4, 101 kPa total pressure, balance He, (◆) 1.8 kPa O_2, H_2O removed; (●) 1.8 kPa O_2, steady state reaction; (■) 1.8 kPa O_2, 0.4 kPa H_2O added; (□) 1.8 kPa O_2, 0.9 kPa H_2O added; (○) 0.9 kPa O_2, 0.4 kPa H_2O added). Reproduced from Takanabe et al.[60] Copyright 2009 American Chemical Society.

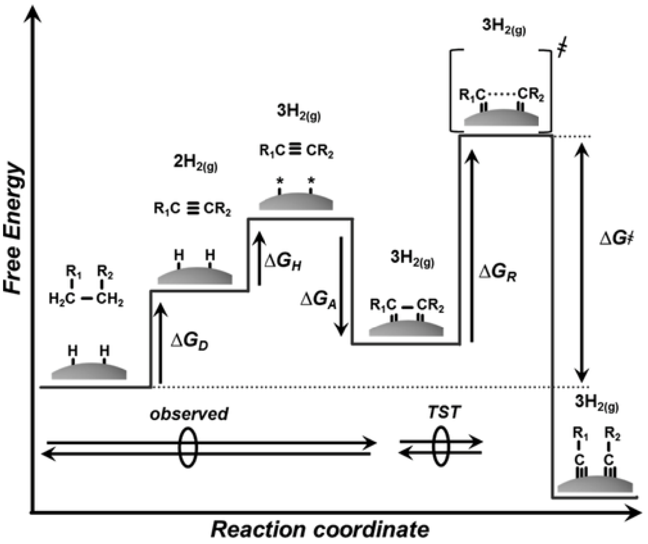

Figure 7. Thermochemical cycle accounting for free energy changes for the reaction sequence that forms transition states for C−C bond cleavage on H*-covered surfaces, depicted here for $^2C-^2C$ bond cleavage in alkane $R_1(H_2C)(CH_2)\ R_2$. Free energy changes are shown for lumped steps that dehydrogenate the alkane (ΔG_D), desorb hydrogen (ΔG_H), adsorb the dehydrogenated hydrocarbon (ΔG_A), and rupture the C−C bond (ΔG_R). (⇄ denotes groups of quasi-equilibrated steps that are observed directly or implied by transition-state theory (TST); and the moles of gas-phase H_2 indicated are cumulative along the reaction coordinate). Measured activation free energies, $\Delta G‡$, equal the sum of free energy changes for all preceding steps and depend in part on the free energy of the transition state ($G‡$) and the gaseous H_2 (G_{H_2}) that is produced in quasi-equilibrated steps that form the transition state. Reproduced from Flaherty et al.[62] Copyright 2014 American Chemical Society.

C_2-C_{10} alkanes and cycloalkanes on Pt, Rh, Ru, and Ir metal clusters of different size and provide guidance on how surface coordination, temperatures, and H_2 pressures can be used to control hydrogenolysis selectivity. The concepts and methods from this work are wide-ranging and extend to C−X bond cleavage (where X = O, S, and N atoms)[67] more broadly. An important learning from this extensive body of work is that the quest to measure rates that are “interpretable” may involve wide variations in experimental reaction conditions (e.g., high H_2:alkane ratios) that allow otherwise complex catalytic surfaces to become dominated by a single MASI species (e.g., H*).

5. NO DECOMPOSITION AND CONVERSION

In addition to the numerous examples of catalytic chemistries useful in the production of energy carriers, fuels, and chemicals, Enrique also studied those relevant for environmental protection and pollution abatement. LSAC began investigating the conversion of nitrogen oxide compounds (NO_x) around the early 2000s, in their same hallmark approach that combines steady-state and transient kinetic, isotopic, and spectroscopic probes with theory to understand site requirements and mechanistic details for NO decomposition,[68−70] oxidation,[57,58,71−75] and hydrogenation[76] on a variety of catalysts. This work provided clarity on mechanisms that mediate reactions relevant to the catalytic treatment of exhaust from combustion engines and demonstrated important fundamental principles in kinetics and thermodynamics that are connected to other areas of catalysis.

5.1. NO Decomposition on Cu-ZSM-5. In the early 2000s, Moden, Da Costa and Iglesia probed active sites and the redox mechanism for NO decomposition to N_2, N_2O and O_2 on Cu exchanged ZSM-5.[68−70] Temperature-programmed reduction by H_2 and CO and desorption of O_2 for samples with varying Cu/Al ratios to quantify the different types of Cu species, along with X-ray absorption spectroscopy, were used to identify reduced Cu centers. Isolated Cu^{2+} monomers and oxygen-bridged Cu^{2+} dimers interacting with Al−Al next-nearest-neighbor pairs were found to be the dominant Cu species, with dimers being more reactive for NO decomposition. Transient product evolution rates after switching from He to NO streams confirmed the redox nature of the catalytic cycle and the role of labile bridging O atoms in forming oxygen vacancies ($(Cu^+-[O_v]-Cu^+)^{2+}$) and replenishing them in Cu dimers ($(Cu^+-O^{2-}-Cu^+)^{2+}$). Kinetic data showed that N_2O and N_2 form via donation of oxygen from NO pairs and N_2O, respectively, to reduced ($Cu^+-[O_v]-Cu^+)^{2+}$ centers. O_2 evolution involved quasi-equilibrated formation of NO_2 from NO at $(Cu^+-O^{2-}-Cu^+)^{2+}$, which acts as an O atom shuttle between nonvicinal dimers, and the addition of NO_2 at $(Cu^+-O^{2-}-Cu^+)^{2+}$ to form a nitrate intermediate that leads to O_2, NO and $(Cu^+-[O_v]-Cu^+)^{2+}$. A key insight that emerged is the role of NO as a reductant and an oxidant in the redox cycle. This work, while confirming some earlier proposals, provided a more complete mechanistic framework and provided some relevant insights for subsequent advances in understanding NOx selective catalytic reduction (SCR) pathways.

5.2. NO Oxidation on Supported Metal Clusters and Oxides. Weiss and Iglesia used kinetic and isotopic tracer methods to unravel the mechanism of NO oxidation on Pt, Pd, Rh and Co catalysts supported on alumina.[57,58,71,72] Despite the prevalence of metallic forms of Pt and oxidized forms of other metals, all catalysts showed NO oxidation rates with the same apparent reaction orders in reactant and product pressures (Figure 8), which together with the comparison of NO oxidation and $O^{16}-O^{18}$ exchange rates, showed that rates are determined by the rate of O_2 dissociation at vacancies on an O atom covered surface. The surface vacancy concentration and the oxygen chemical potential are determined solely by NO-NO_2 equilibrium, which can be used to define a virtual O_2 pressure that accurately captures the NO_2 inhibition effects on forward rates. NO_2 inhibition can be alleviated by barium carbonate or oxide domains that capture NO_2 as nitrates, and these require close proximity to Pt clusters but not atomic contact. Such site proximity effects are a recurring subject of investigation in LSAC, leading to rigorous demonstration in many cases that molecular shuttles are more efficient in transporting chemicals between distant sites than is through-surface migration or “spillover”.[77,78]

In contrast to unassisted O_2 dissociation in Pt, PdO, RhO_2 and Co_3O_4 catalysts, the work of Iwasaki and Iglesia showed that NO oxidation on WO_3-CeO_2 catalysts requires kinetically relevant NO-assisted O_2 dissociation.[73] WO_3 domains act as promoters that enhance the reaction rates by modifying the redox properties of CeO_2 domains in atomic contact. This work also demonstrates the use of transient UV−visible spectroscopy to probe the intrinsic rates of redox cycles, which together with the global rate of product formation at steady-state, can give an accurate count of the number of active sites in oxides with nonuniform domains that preclude the use of titration methods for quantifying active sites. A similar method

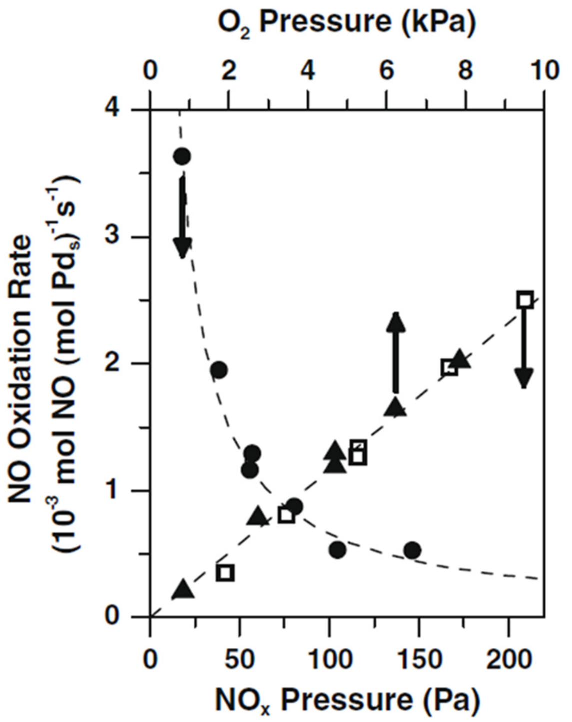

Figure 8. NO oxidation rate on Pd/Al_2O_3 (0.33 dispersion) at 603 K versus NO_2 (●), NO (☐), and O_2 (▲). The partial pressure of each gas was varied independently while the others were held constant at 5 kPa O_2, 0.056 kPa NO_2, and 0.112 kPa NO. Reproduced with permission from Weiss et al.[58] Copyright 2010 Elsevier.

was applied earlier for alkane activation on vanadium oxide by Argyle and Iglesia.[79]

5.3. NO Oxidation in the Gas Phase and within Zeolite Voids. Artioli, Lobo, and Iglesia showed that NO oxidation on purely siliceous zeolites (MFI (SIL-1), CHA, BEA) occurs at remarkably high rates near ambient temperatures (Figure 9), in contrast to the high temperatures required on metal catalysts.[74] This nonsite-specific zeolite-catalyzed reaction exhibits reaction kinetics identical to gas-phase NO oxidation mediated by a termolecular transition state, but at several orders-of-magnitude higher rates and significantly more negative activation energies due to the physical confinement of termolecular transitions state within voids of molecular dimensions. Maestri and Iglesia later performed computational work corroborating these interpretations.[75] This work highlights the importance of enthalpic stabilization of transition states via van der Waals forces and the more influential enthalpic than entropic contributions to Gibbs free energy at low temperatures, a recurring insight across many catalytic systems examined within LSAC.

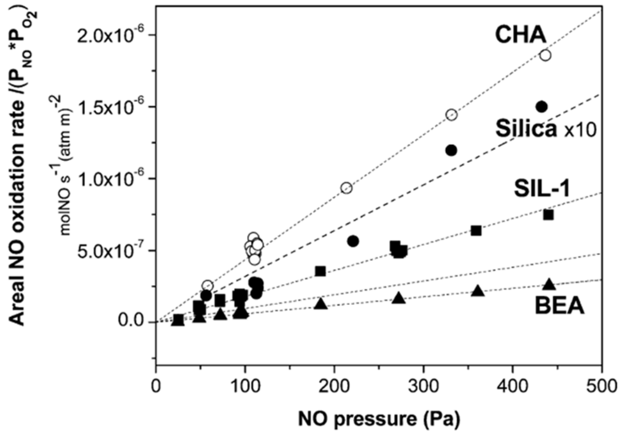

Figure 9. Areal NO oxidation (forward) rates divided by NO and O_2 pressures (50−450 Pa NO, 1−10 kPa O_2) on MFI (SIL-1) (0.1 g) (■), BEA (0.1 g) (▲), CHA (0.3 g) (○), and silica (0.8 g) (●) as a function of NO pressure at two temperatures of (a) 305 K and (b) 331 K. Reproduced from Artioli et al.[74] Copyright 2013 American Chemical Society.

NO/NO_2−O_2-hydrocarbon mixtures react in the gas-phase via complex networks that generate $OH^\bullet$, which in turn selectively abstract strong H atoms in alkanes. Zalc, Green, and Iglesia performed kinetic simulations for NO/NO_2−O_2-CH_4 reactions using rate parameters available from combustion chemistry studies to analyze experimental reports of selective HCHO formation.[80] This work demonstrated that almost all CH_4 molecules are activated by H-abstraction by $OH^\bullet$, while weaker abstractors such as NO_2 activate oxygenates with weaker C−H bonds that are formed at short residence times. The high abstractor strength of $OH^\bullet$ leads to early C−H activation transition states that are insensitive to C−H bond strength and improve selectivity to strong bonds in comparison to weaker abstractors that prefer weaker C−H bonds. This insight is also important for oxidative coupling of methane[59,60] and has recently found relevance in selective propane oxidative reactions that proceed via gas-phase alkane activation by surface generated radicals.

5.4. NO Reduction by H_2 on Supported Metals. Iglesia and co-workers also examined the reduction of NO by H_2 to form a mixture of N_2, NH_3, and N_2O on supported Pt[76] and Rh catalysts using a combination of kinetic studies and theoretical techniques. Product formation rates on Pt/Al_2O_3 (0.6 wt % Pt) catalysts were independent of space velocity (and NO conversion), indicating that all three products are formed from a single sojourn to the catalyst surface. Additional studies with cofed NH_3 and N_2O confirmed that these products were unreactive at NO-H_2 reaction conditions (423−453 K, 0.3 kPa NO, 1.5 kPa H_2) and H_2-D_2 exchange rate measurements during NO-H_2 reaction conditions confirmed that H_2 dissociation was reversible and quasi-equilibrated during the reaction. NO consumption rates were first-order in H_2 pressure at low H_2 pressures (<5 kPa) and became zero-order in H_2 at very high H_2 pressures (>500 kPa), suggesting that H* can block sites at very large H_2/NO ratios. Increasing the NO pressure increased the NO consumption rates at high H_2 pressure and decreased the NO consumption rates at low H_2 pressure, suggesting that the surface is blocked by NO* at low H_2/NO ratios and inhibited by NO at those conditions. Taken together, this leads to a rate equation that suggests that NO and H_2 (or two H -atoms derived from H_2) are involved in the rate-determining step, and that the surface is covered by either H* or NO* based on the H_2/NO ratio.

DFT calculations were used to contrast four different NO activation mechanisms: direct NO* dissociation to form N* and O*, NO*-assisted NO* dissociation to form N_2O and O*, and H*-assisted NO* dissociation that first reduces NO to either NOH* or HNOH* prior to a kinetically relevant N−O cleavage step. Among these, DFT-calculated free energy barriers were lowest for the two H*-assisted pathways, while the kinetic trends were consistent with a two H atom reduction of NO* via the quasi-equilibrated formation of *HNOH* prior to dissociation. The produced NH* fragments would then react either with H* to produce NH_3, with NO* to produce N_2O, or with other NH* species to produce N_2, leading to changes in product selectivity with reaction conditions. These DFT calculations focused on close-packed Pt(111) surfaces at mild (~0.5 ML) NO* coverages and showed that bimolecular assisted NO* dissociation pathways were preferred to direct unassisted NO* dissociation pathways on the flat and crowded surfaces that dominate metal catalysts (further discussed in Section 9).

6. REDOX CATALYSIS

Since the beginning of his academic career, Enrique has had a strong focus on oxidation reactions, including on metal nanoparticle surfaces (Section 4) and supported metal oxide catalysts. In his first decade at Berkeley with Chen, Argyle, and Liu, Enrique repeatedly returned to alkane oxidative dehydrogenation (especially of ethane and propane) and alcohol oxidation (especially of methanol, dimethyl ether, and ethanol) as a platform to understand the redox properties of supported metal oxides, especially MoO_x[81−89] and VO_x[79,90−101] and their promoted and modified analogs. The larger reaction network of ethane to acetic acid over Mo−V−Nb oxides was also investigated stepwise in a series of papers by Li.[102−105] Under most conditions studied, these reactions occur by Mars-van Krevelen mechanisms, where rates are sensitive to the kinetics of C−H bond activation steps and not surface reoxidation steps. In many cases, reaction networks are relatively simple and are very far from equilibrium under typical reaction conditions, readily allowing experimental measurements of intrinsic rate constants. In doing so, this system provided LSAC with access to one of their fondest strategies of relating intrinsic rate constants to discernible, measurable, and predictable properties of the catalyst.

Although analyzing the kinetics of these reactions and materials is consistent with the approaches discussed elsewhere in this perspective, these catalysts and reactions represent somewhat of a departure from the other research inquiries in LSAC. First, much of the early research on this topic was carried out by co-mentored students and postdocs in collaboration with Enrique's faculty colleagues at Berkeley, unlike many of his other research projects. This research area thus became somewhat of a testing ground, as ideas from Enrique's group percolated across Berkeley's campus, and techniques or strategies from other groups were adopted within his.

Second, while the reaction network of alkane oxidative dehydrogenation provides many opportunities to teach the observant scientist about the fundamentals of redox behavior and C−H bond activation, these same fundamentals dictate that a commercially viable process in a simple reactor is euphemistically very challenging to envision. As students of that era saw frequently, the "triangle kinetics" of alkane oxidation directly to CO_2 or to the alkene and then onward to CO_2 disfavor the accumulation of high concentrations of the intermediate. This contrasts with much of LSAC's research output on other topics, which focused on understanding the fundamentals of commercial or near-commercial reactions. By that same token, the level of fundamental understanding that arose from these studies also sheds light on what types of reactor-scale innovations might be required to see progress on these reactions. In one memorable group meeting discussing the role that staged O_2 could play in improving reactor performance,[106] Enrique noted (here, we paraphrase): "If we were in the business of making money, we could make *a lot* of money." Rest assured, there was much discussion following the meeting about why exactly the group could not be in the business of making money. Regardless, the sentiment highlights how Enrique's approach to catalysis science is rooted in gaining fundamental insight, even in the context of addressing technical challenges. What is distinctive about this approach is the focus on creating knowledge and not just data for technologically relevant catalytic systems.

Third, the structures of the supported oxides primarily used in this work are, relative to most of the materials discussed in this review, poorly defined and still debated. Spectroscopies such as UV−visible or Raman, which can be sensitive to longer-range structures, in some places replace X-ray spectroscopy techniques. Local disorder with respect to both the connection to the support and the number and type of metal oxide clusters continues to present challenges for mechanistic understanding. A desire to work with better-defined metal oxide structures led to some additional collaborations on "site-isolated" oxides,[107,108] but most work used relatively "conventional" supported oxides. However, early work within the group led to adoption of three distinct structural regimes where reactivity could be categorized as having "submonolayer", "near-monolayer", and "bulk oxide" characteristics. While quantitative measures of dispersion remain difficult to obtain, this work was part of a shift by some practitioners in the field away from information-poor descriptors of oxide catalyst surfaces, such as "20 wt % MoO_3", to descriptors that could be used across materials families, such as "4.6 Mo atom.nm^{-2}". A related effort was to emphasize site titrations and correlations between oxide and substrate properties, over wide ranges of reactivity, surface density, and oxide electronic structure, a continual theme in the research approaches throughout this review.

The intrinsic complexity and disorder of most oxide catalyst surfaces also provoked a transition away from conventional supported oxide surfaces toward the use of Keggin-type polyoxometalates (POMs) in later years,[109−112] which proved useful in other lines of research inquiry on solid acid catalysts (Section 8). The use of well-defined structures allows computational modeling to capture the properties of the catalyst with greater fidelity. The starting state of a POM is crystallographically regular and these materials are stable at reaction conditions, requiring far less faith when connecting predictions of a quantum chemical model and experimental measurements of properties of the material under interrogation. POM structures also generate isolated acid sites whose kinetic behavior can be described satisfactorily by using Langmuirian models. This is in contrast with most supported oxides, where irregular surfaces create a heterogeneous ensemble of sites in which a potential minority, highly active species may exist.

Persisting through these challenges, significant insights into surface redox chemistry were made. Eschewing review and perspective articles, the LSAC preferred to periodically publish comprehensive studies that collected the trends and overarching principles gleaned to date. Several landmark reports that unified concepts in redox catalysis appeared in 2002 by Chen,[113] 2008 by Macht,[110] 2009 by Zboray,[114] and 2016 by Deshlahra.[115] These tied together studies to show how empirical parameters (e.g., loading) determined oxide structure and how this combined with composition to determine their

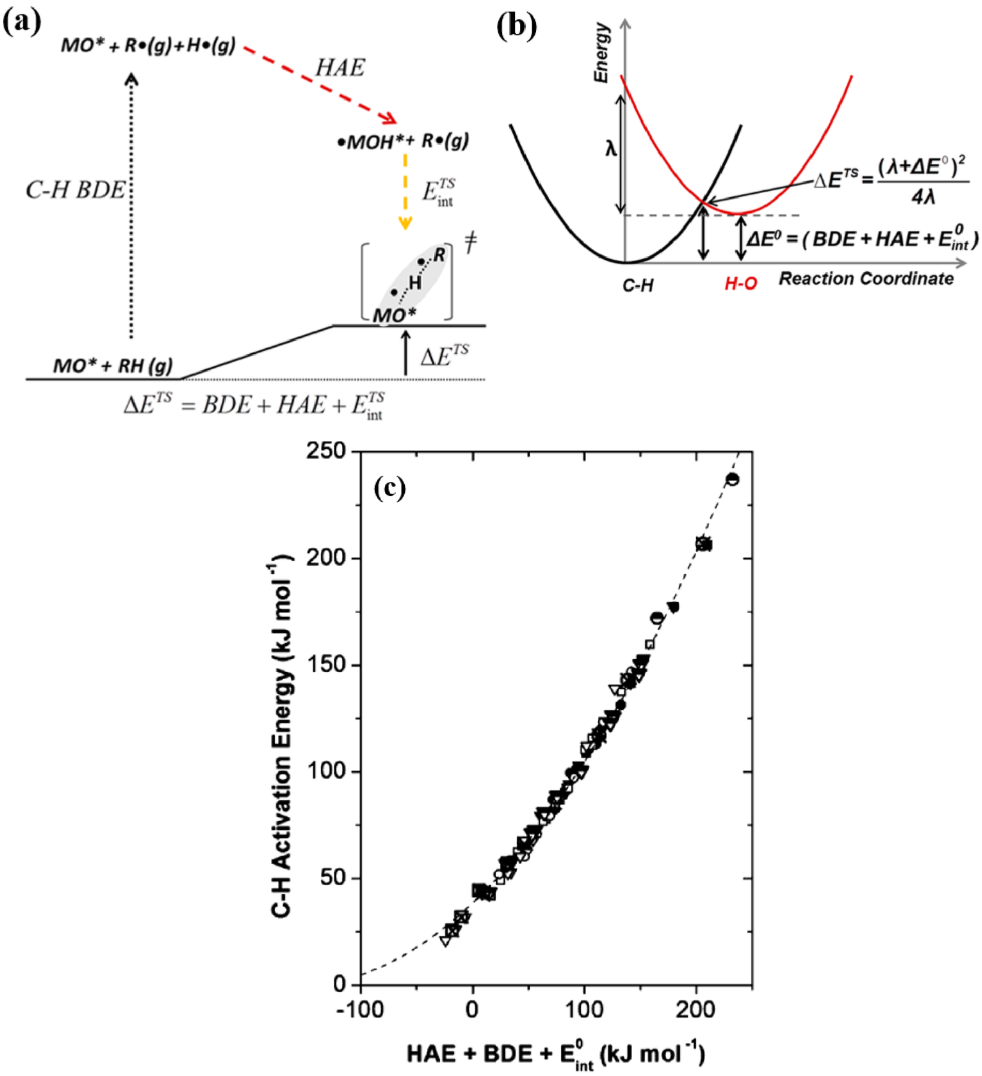

Figure 10. (a) A Born−Haber cycle description of the C−H bond activation energy for gaseous reactants on metal oxides (MO*) as a sum of C−H bond dissociation energy (BDE), the H atom addition energy (HAE) of lattice O atoms and a radical-surface interaction energy ($E_{\text{int}}^{\text{TS}}$), (b) A crossing potential model describing the relation between the transition state and the product state energies using the geometric crossing point of harmonic potential energy surface for stretching of C−H bond in reactant and the surface O−H bond, and (c), DFT derived C−H bond activation energies in alkanes (closed symbols), alkanols (open symbols), alkenes (half-filled symbols), and alkanals (crossed symbols), as a function of the sum of the C−H BDE of reactants, the HAE of abstractors, and the product state interaction energy (E_{int}^{0}). Dashed curves represent best fits to the functional form of the expression for ΔE^{TS} in (b) where λ is a parameter that depends on the curvature of the potentials and the bond distances involved in the C−H activation. Reproduced from Deshlahra et al.[115] Copyright 2016 American Chemical Society.

redox properties. Finally, the combination of metal oxide redox strength and the C−H bond strengths in molecules combined to predict reactivity (Figure 10). Specifically, Deshlahra and Iglesia showed that C−H bond activation energies across a diverse set of bonds in alkanes, alkenes, alkanols, and alkanals do not obey a single universal dependence on the C−H bond strength and the H atom addition energy (HAE) of the lattice O atoms in oxides, which are independent descriptors of the properties of the reactant and the catalyst, respectively. Instead, these dependencies exhibit different slopes and y-intercepts for C−H bonds with different substitution around the C atom due to the variations in the radical-surface interaction energies in transition states involving incipient radical formation ($E_{\text{int}}^{\text{TS}}$, Figure 10a). This study showed that the relevant interaction energies can be described using a product state interaction energy (E_{int}^{0}) that was independent of the lattice O atom involved and a harmonic crossing-potential model that describes changes in the lateness of the transition state along the C−H cleavage path (Figure 10b). This crossing potential model allows for a more complete description of activation energies for different types of C−H bonds based on a single-valued relation that combined the independent properties of the molecules and catalysts involved. Crucially, this analysis also allowed predictions of selectivity in sequential reactions involving competing C−H bond activation pathways in the reactant and desired product.

A critical final conclusion from this work is that this is *not* the end of the story. It is tempting to overgeneralize in this area and leave with the notion that selectivity is solely determined by C−H bond strength. However, because these reactions are primarily surface-catalyzed, unlike oxidative coupling of methane, for example, there remain opportunities for specific surface-substrate interactions to play a role, enabling some reactions to be more selective than would be predicted simply from bond dissociation energies.

Of note are two side excursions from alkane and alcohol ODH in the realm of redox-active oxides. In a series of papers from 2004 to 2007,[116−119] Iglesia (and principally Moden) examined the curious case of regioselectivity of alkane hydroxylation for Mn-exchanged zeolites. Prompted by earlier work by Thomas using Mn-exchanged AlPO materials,[120] Moden was persuaded to investigate claims of high selectivity to terminal hydroxylation that did not entirely align with prior kinetic assumptions. After reluctantly abandoning short contact time differential flow reactors, the intrinsic rate constants of this reaction were eventually established to the satisfaction of the LSAC group members. In general, these were not consistent with the exceptional results claimed in the earlier work, but transient conditions were found in which the much-desired high selectivity to terminal hydroxylation could be replicated. This study was a rare example where LSAC sought to address a specific finding in the literature. In most other cases, this task was incorporated as a critical education component of group meetings, but the group was otherwise encouraged to continuously push forward rather than perpetually circling back to reconcile inconsistencies in the published literature.

Most recently, the story of LSAC research into redox catalysis returns to the role of the O_2 activation. At the beginning of this section, it was mentioned that C−H bond activation is rate-limiting under the typically employed conditions, leaving O_2 activation steps kinetically invisible. Although studies using site counting, isotopic tracers, and spectroscopy showed conclusively that framework O atoms were kinetically relevant and equilibrated in the ODH catalysis, the specific mechanism by which molecular O_2 became a framework O atom was unclear. Again, because this step was not kinetically visible for benchmark catalysts, it became common practice, especially within the computational modeling literature, to consider only the thermodynamics of active site reoxidation, rather than its kinetics. This led to tortured mechanistic constructions where "1/2 O_2" is invoked to reoxidize isolated metal sites. In some of the most recent work from the Iglesia group, Kwon and Deshlahra[111,112] examined the reoxidation half reaction and showed that one of the O atoms could be recaptured by alkenes via transient hydroperoxy species. This work begins to shed light on the complex oxygen surface chemistry (e.g., peroxo, superoxo, hydroperoxo, or oxo) present under the ODH conditions, which is relevant for understanding and improving product selectivity. It also points toward a route by which careful coupling of kinetic cycles might enable progress in one of the grand challenges in selective oxidation chemistry, epoxide synthesis using O_2.

7. ACID-BASE CATALYSIS

Catalysis by solid acids and bases is another major area that Enrique has studied throughout his career, which played a major role in shaping understanding of the relevant mechanistic details and structure−function relationships in this field. His early research focused on the mechanistic details of bifunctional catalysis often involving Brønsted acid sites or acid−base pairs in multicomponent or supported oxides together with metal or redox functions that typically facilitate C−H bond activations. In later years, research investigations involved a greater emphasis on understanding compositional consequences and reactivity descriptors for each of the functions using a combination of experimental measurements and DFT calculations.

7.1. Bifunctional Catalysis Involving Solid Acids and Acid−Base Pairs. In the early 1990s, Ribeiro, Iglesia and co-workers reported unique effects of surface oxygen on tungsten carbide catalysts in inducing large shifts in selectivity for alkane conversion from hydrogenolysis to isomerization products.[28,121−124] Using kinetic and isotopic measurements, they demonstrated that isomerization involves sequential alkane dehydrogenation and alkene isomerization steps, with the product distributions in the latter step resembling those in typical carbenium ion rearrangements on Brønsted acid sites on WO_x. These observations led to an important insight that surface oxygen species lead to nonuniform surfaces in which WC_x domains and WO_x domains catalyze dehydrogenation/hydrogenation and isomerization steps, respectively, with gas-phase diffusion mediating the transfer of alkenes between these sites. Concurrently with these WC_x-WO_x studies, Soled and Iglesia investigated analogous $Pt/ZrO_2{-}SO_4$ bifunctional catalysts,[125,126] where Pt sites catalyze alkane dehydrogenation and strong acid sites on sulfated zirconia catalyzed isomerization. Here, the addition of small quantities of adamantane improved *n*-heptane isomerization rates and selectivity over cracking because kinetically relevant hydride transfer steps mediated by this hydrocarbon co-catalyst enhance carbenium ion termination rates decreasing surface residence times of species that might undergo cracking. This type of bifunctional approach to converting saturated alkanes and alkanols, where C−H activation functions are used to maintain low and known concentrations of unsaturated species, became a recurring feature in LSAC research investigations, with isomerization on Brønsted acids such as POMs and zeolites (Section 8) and alcohol condensation on acid−base pairs as prominent examples.[30]

Hilmen[127] and Xu[128] probed the reactivity of alkali promoted $Cu_yMg_5CeO_x$ and $Cu/ZnO/Al_2O_3$ for synthesis of alcohols from CO/H_2. Here, Cu sites catalyzed CO hydrogenation steps and acid−base pairs in $MgCeO_x$ and ZnO/Al_2O_3 led to aldol-type condensation steps beyond the direct initial formation of ethanol from CO, while alkali ions titrated Brønsted acid sites to prevent alcohol dehydration. Wang and Iglesia studied alkanol condensation using bifunctional catalysts involving physical mixtures of Cu with TiO_2 or ZrO_2,[129−131] accurately quantifying accessible acid−base pairs via titration with propanoic acid during reaction to derive turnover rates and combining measurements with DFT calculations to understand how reactivity and selectivity depend on molecular properties and strengths of acid and base sites in Ti−O and Zr−O pairs. Rates were limited by enolate formation and DFT-derived activation barriers correlated with C−H bond dissociation energies of α-carbons of the aldehydes. Condensation versus esterification rates depend on barriers for C−C and C−O coupling, respectively, between the enolate and a second aldehyde. C−C coupling activation barriers increased more sensitively with aldehyde size ($>C_2$) and branching due to the steric hindrance involved in its transition state. An important insight was that the anomalously high rates of the cross-coupling of formaldehyde with enolates (>1000-fold higher than acetone) originated not from enthalpic effects, because lower hindrance was compensated with weaker van der Waals stabilization for smaller formaldehyde reactants, but instead from the smaller entropic loss in forming tighter C−C transition states using formaldehyde.[131] The Iglesia group has continued to develop new insights on catalytic properties of acid−base pairs in nonreducible oxides with recent reports by Kwon et al.[132,133] on formic acid dehydration on crowded TiO_2 surfaces, and ongoing work on alkane dehydrogenation on ZrO_2.

7.2. Brønsted Acid Catalysis in Supported Oxides and by Polyoxometalate Clusters.

Following the initial studies on the bifunctional WC_x-WO_x system, the nature of acid sites on supported WO_x domains in contact with other oxides and their reactivity for isomerization, cracking, and dehydration reactions became a subject of investigation within the group for the next several years. Barton et al. found that, for WO_x-ZrO_2 and WC_x-WO_x catalysts, Brønsted acid sites form when some W^{6+} cations are replaced by a lower valent cation or are partially reduced, and that H_2 is involved in the generation and maintenance of these sites.[31,134,135] Macht et al. extended these results to WO_x domains on a broader range of supports including Al_2O_3, MCM-41, and SnO_2 and investigated relationships between acid and redox properties detected by UV−visible absorption edges and pre-edge features.[136] This work revealed that the number of acid sites, but not their reactivity, is correlated to the support redox properties.

Investigations involving Keggin-type POMs as catalysts with known structure and uniform sites but with diverse acid and redox properties, have been an important part of the work performed by LSAC since the early 2000s (also mentioned in Section 6). The known structure of POMs allows experimental measurements to be combined with reliable computational representation, underpinning an extensive collaboration with the Neurock group that led to rigorous understanding of structure−function relations via seamless combination of experiment and theory.

Liu et al. used POM clusters with Mo and V oxide shells enclosing a central heteroatom oxyanion to probe interactions between acid and redox functions in clusters for bifunctional methanol conversion.[137−139] Following these studies, Macht et al.[140−142] and Carr et al.[143] measured turnover rates as a function of reactant pressures for alkanol dehydration reactions on nonreducible W-oxide based POM clusters containing different central heteroatoms; the number of charge balancing protons also change with central atom identity, but this was appropriately accounted by normalization. In initial studies, Macht et al. correlated experimentally measured 2-butanol dehydration rate constants and butanol dimer formation equilibrium constants with DFT-derived acid strength (deprotonation energy and DPE values) in collaboration with the Neurock group. These were compared to kinetic parameters measured on BEA zeolite, whose DPE values had been calculated in prior literature.[140] Rate constants for butanol dehydration (k_2 in Figure 11) decreased exponentially with linearly increasing DPE values, because this rate constant reflects the formation of a cationic transition state from a neutral precursor. Furthermore, the rate constant for butanol dehydrogenation in zeolite BEA was noted to fall on the same correlation as that established for the reaction on the series of unconfined W-based POM acid sites, indicating that the impact of solvation (confinement) is weak for this monomolecular reaction whose transition state is of a similar size to its precursor. The equilibrium constant for the formation of butanol dimers (K_4 in Figure 11) also decreased exponentially with increasing DPE because, like the rate constant, it reflects the formation of a cationic species from a neutral species. However, the equilibrium constant in zeolite BEA is much larger than the expected value based on the correlation exhibited by W-based POM materials, indicating that zeolite pores confer additional stabilization for forming a butanol dimer (from a butanol monomer) through solvation.

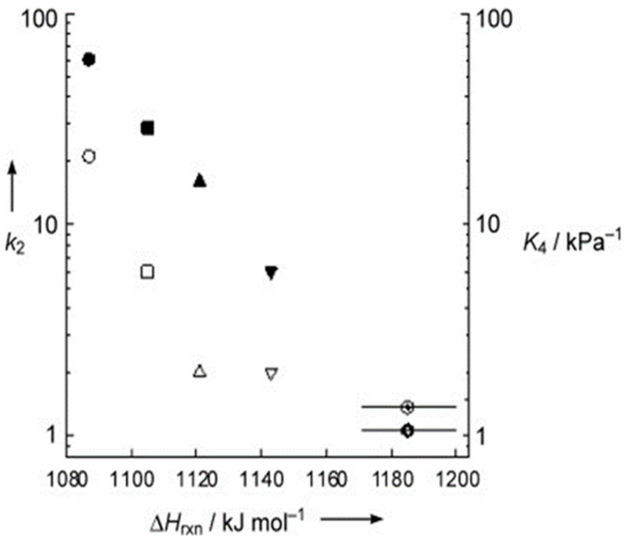

Figure 11. 2-Butanol dehydration rate constant k_2 (in 10^{-3} molecules 2-butanol $(H^+)^{-1}$ s^{-1}) (closed symbols) and dimer formation equilibrium constant K_4 (open symbols) as a function of deprotonation enthalpy, defined as ΔH_{rxn} of HA → A^-+H^+ (HA is the acid, and A^- is the conjugate base) and calculated by DFT. (0.04 H_3PW/Si (●), 0.04 H_4SiW/Si (■), 0.04 H_5AlW/Si (▲), 0.04 H_6CoW/Si (▼), and H-BEA (♦). — denotes the DPE range reported for different zeolite catalysts at the time of this publication. Reproduced with permission from Macht et al.[140] Copyright 2007 Wiley-VCH.

These two observations established the key rules for effects of acid strength and ultimately confinement on rate and equilibrium constants that would be later observed by LSAC across a wide range of chemistries: 1) kinetic parameters for steps that involve charge-separation (e.g., k_2 and K_4 in Figure 11) would decrease exponentially with increasing DPE values (i.e., decreasing acid strength) of the acid site, and 2) kinetic parameters for steps that involve changes in size of the intermediate will be influenced by the structure of the confining environment (e.g., varying size). The latter effects of confinement are explored in more detail in Section 8. In general, it was found that when analyzed within the framework of Born−Haber thermochemical cycles, reactions sense acid strength weakly (i.e., slopes reflecting changes in activation energy with DPE are much less than unity), because the energy required for solid acids to donate a proton to noninteracting distances (DPE) is largely recovered when protonated complexes interact with conjugate anions at transition states. The sensitivity to DPE is further diminished when the measured rate constant reflects the energy of a cationic transition state relative to a partially charged intermediate, instead of a neutral precursor.

DPE relations were also investigated for isomerization reactions, where Macht et al. used reactivity versus DPE relations in isomerization reactions on well-defined POM clusters to determine apparent DPE values for less uniform tungstated and sulfated zirconia materials and to suggest likely structures of active sites on these solid acids that could be assessed by theory.[144,145] Knaeble et al. measured rate constants for skeletal isomerization in acyclic and cyclic alkenes mediated by cyclopropyl carbocation transition states and their sensitivity to DPE for W-POM clusters.[146,147] Transition states of the same size but different substitutions around the cyclopropyl cation, which mediate chain-lengthening, chain-shortening, and methyl-shift steps for 2-methylpentene conversion, exhibited different energies consistent with the formation energies of their gaseous analog. Yet, barriers for forming transition states exhibited the same dependence (slope) on DPE, suggesting that a similar amount of stability is recovered for all three reactions via ion-pair interactions at their transition states. In contrast, larger transition states with more diffuse cationic charges that mediate methylcyclohexene conversion showed a stronger dependence on DPE, indicating less complete recovery of ion-pair interactions with conjugate anions as charges become more delocalized in the cationic transition state (relative to a proton).[146−148] While many Brønsted acid catalyzed reactions are mediated by nearly fully formed ion-pair transition states, reflecting complete transfer of the proton from the acid to the reactive species in the gas phase, Wang et al. found that the proton transfer for Prins condensation occurred earlier along reaction coordinates for weaker acids. This leads to barriers that were more sensitive to DPE for this reaction than for later transition states of similar size that mediated isobutene oligomerization.[149]

Taken together, these studies demonstrate that the DPE of solid acid catalysts and the proton affinity (PA) of reacting molecules determine activation barriers but that ion-pair interactions at the transition state are a necessary component to more fully describe acid−base reactivity. The energy of a given ion-pair transition state is different for same strength acid within different families of acids (e.g., W-POM, Mo-POM, molecular mineral acids and aluminosilicates without accounting for van der Waals components), indicating that ion-pair interactions are different (for the same DPE and PA values) across these families.[150,151] The transition state energy within each family increases with DPE with similar subunity slopes, but correlations for different families do not lie on the same line. To account for the nonuniversal nature of these correlations, Deshlahra et al. expanded on frameworks based on Born−Haber cycles[148,150,151] to account for two different contributions to DPE: a charge reorganization energy required to form a full proton and an anion from the neutral acid, and an electrostatic energy required to overcome Coulombic attraction between full ions. These covalent and ionic components of DPE, and the extent to which each is recovered at the transition state, led to a more complete descriptor of the acid−base reactivity. Specifically, the covalent component of DPE remains essentially unrecovered at full-ion-pair transition states, and as a result, the transition state is less stable on an acid containing a larger covalent component of DPE.

These structure−function relations describe why the reactivity depends on acid strength and how sensitive these dependencies are for different families of reactions and solid acids. POM clusters and zeolites were often probed in conjunction within LSAC to decouple the convoluted effects of acid strength and confinement. This approach overcomes limitations in studies that inaccurately attribute the reactivity and binding properties of probe molecules to imprecise concepts of “acidity”, which tend to conflate the influences of the number and intrinsic strength of acid sites with additional effects of confinement.

8. ZEOLITES AND POROUS SOLIDS

LSAC has studied catalytic reactions that occur within the confined spaces of zeolites and porous solids since its foundation, with early work using zeolites as supports for Mo-based active sites for methane dehydroaromatization and related alkane dehydrogenation reactions (Section 4). These reactions involved complex networks comprising alkene interconversion and hydride transfer and cyclization reactions, which highlighted the sensitive interplay between the reaction and diffusion within zeolitic voids, foreshadowing later work that used the Brønsted acid sites of zeolites themselves as active sites. Unraveling the details of these complex reaction networks required careful kinetic studies and understanding of the pervasive interplay between reaction and transport phenomena that are both affected by the zeolite voids where catalysis occurs. In particular, LSAC research has disentangled and clarified the roles of acid strength and solvation by confinement, the latter of which is defined by solvating van der Waals interactions between inorganic zeolitic hosts and organic guest moieties; together, acid strength and confinement endow zeolites with the reactivity and selectivity characteristics that underpin their ubiquity in industrial practice. The group’s work in zeolite catalysis, and more broadly in solid acid catalysis, has strived to replace qualitative heuristics with quantitative concepts such as enthalpic and entropic drivers that can represent host−guest interactions, the size and topology of the host, and primary and (diffusion-enhanced) secondary reactions, all of which have now become consistent themes in the literature.

8.1. Assessments of Acid Strength.

Inspired by the structure−function relations for acid strength using POM clusters, Jones and co-workers[152] demonstrated that DPE values for isolated protons in aluminosilicates were essentially invariant with differences in either long-range or local geometric structural properties, such as the framework topology or crystallographically distinct tetrahedral sites (T-sites) within a specific zeolite topology. This work established that isolated Brønsted acid sites in aluminosilicate zeolites are of similar intrinsic acid strength (i.e., DPE), because the stabilities of conjugate anions formed upon proton removal were similar among all sites due to the similar localization of negative charge among the four lattice oxygen atoms coordinating the Al site, a consequence of the predominantly SiO_2-framework functioning as an electronic insulator. Thus, differences in measured reactivities or probe molecule (e.g., NH_3) binding energies that are commonly used imprecisely as proxies of acid strength across zeolite topologies can instead be attributed to differences in confining environments. This attribution was systematically affirmed in LSAC research for a large class of Brønsted acid-catalyzed reactions in zeolites.

Although the local environment around Al atoms in zeolite framework lattices only weakly affect DPE, substitution of SiO_2-frameworks with trivalent heteroatoms (e.g., B, Ga, Fe) other than Al increases DPE. These differences in acid strength were examined without the conflating contributions of different voids by using a series of MFI zeotypes with isomorphously substituted heteroatoms, samples that were synthesized frequently by his collaborator Stacey Zones at Chevron. Rate and equilibrium constants were experimentally measured for acid-catalyzed methanol dehydration reactions by Jones and co-workers,[153] alkene oligomerization reactions by Sarazen and co-workers,[154] alkene isomerization by Noh and co-workers,[155] and acetone condensation by Herrmann and co-workers.[156] After normalization of kinetic constants by the number of Brønsted acid sites measured by temperature-programmed desorption of NH_4^+-exchanged zeolites or *in situ* titration using site-selective pyridine bases, rate constants (per H^+) showed similar trends with DFT-calculated[153] DPE values for measurements on Keggin POM acids for several reactions. The slope of the semilog dependences of rate constants on DPE reflect the sensitivity of ion-pair transition state stability, which differs in its extent and localization of separated charges relative to the case of a proton, to changes in the conjugate base stability. Rate constants for a given reaction decreased exponentially with increasing DPE values, with similar sensitivity for POM acids of varied strength and for MFI zeotypes. Notably, however, rate constants for zeotypes were greater (by orders of magnitude) than predictions based on extrapolation of measurements on POM acids to the higher DPE values characteristic of zeotype acids (Figure 12). These larger rate constants reflect the increased stabilization (by solvation) of larger bimolecular transition states relative to smaller monomolecular precursors in confined environments.

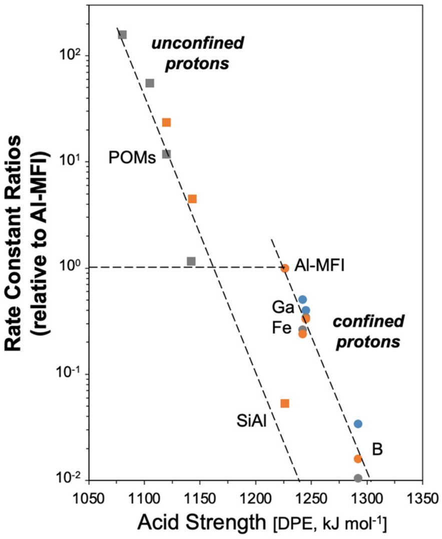

Figure 12. Relative rate constants for methanol dehydration (gray, ■/●), propene dimerization (orange, ■/●), and acetone condensation (blue, ●) referenced to the value measured on Al-MFI as a function of DFT-calculated DPE values for varied reactions on Keggin POMs and mesoporous silica−alumina (■) and X-MFI (●). Original figure with data reported in Jones et al.,[153] Sarazen et al.,[154] and Hermann et al.[157]

8.2. Confinement Influences on Catalytic Reactivity and Specificity.

This conceptual framework, extending the Born−Haber thermochemical analysis developed for POM acids to zeolitic acids, allowed for decoupling the separate influences of acid strength and confinement on the reactivity of isolated protons located in zeolites and porous materials, and eventually to more precise explanations for catalytic diversity among aluminosilicate zeolites that in many cases had been misattributed to differences in acid strength and further conflated by the near-range and farther-range effects of the surrounding voids (i.e., diffusion). Now, it is well recognized that protons confined only within certain voids of a given zeolite may catalyze a certain reaction because these voids are able to preferentially stabilize the transition state, moving beyond conventional concepts in shape selectivity based on heuristic arguments of size, shape, and access to and from the active site. The first example of this was through the work of Cheung, Bhan and co-workers to study the low-temperature (<523 K) carbonylation of dimethyl ether (DME) to form methyl acetate, which led to the recognition that rates (per H^+) were highest on zeolites that contained 8-MR voids and pockets (e.g., FER, MOR),[158,159] despite the similar intrinsic acid strength of protons among these materials. IR spectra of OH stretching bands were used to distinguish and quantify acid sites in 8-MR pockets, after titration or perturbation of acid sites in 12-MR channels by bulkier base titrants such as *n*-hexane or pyridine (Figure 13a).[158] Reactions of DME and CO were found to occur at acid sites specifically within the small 8-MR pockets (Figure 13b), through a backside nucleophilic attack by CO on a bound methyl derived from DME and subsequent methoxylation of acyl groups to reform methyl groups and yield methyl acetate products. Theoretical calculations from the Neurock group[160] showed that transition state stabilities were similar at protons confined within 8-MR and 12-MR voids of MOR when assessed with DFT functionals that did not include dispersion corrections, but that transition states were significantly more stable when assessed using DFT functionals with dispersion corrections, again corroborating the dominant role of van der Waals stabilization of the transition state upon confinement and the enzyme-like specificity of 8-MR voids for this carbonylation chemistry. This represents the first report of selective (>99%) and stable (>100 h) carbonylation catalysis by solid acids, especially one that is halide-free. This work was one of the early contributions from a long-standing collaboration with BP through a multiuniversity consortium MC^2 (Methane Conversion Center), which later became XC^2 upon expansion of the scope of work to include light hydrocarbons and biomass derived feedstocks. The ability of acids within the 8-MR side-pockets to catalyze DME carbonylation at much higher rates than those in 12-MR pores indicate that zeolite voids did more than prevent reactions on the basis of size exclusion, but could selectively promote reactions through van der Waals interactions (i.e., solvation) by matching transition state size and shape with that of the confining void.

The consequences of confinement on zeolite acid catalysis were explored further by Gounder and Iglesia in examining protolytic alkane cracking and dehydrogenation in MOR zeolites.[161−164] For high-temperature reactions (>700 K), differences in activation entropies were found to control the relative reaction rates between sites in MOR 8-MR side pockets and the 12-MR channels. These reactions, unlike DME carbonylation, are expected to occur at the interface between those environments for acid sites in the 8-MR side pockets, resulting in partial confinement of transition states in those environments. Transition states at pore mouths catalyzed by acid sites within 8-MR side-pockets exhibit greater entropy than those at acid sites within the 12-MR channels. Furthermore, these effects of transition state entropy vary among different C−C and C−H activation pathways within the same reactant molecule, resulting in changes in selectivity between dehydrogenation and cracking. The role of entropy on binding and on the stability of the relevant transition states is now ubiquitously considered in the analysis of reactivity within confined spaces, in the context of its balance with the enthalpic stabilization provided by ion-pair interactions, mediated by acid strength, and by dispersion forces imposed by van der

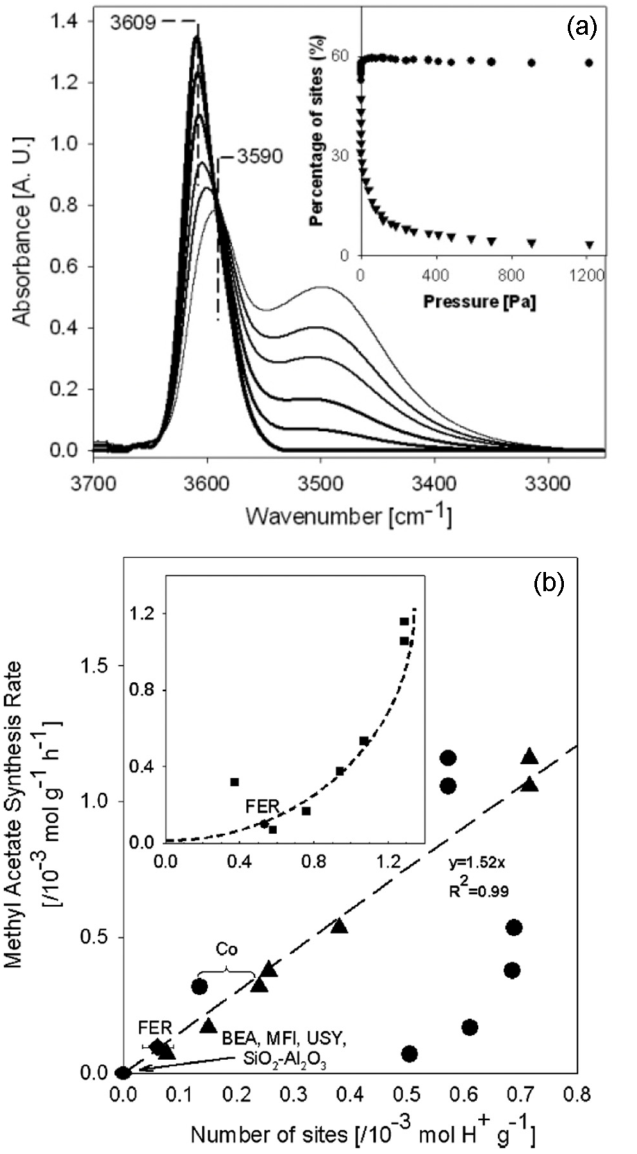

Figure 13. (a) Infrared spectra of the OH stretching region of H-MOR (Si/Al = 10, Zeolyst) upon *n*-hexane adsorption at 303 K; inset shows the percentage of H^+ sites determined from band deconvolution analysis in 8-MR (circles) and 12-MR (triangles) channels with increasing *n*-hexane pressure. (b) DME carbonylation rates per unit mass (438 K, 3.34 cm^3 s^{-1} g^{-1}, 0.93 MPa CO, 20 kPa DME, 50 kPa Ar) plotted against the number of H^+ sites per unit mass in 8-MR channels of MOR (triangles; Si/Al = 10, Zeolyst) and FER (diamonds; Si/Al = 33.5, Zeolyst) and 12-MR channels of MOR (circles). Inset shows DME carbonylation rates plotted against the total number of H^+ sites in these samples (squares). Reproduced from Bhan et al.[158] Copyright 2007 American Chemical Society.

Waals interactions. The consequences of entropy become more influential for reactions at higher temperatures, such as those (>700 K) where protolytic alkane activation prevails; thus, reactions are preferred in locations that increase transition state entropies, because such entropic gains are able to more than compensate the higher activation barriers required, ultimately leading to lower Gibbs free energies of activation.[165,166]

Confinement was also used by Gounder, Iglesia, and co-workers to attribute the higher reactivity of protons in hydrothermally "steamed" zeolites to the additional dispersive interactions provided by extraframework Al species confined within the same voids as the carbocationic transition state,[167] rather than an increase in intrinsic acid strength (attributed in prior work to "super-acidity"). It also allowed them to later (in 2020) unravel the mechanistic details and kinetic contributions of lower barrier pathways often measured and reported on acidic zeolites for alkane dehydrogenation to the presence of carbonaceous deposits that form in proton-free voids during reaction in H_2-deficient regions of catalytic packed beds,[168] rather than to changes in the intrinsic reactivity of proton sites attributed to changes in acid strength or to alternative (nonprotolytic) reaction mechanisms.

These studies of isolated transition states are often obfuscated by the "unselective" nature of protons, even in these "selective" pores. Complex reaction pathways, including alkanol/alkene/alkane chain growth cycles that are connected with isomerization, β-scission, and hydride transfer, can nevertheless be investigated using mechanistic analysis including how the pores and their connectivity dictate rates and selectivity, or relative rates, allowing frameworks to utilize confinement to select among various reaction steps (and molecules) in complex chain growth chemistries.[169,170] This work began with the selective homologation of methanol or DME on solid Brønsted acids (400−500 K), which involves the methylation of C_{n-1} alkenes by DME-derived adsorbed C_1 species to form C_n homologues, which can desorb as an alkene, isomerize to a C_n intermediate with a different backbone, undergo subsequent methylations, or desorb as a C_n alkane after hydride transfer from a H-donor. Methylation of C_n ($n < 7$) intermediates occurs in positions that form the most stable carbenium-ion at transition states, which tend to preserve a branched four-carbon backbone, resulting in the selective formation of 2,2,3-trimethylbutane (triptane).[171,172] Simonetti and co-workers showed from kinetic and isotopic studies that chains that grow to C_{8+} intermediates undergo facile β-scission to form isobutane, as well as smaller alkenes that re-enter chain growth cycles.[173,174]

These "rules" result in triptane and isobutane as the preferred termination products of DME homologation routes on solid acids, although this preference and rates of formation can vary. Ahn and co-workers initially showed that BEA zeolite was not only the most selective catalyst for triptane synthesis,[171] but also had the highest rates; among acids with decreasing void size (SiO_2−Al_2O_3, FAU, BEA, MFI; 10−0.55 nm diameter), triptane and isobutane selectivities go through a maximum in the BEA framework (0.7 nm diameter), indicating that methylation and hydride transfer of C_n intermediates become favored over isomerization within smaller voids, until the larger bimolecular transition states required for hydrogen transfer no longer fit (as observed within MFI voids). This was further corroborated in alkene-alkane "alkylation" mediated by hydride transfer reactions by Sarazen and co-workers, where BEA showed the highest hydride transfer rate constant between alkene-derived alkoxides on the surface with cofed alkanes (isobutane, *n*-butane, isopentane).[175] Solid zeolitic acids, differing in confining environments, become competent for these reactions as long as their voids are sufficiently large to accommodate large bimolecular transition states.

LSAC's contribution to what it means to be able to "accommodate" transition states came through the quantification of the confining environment. This confinement, or the strength of van der Waals interactions, depends on both the size of the guest moiety (ion-pair TS) and its host. Hence, rates differ among aluminosilicates based on their ability to confine transition states and the number (but not the strength) of the protons, the latter of which can be accounted for by proper normalization. When transition states are larger in size (e.g., bimolecular) than their relevant precursors (unlike the butanol dehydration example), measured rate constants increase with decreasing container size but only up to the point at which the size of the transition state approaches that of the confining void, beyond which the rate constant decreases with further decreases in container size (Figure 14). In other words, a "tight fit is the right fit". LSAC established these trends for several classes of proton-catalyzed chemistries, including methanol dehydration to dimethyl ether (DME), alkene dimerization, alkylation, isomerization, β-scission, and aldol and Prins condensation reactions. Figure 14 shows that for the slightly larger transition state of acetone condensation rate constants begin to decrease on 10-MR zeolites, while rate constants for propene dimerization continue to increase. There are nuances of "shape", however, which is why BEA and MFI rate constants overlap for propene dimerization but differ for acetone condensation (Figure 14) and also for the hydride transfer between C_6-alkoxides and cofed C_4 alkanes.[175] Thus, further exploration went into assessing descriptors that capture the nuances of how the transition state interacts with the surrounding environment. Energetic descriptors, such as molecular adsorption energies, are more accurate proxies that account for such effects. Jones and co-workers used the dispersive contribution to adsorption enthalpies of DME, a proxy in shape and size for the transition states involved in methanol dehydration to DME, calculated using DFT and Lennard-Jones interactions on FAU, SFH, BEA, MOR, MTW, MFI, and MTT zeolites and ensemble-averaged over all proton locations; first-order rate constants depended exponentially on such enthalpies.[176] This work was further developed by Herrmann, Sarazen and co-workers,[154,156] who used the actual transition state to sample the zeolite void, calculating dispersive interactions for each structure and ensemble-averaging all values.

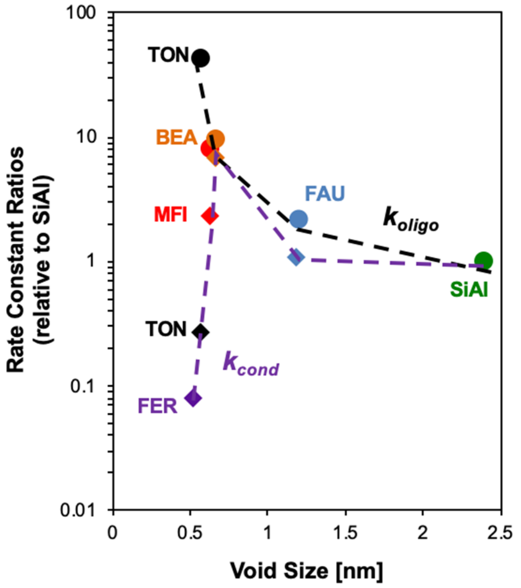

Figure 14. Rate constants for propene dimerization (●) and acetone condensation (◆) on aluminosilicates as a function of void size relative to those measured on mesoporous silica−alumina. Original figure with data reported in Sarazen et al.[154] and Herrman et al.[156]

The identity of the zeolite affects not only rate constants but also selectivity; in part, selectivity is driven by the selection among transition states that differ in size and thus their ability to optimally fit within different zeolite environments and in part due to diffusional restrictions imposed differently on differently sized molecular intermediates, which can increase intracrystalline residence time and thus reactivity. In DME homologation, triptane was selectively formed on BEA due to lower cracking and higher hydride transfer rates.[172,175] MFI, however, favors related MTH chemistry dictated by a hydrocarbon pool. If an alkane[177] or alkene[178−180] is fed instead of MeOH/DME, MFI also favors alkene cracking cycles, due to the fact it has larger voids accessible via smaller channels. Sarazen and co-workers used light alkene oligomerization to determine the effects of channel connectivity, void environment, and acid strength on the relative rates of C−C bond formation, β-scission, and isomerization reactions and the extent of diffusion-enhanced secondary reactions. Skeletal and double bond isomerization resulted in equilibrated alkene pools of a given carbon number on all catalysts, consistent with rapid hydride and methyl shifts of alkoxide intermediates and their rapid adsorption/desorption. The size distribution of the chains is dictated by the void environment, however, where zeolites with one-dimensional pores predominantly preserve the chain-growth product because their growth would not inhibit their diffusion through essentially cylindrical channels. Three-dimensional zeolites, like MFI, frequently contain voids larger than their interconnecting paths that facilitate the formation of oligomers that are too large and branched to readily diffuse through smaller interconnecting paths, requiring β-scission events to form smaller and faster-diffusing chains. These framework undulations, defined by the ratio of the largest cage size to the smallest window size, thus determine the extent to which secondary β-scission and subsequent oligomerization steps contribute to observed product distributions (Figure 15a).

This complex reaction-diffusion interplay is an inherent aspect of zeolitic materials. Small pores confer high reactivity to protons via solvation and confinement effects but also regulate access to guest molecules based on their size and their degree of branching. As a result, understanding and decoupling these effects is crucial, as shown by studies of bifunctional heptane isomerization and β-scission that examined the interplay between reaction and diffusion on the length scale of zeolite crystallites. These reactions involve skeletal isomerization of linear heptenes to methylhexenes and dimethylpentenes, which act as the sole precursor for β-scission to form smaller C_3 and C_4 products.[77,181] Notably, for such a reaction network, secondary reactions can occur before primary products can be detected in the bulk fluid phase. Similar formulations of the undulation parameter were utilized to collapse trends of extrapolated β-scission selectivity for *n*-heptane reactions, as in oligomerization (Figure 15b). Reaction-diffusion formalisms, taken together with selectivities measured during the desorption of a weakly bound titrant, were used to unambiguously demonstrate that cracking products were formed in secondary reactions; their formation reflected not differences in acid strength, but instead the inability of primary products to emerge from zeolite crystallites intact.[182] In fact, weaker acid sites, present in B-containing MFI zeotypes, had a higher intrinsic selectivity to β-scission

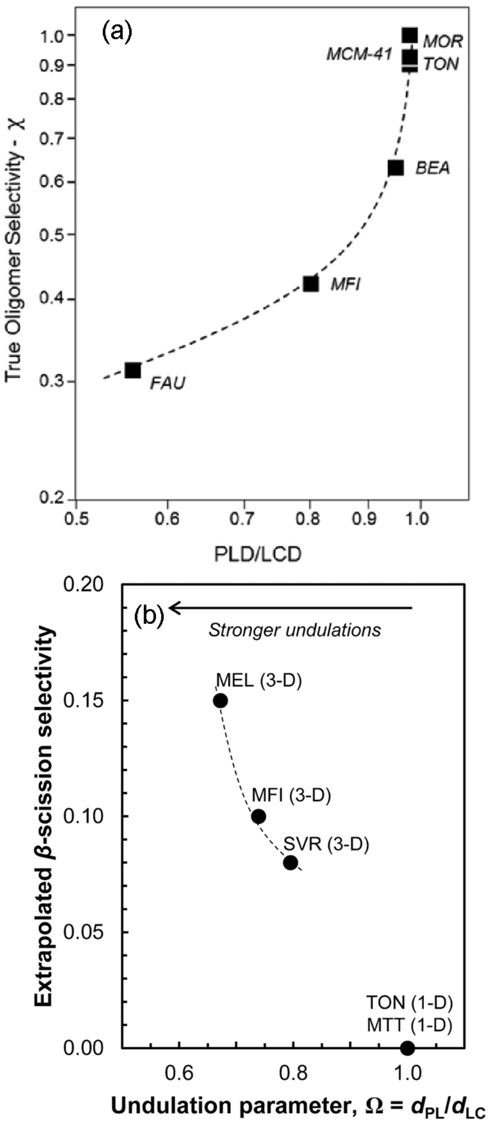

Figure 15. (a) True oligomer selectivity parameter for C_3H_6 oligomerization at <1% conversion (inverse of β-scission selectivity) reproduced with permission from Sarazen et al.[178] and (b) extrapolated β-scission selectivity for n-heptane reactions as functions of pore limiting diameter/largest cavity diameter (PLD/LCD) adapted from Noh et al.[181] Copyright 2019 Elsevier.

compared to isomerization, in contrast to the prevalent claim of cracking indicating higher "acidity".[155] These intrinsic (single-sojourn) selectivities instead reflect the greater charge delocalization in the isomerization transition state carbocation compared to that for β-scission. As a result, isomerization rate constants decreased more sensitively with decreasing acid strength than did the β-scission rate constants.

Hindered diffusion in micropores, however, is neither necessary nor sufficient to diagnose the diffusional enhancement of secondary reactions. Similarly, the use of catalysts lacking micropores is also not a guarantee of the absence of reaction-diffusion coupling. The coupling of reaction and diffusion can occur across all length-scales relevant to catalysis science: macroscopic convection, external diffusion of molecules between the extra-pellet fluid phase and the catalyst pellet surface, and internal diffusion of molecules within a given pellet. These different length scales are governed by different dimensionless numbers (e.g., Damköhler numbers and Thiele moduli) that represent the ratios of reaction rates and mass transfer rates. In fact, the selection of specific reaction networks (hexane isomerization)[146] and the use of catalyst deactivation as a tool to decrease active site density (methylcyclohexane ring contraction)[147] were both used to carefully decouple reaction-diffusion phenomena for acids supported on mesoporous SiO_2. Similarly, for isomerization and β-scission of heptanes on zeolitic materials, NH_3 was preadsorbed to the catalyst as a weakly bound titrant; product selectivities were measured as the titrant desorbed, permitting quantitative agreement with selectivities theoretically modeled using differential mole balances.

Decoupling reaction and transport phenomena has been a prevalent theme throughout Enrique's work. Over his career, his work has included frequency response measurements,[183] Monte Carlo simulations for tracer diffusion, and adsorption of probe molecules to quantify diffusion phenomena.[184−186] While his initial focus was on Fischer−Tropsch synthesis and understanding the extent to which diffusion and readsorption of primary products altered rates and selectivities,[187] his more recent work has used numerical methods (finite differences, finite elements) routines together with convective integral bed models.

8.3. Toward Design of Zeolite Catalysts through Synthesis. In some of these kinetic studies, bifunctional metal/zeolite systems were needed to mitigate deactivation, and the idea of designing these bifunctional systems with the zeolite acting as a support or a host for active sites other than protons grew into a synthesis-focused endeavor. Bolstered by his collaboration with Stacey Zones and Chevron and the synthesis of encapsulated metals in zeolites of varying structure and composition through direct hydrothermal syntheses and interzeolite transformations, the latter was expanded to include the synthesis of zeolites without metals. These studies resulted in model materials for investigating the fundamentals of catalytic reactions and developing materials for applications in shape-selective catalysis on protected metal clusters. The one-pot methods for confining ligand-protected precursors to metal nanoparticles during hydrothermal crystallization of small and medium pore zeolite frameworks, which are precluded from methods involving postsynthesis exchange, were initially developed by Choi[188] and expanded by Goel[189,190] and Wu.[191] Such procedures led to >95% encapsulation selectivities for materials inaccessible through alternate synthesis protocols and to nanoparticles uniquely resistant to sintering and inaccessible to large titrants. Otto and co-workers further developed these procedures to encapsulate monometallic Au,[192,193] which suffers from difficulty in synchronizing the rate of nucleation of nanoparticles and zeolite crystallization given the high reducibility of Au, bimetallic nanoparticles,[194] and base metal oxides.[195,196] The same emphasis on mechanistic details on reaction pathways was applied to synthesis pathways, leading to a search for interzeolite transformations[190] driven by common structural building units, so as to allow nanoparticle encapsulation for systems where precursors could not be stabilized by ligands at the conditions required for zeolite crystallization. This was guided by an increasingly detailed working model of framework nucleation and growth, which was then used to crystallize many zeolites typically requiring organic templates (e.g., CHA, MFI) via intrazeolite transformations without using such structure-directing agents. These contributions find applications for catalytic processes at high temperatures and with impure reactant feedstocks.

8.4. Metal-Exchanged Zeolites and Other Porous Solids. Additional work from LSAC using metal-exchanged zeolites extended beyond Mo and Cu in MFI described above for nonoxidative methane conversion and NO decomposition, respectively; in particular, activation of larger alkanes (primarily ethane and propane) was investigated. Alkane reactions on H-MFI at high temperatures were found to form a variety of products (including alkenes and cycloalkanes/alkenes), resulting from the "zoo" of unsaturated intermediates that formed within intrazeolitic void spaces. It was found that C−H activation is not the only reaction of importance but H-recombination and desorption are as well. Work by Baumgartner,[197−199] Meiztner,[200,201] Biscardi[202−204] incorporated Zn and Ga cations onto H-MFI supports to help facilitate reactions that scavenge H as H_2, altering alkane activation rates and selectivity to unsaturated products. The insights into hydrogen transfer, C−C bond formation, cracking, and cyclization reactions that occur simultaneously[205] were instrumental in later work without metal cations of DME homologation,[173] alkene oligomerization,[178] and alkene/alkane alkylation[175] discussed above. More generally, these early studies in LSAC set the stage for site identification and quantification, detailed kinetics (turnover rates and selectivities), and isotopic studies that inspired a high level of quality and rigor for work carried out by subsequent generations.

Reactions within zeolites are solvated by the inorganic framework via van der Waals interactions that depend on the size and shape of the surrounding voids and the reaction intermediates and transition states they confine,[166] and further influenced by the presence of debris within the pores.[167] More recent work from LSAC examined the role of solvation by a coadsorbed organic phase within mesopores. Studies of Ni^{2+} species grafted within mesoporous aluminosilicates (i.e., Al-MCM-41) for ethene dimerization at subambient temperatures revealed the effects of the capillary condensation of liquid-like ethene within mesopores on reaction stability, selectivity, and reactivity.[206,207] Titrations, kinetic assessment and DFT treatments suggest isolated $(Ni{-}OH)^+$ as the active sites for kinetically relevant C−C formation without the activators or cocatalysts needed in organometallic Ni-based catalysts.[207] However, the reaction rapidly deactivates at ethene pressures that are too low to cause capillary condensation. The catalyst could be regenerated by thermal treatments in either an inert (He) or oxidizing (O_2) environment, indicating deactivation occurs because desorption of large oligomers is limited and not because of coke formation. First-order deactivation rate constants decreased to undetectable values at temperatures and relative pressures that led to the capillary condensation of ethene within mesopores. The intrapore liquid stabilizes the desorption of bound 1-butenes before subsequent isomerization or further oligomerization, resulting in rates that are both stable and highly selective to 1-butene. This work was extended to propene and 1-butene dimerization reactions,[208] where high turnover rates and low deactivation rates were observed at the relative pressures required for alkene capillary condensation even in catalysts with differing mesopore diameters and even when the intrapore liquids consist of unreactive alkanes (Figure 16). These solvation effects conferred by noncovalent dispersive interactions highlight the need to incorporate thermodynamic nonideality in terms of transition state formalisms of chemical dynamics and became part of an enduring canon of LSAC research into catalysis within condensed phases and on crowded surfaces.

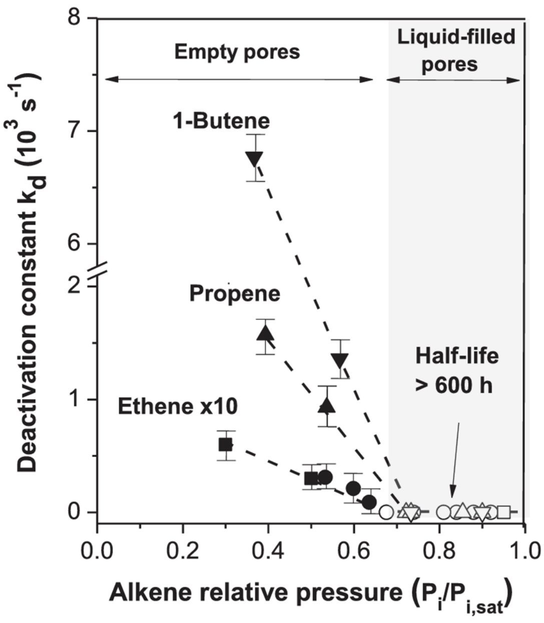

Figure 16. First-order deactivation constants during alkene dimerization at 248 K on Ni−Al-MCM-41 (Ni^{2+}:H_0^+=5.0) for ethene (●), ethene/ethane mixtures (■), propene (▲) and 1-butene (▼) as a function of the alkene relative pressure ($P_i/P^{i,sat}$). Reproduced with permission from Agirrezebal-Telleria et al.[208] Copyright 2020 Elsevier.

9. FISCHER−TROPSCH SYNTHESIS AND CATALYSIS ON CROWDED SURFACES AND IN CONDENSED PHASES

Few catalytic processes have garnered Enrique's attention as persistently as the Fischer−Tropsch synthesis (FTS), as evidenced from his patent and publication record at Exxon (1984−1997), throughout his work at Berkeley, and up to his recent perspective in *Journal of Catalysis*.[209] Enrique's study of FTS spans catalysis synthesis and optimization and kinetic and isotopic analysis to establish reaction and transport effects that govern product distributions and to establish reaction mechanisms along with atomistic-scale modeling of surface reactions with DFT. Like so many other areas Enrique has focused on, his work in FTS is characterized by elucidating and rationalizing long-held (and often contradictory) observations. Efforts to establish detailed understanding of Fe-based FTS catalysts were, and are, limited by the *in situ* carburization of Fe catalysts and the complex surface it creates. Co and Ru, in contrast, maintain their metallic state (when operated under the strongly reducing conditions that mimic industrial practice) and thus lend themselves most readily toward mechanistic insights. His work in FTS, particularly at Berkeley, created and reinforced some widely applicable "lessons" about how water can assist in H-addition reactions,[22,23,210,211] how bimolecular reactions are often preferable at the high coverages typical of metal-catalyzed reactions under practical (not UHV) pressures,[22,23,25,26,187,210−212] and how adsorbate−adsorbate interactions within those dense adlayers can influence reaction rates.[210,212,213] Under such conditions of high coverage, Langmuirian models of catalytic surfaces are no longer adequate to describe kinetic behavior. Lessons in coadsorbate interactions within crowded surfaces were, recently, directly translated into studies of reactions within crowded pores (condensed phases) often present at high pressures in micro- and meso-porous catalysts.

9.1. The Effects of Water on FTS Rates and Other Chemistries. H_2O is the main O-containing product of FTS, with CO_2 also observed at lower H_2 pressures on Fe catalysts or at conditions of significant water gas shift ($H_2O + CO \rightarrow H_2 + CO_2$). FTS rates increase with increasing CO conversion, which increases the H_2O pressure but also decreases the CO and H_2 pressures, making the kinetic origin of this rate increase less certain. Studies co-feeding water directly measure the rate and selectivity impacts of water and were first reported to increase FTS rates and selectivities to desired (C_{5+}) products within the patent literature.[214] What followed was a number of publications (including by Iglesia in 1997[187]) establishing that water could increase or decrease FTS rates depending on the nature of the metal, support composition and pore size. This variation in behavior is caused by a combination of promotional effects (discussed herein) and inhibitory effects (site-blocking and surface oxidation) that can occur on materials that are more easily oxidized (i.e., small Co nanoparticles).

Krishnamoorthy and Iglesia contrasted potential explanations for why H_2O increases CO consumption turnover rates on Co/SiO_2 catalysts.[22] This work used *in situ* spectroscopic studies to show that water does not influence the density or structure of adsorbed CO* intermediates thus establishing that water was neither creating nor alleviating CO transport restrictions and was neither cleaning the surface of carbonaceous debris nor polluting the surface with H_2O-derived species, as any of these would influence surface coverages. It also showed that H_2-D_2 kinetic isotope effects were invariant with H_2O pressure and that H_2O/D_2O showed no kinetic isotope effect. Taken together, this work implied that water was increasing intrinsic reaction rates yet was not directly involved with the kinetically relevant step. This inconsistency would remain unresolved[215] until theoretical tools advanced to the level necessary to model high coverage CO-H_2 reactions.[23,210]

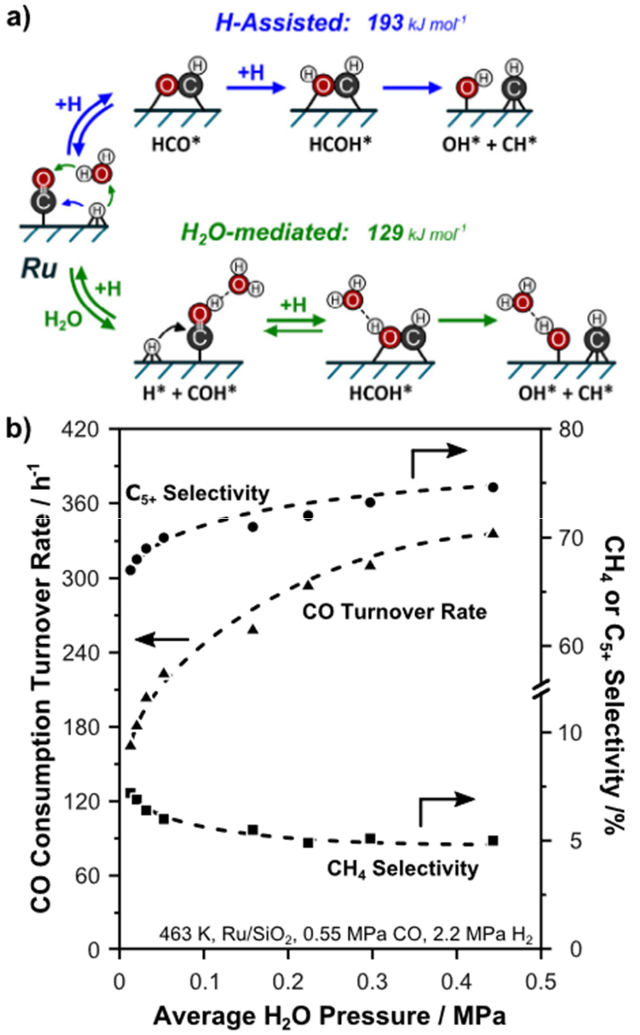

Figure 17. (a) H-assisted CO activation can be further mediated by proton coupled electron transfer reactions that facilitate O−H bond formation and ultimately C−O cleavage via HCOH transition states. (b) CO turnover rates increase with increasing H_2O pressure as CH_4 selectivity decreases and the selectivity to C_5 species increases (463 K, 0.55 MPa CO, 2.2 MPa H_2, Ru/SiO_2). Reproduced with permission from Hibbitts et al.[23] Copyright 2013 Wiley-VCH.

In 2013, Loveless, Hibbitts, Neurock, and Iglesia examined CO activation routes[23,210] informed by kinetic studies combined with DFT calculations performed on 201-atom Ru nanoparticles at CO* coverages at (or above) 1 monolayer (ML). CO turnover rates were found to be first-order in H_2 pressure and inhibited by CO pressure on Ru/SiO_2 catalysts,[210] consistent with prior reports on Co catalysts.[25,26,216] Rates, furthermore, were found to increase with H_2O pressure (Figure 17b), with H_2O effects approaching saturation as H_2O pressure increased,[23] as also observed in Krishnamoorthy et al.[22] DFT calculations were used to contrast CO* activation with a nearby vacancy (to form C* and O*) and a route assisted by coadsorbed H* (via C−O cleavage in *HCOH* intermediates). Among these paths, the H*-assisted route had barriers ~100 kJ mol^{-1} lower than those for direct CO* dissociation at high CO* coverages. The water-mediated path involved a H*-assisted route in which H* first reacted with H_2O to form a short-lived H_3O intermediate which reacted with CO* to form COH* in a proton-coupled electron transfer that reforms H_2O. This was followed by hydrogenation of COH* to form *HCOH*, which then underwent C−O dissociation to form CH* and OH* fragments. This water-involved route had an effective enthalpy barrier ~60 kJ mol^{-1} lower than that for the anhydrous route (Figure 17a), but the entropy loss associated with H_2O adsorption made the effective free energy barrier nearly identical to the anhydrous route, consistent with both the anhydrous and water-mediated routes contributing at mild H_2O pressures and the nonzero *y*-intercept in Figure 17b. H_2O alters the mechanism as a cocatalyst, but only hydrogen-bonds with *HCOH* during its dissociation, which is the kinetically relevant step in both the anhydrous and water-mediated routes. These findings thus resolved how water could increase the intrinsic rate and present no kinetic isotope effect, as seen by Krishnamoorthy et al.[22]

H_2O assists in CO activation during CO-H_2 reactions, while H_2O was shown to assist in O_2 activation during CO oxidation reactions on Au in prior work by Ojeda and Iglesia.[217] Single crystal Au(111) surfaces are incapable of activating O_2 at the ambient temperatures typical of CO oxidation on Au.[218] This led to proposals that active sites for O_2 dissociation involve defects on the Au surface (i.e., corners or step-edges) or bifunctional sites at Au-support interfaces. Lending credence to the latter claims was that Au/TiO_2 was much more reactive than the Au/Al_2O_3 surfaces. However, while large support effects were observed during "anhydrous" CO oxidation reactions, even small water cofeeds (~0.5 kPa) would dramatically increase CO oxidation rates and eliminate any benefit of the TiO_2 support (over the Al_2O_3 support). Kinetic measurements of CO oxidation rates on Au/Al_2O_3 showed that cofeeding 0.2 kPa H_2O increased rates by a factor of ~20 and that rates went through a maximum near 0.4 kPa H_2O before gradually decreasing with further increases in H_2O pressure. This kinetic behavior is consistent with a reaction mechanism in which H_2O* reacts with O_2* to make OH* and OOH*, the latter of which reacts with CO* in the kinetically relevant step to generate CO_2* and OH*. H_2O-assisted O_2 activation to form OH* was also reported during aqueous-phase alcohol oxidation on Au catalysts.[218] The two OH* generated then disproportionate to form H_2O* again, and an O* adatom that can react with a second CO* to form CO_2*. Thus, H_2O behaves as a cocatalyst and the lack of support effects at mild H_2O pressures suggest that support effects at anhydrous conditions likely reflect differences in trace amounts of H_2O adsorbed on the supports and not on the presence of kinetically relevant Au-support interfacial sites.

9.2. Coadsorbate Effects on FTS Initiation and Growth Rates. In the early 1980s, Brady and Pettit showed that feeding diazomethane (CH_2N_2) with or without CO* readily led to hydrocarbon products by its decomposition to form CH_2* species (the carbene mechanism).[219] The rapid incorporation of CH_x* species into a hydrocarbon chain would suggest that chain initiation and propagation would both be limited by the formation of CH_x* and thus occur at similar rates. Isotopic-switch studies (^{12}CO to ^{13}CO) by Mims and McCandlish[220] followed by NMR analysis of α-olefin products revealed that long-chain hydrocarbons grew so rapidly that their isotopic content (% ^{12}C) was constant along their backbone and did not, as one might expect, show a gradient of decreasing ^{12}C content toward the C=C double bond that involves C atoms most recently added to the chain. These data imply that chain initiation is much slower than chain propagation and prompted many researchers to propose that hydrocarbon chains (once initiated) reacted quickly with CO* as the chain-growth monomer (the CO-insertion mechanism). Thirty years later, and again assisted with insights from DFT, Hibbitts, Neurock, and Iglesia[213] reconciled this point by showing that hydrocarbon chains disrupted CO* adlayers to facilitate CO* activation at nearby sites, thus leading to two CO* consumption pathways: 1) a slow activation to initiate a chain, and 2) a facile activation near a chain to produce CH_x* monomers. The facile activation occurred with enthalpy barriers ~60 kJ mol^{-1} lower than the slow chain initiation (~130 kJ mol^{-1}), consistent with measured activation barriers in FTS.[210,216] This work explained how chains could initiate slowly and also grow rapidly, despite both processes occurring through the same CO activation mechanism. H_2O, by promoting CO* activation, would then lead to an increase in the ratio of chain-propagation to chain-termination events, and thus lead to the observed increase in the selectivity of desired C_{5+} hydrocarbons.

9.3. Bimolecular Pathways Facilitate Strong-Bond Activation in FTS and Other Chemistries. Molecules with strong double or triple bonds (e.g., NO, CO), dissociate with relatively high barriers on the close-packed surfaces that make up the abundant fraction of transition metal nanoparticles (>1 nm in diameter). This has led to proposals that under-coordinated defect sites (e.g., corners or step-edges) are responsible for their dissociation, such as for N_2 on Ru during NH_3 synthesis, NO on Rh and Pt during NO reduction reactions, and CO on Co and Ru during FTS. Similarly, the inability of Au(111) surfaces to directly dissociate O_2 has led to proposals of bifunctional sites at interfaces between the metal and oxide supports that are responsible for those dissociations. These claims of rare defects responsible for the dissociation of recalcitrant reactants have been supported by UHV surface science experiments and DFT calculations at the low coverages characteristic of UHV. However, as the total system pressure increases to that of practical catalysis, adsorbate coverages increase dramatically, which 1) block highly reactive defects with strongly bound species and 2) create opportunities for bimolecular reaction pathways that would be rare at UHV conditions.

As described above, Enrique's work in FTS established that CO is activated following hydrogenation events (i.e., through bimolecular CO-H_2 reactions) which reduce the strength and bond order of the CO bond prior to its activation. This work was performed on Co (with Ojeda, Mavrikakis, and others)[25,26] and Ru (Loveless, Hibbitts, and Neurock)[23,210,221] using a combination of kinetic measurements and DFT calculations. These kinetic measurements were consistent with prior reports on Co,[216] and many subsequent studies have established the similarities (in kinetic behavior) between Co and Ru catalysts.[26,187,210,216,222] This H-assisted pathway gives a natural explanation for the first-order dependence in H_2 pressure observed on both catalysts and explains why close-packed surfaces, Ru(0001) and Co(0001), are the active sites for this chemistry as suggested by increasing turnover rates with increasing particle size (which expose a greater fraction of their surface in close-packed terraces).

NO-H_2 reactions occur by a similar H-assisted pathway in which NO is first reduced to NOH* or *HNOH* intermediates prior to N−O dissociation on NO*-covered Pt(111) surfaces.[76] Similarly, Iglesia showed that CO-O_2 reactions occur by a CO-assisted O_2 dissociation reaction on CO*-covered Pt surfaces,[223] and by H_2O-assisted O_2 dissociations on Au surfaces.[217]

9.4. Nonideal Environments of Crowded Surfaces (and Pores). Enrique (and others) have shown through spectroscopic, kinetic, and theoretical studies that CO* and NO* often dominate transition metal catalyst surfaces, leading to high coverages for CO-H_2, CO-O_2, NO−CO, and NO-H_2 reactions.[211] Reactions require desorption from these dense adlayers to create vacancies, leading to inhibition by CO or NO in kinetic rate expressions. Furthermore, these dense adlayers modify adsorption/desorption, reaction, and activation energies through coadsorbate interactions that are mostly repulsive in nature on dense metal surfaces. These coadsorbate interactions can be understood through nonideal kinetic formalisms, such as in work by Hibbitts and Iglesia focusing on Ru-catalyzed FTS.[212] The reaction rate expression implies that the number of CO* that must be desorbed to form the kinetically relevant transition state is between 0 and 2, depending on the value of $\beta^* P_{CO}$ relative to unity:

$$r_{CO} = \frac{\alpha P_{H_2} P_{CO}}{(1 + \beta P_{CO})^2} \quad (1)$$

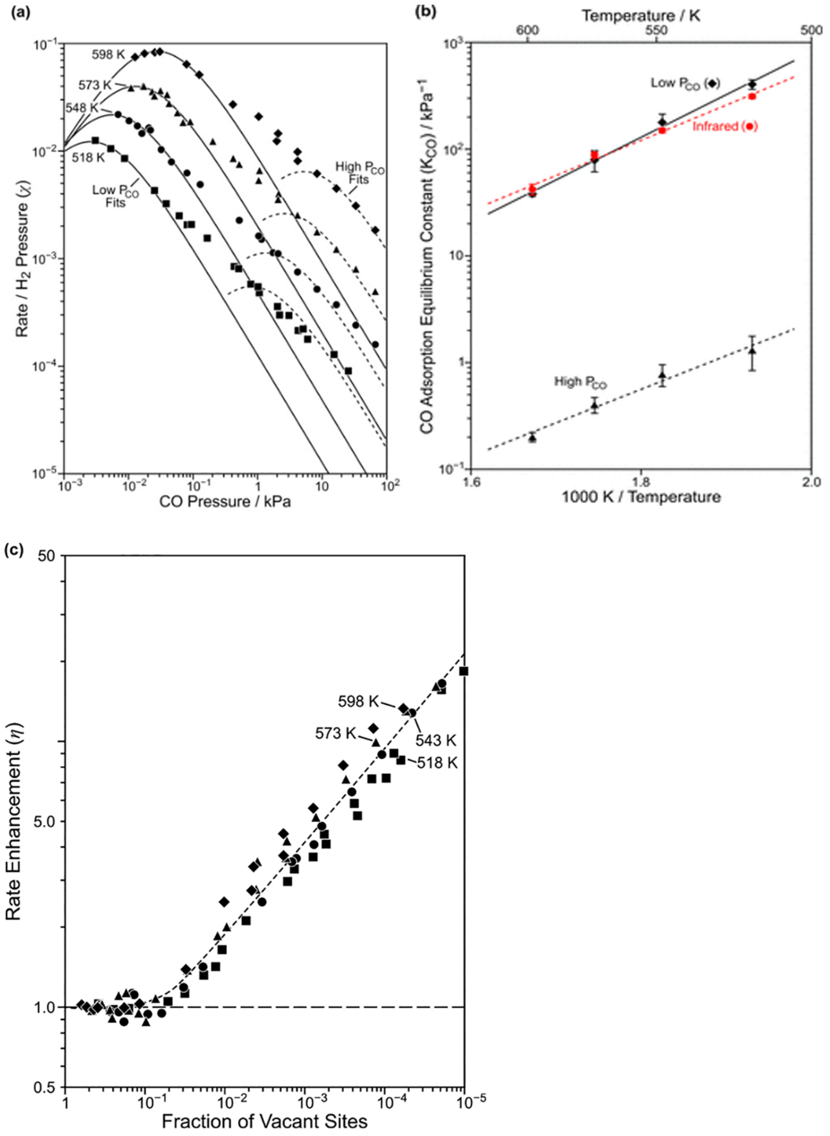

Figure 18. (a) Effects of CO pressure on CO-H_2 turnover rates (divided by H_2 pressure) on 5% wt. Ru/SiO_2 (7.5 nm) at 518−598 K. Solid lines show rates predicted from eq 1 using K_{CO} values regressed from low-pressure data while dashed lines show predicted rates using K_{CO} values from high-pressure data. (b) Regressed K_{CO} values from IR data (●), low-pressure rate data (10^{-3}−10^{-1} kPa CO,◆), and high-pressure rate data (10−100 kPa CO, ▲). (c) Ratios of measured to predicted CO-H_2 turnover rates (η) as a function of CO* coverage at 518−598 K. Reproduced from Liu et al.[212] Copyright 2017 American Chemical Society.

where β value in eq 1 reflects the CO adsorption equilibrium constant (K_{CO}). At methanation conditions (518−598 K, 0.01 to 10 kPa of CO), regressed K_{CO} values match those regressed from adsorption isotherms generated from CO FTIR data, and rates can be well-predicted through the Langmuir−Hinshelwood rate equation shown above. At higher pressures (10−100 kPa CO), however, regressed K_{CO} values are ∼200-times lower and rates exceed those predicted by low-pressure fits to eq 1 (Figures 18a and b). This enhancement factor (η) increases with increasing CO pressure and decreasing temperature, or rather, it increases with CO* coverage and can be rationalized by writing a rate equation for reactions in nonideal media.

Reactions in nonideal solutions with varying ionic strength lead to the inference that rates are proportional to the concentrations, and not the activities, of the activated transition state complex,[224] with Eckert and Boudart showing that the same holds for gas-phase reactions in their 1963 study of hydrogen iodide pyrolysis.[225] Madon and Iglesia later expanded those efforts to describe nonidealities present between adsorbed species and a contacting liquid phase.[226] Hibbitts and Iglesia then used those formalisms to describe nonidealities present among coadsorbed species in 2013.[212]

Transition state concentrations can then be related to the concentration of reactants and the activity coefficients of the reactants and transition state. For CO-H_2 reactions on crowded metal surfaces, this rate equation is written in terms of reactant pressures and the activity coefficients of the kinetically relevant transition state and the chemisorbed CO* that it replaces (eq 2):

$$r_{CO} = \frac{k_B T}{h} \frac{K^{\ddagger}}{K_{CO}^{2}} \frac{\gamma_{CO^*}^{2}}{\gamma_{\ddagger}} \frac{P_{H_2}}{P_{CO}} \tag{2}$$

This rate equation assumes that surfaces are fully saturated in CO*; thus, the unity term in the denominator of eq 1 is negligible. Equilibrium constants describing CO adsorption

(K_{CO}) and transition state formation ($K^‡$) are treated as corresponding to those processes at low coverage (absent coadsorbate interactions) and γ terms reflect nonidealities caused by coadsorbate interactions and thus are CO*-coverage dependent. Using this formalism, the enhancement factor (η) becomes the ratio of activity coefficients and is a single-valued function of the CO* coverage[212] across a wide range of pressures (0.01 to 100 kPa CO) and temperatures (518−598 K), as shown in Figure 18c. At low CO* coverages, the enhancement factor is unity, indicating that the system is ideal (no coadsorbate interactions), while at higher CO* coverages, the enhancement factor is >1. Kinetic analysis showed that this ratio changes but could not be used to rationalize or independently describe γ^2_{CO*} and $\gamma_‡$. A complementary set of DFT studies provided these insights.

As the CO* coverage increases, DFT-calculated CO* desorption free energies decrease, consistent with an increase in γ^2_{CO*} while transition state barriers do not change, indicating that $\gamma_‡$ is nearly independent of coverage. This difference in the behaviors of γ^2_{CO*} and $\gamma_‡$ can be rationalized by considering their size on the catalyst surface. A pair of vicinal CO* surface-bound species occlude (or occupy) 16 Å^2 of the catalyst surface (as estimated from DFT-derived structures and common space-filling atomic models), while the transition state occupies just 12 Å^2. The smaller species is repulsed to a lesser extent by densifying the CO* adlayer around it, and thus, the enhancement factor increases. The change in the area of the surface-bound species upon transition state formation represents an activation area, and like activation volume, it can predict how observed rate constants will change with increasing pressure for homogeneous reactions in liquid and high-pressure nonideal gas phases. Here, the negative activation area predicts that effective rate constants (which include activity coefficients) will increase with increasing CO* density, as observed (Figure 18c).

10. ENRIQUE'S MENTORING AND ADVISING OF LSAC

Enrique's intellect and clarity of thought, his ability to distill complex problems into their most essential components, and his perspective on scientific problems of relevance in catalysis are what LSAC alumni recall after their stay in the group. LSAC kept you on your toes in terms of both a high-achieving peer group and a mentor who demanded nothing short of excellence in your experiments, analysis, and presentation. We were challenged to examine in-depth problems in catalysis from the vantage point of generating new insight, "recyclable" knowledge, and at the same time to balance rigor, applicability, and clarity. Manuscript revisions for the *n*th time, practice talk after practice talk, and progress reports were always given feedback that was incisive and meant to instruct, often with a tone of humor. These outputs of scientific communication had their signature "style", one that was enforced with fair diligence (in hindsight) for clarity and logic, and one that many of his mentees have adopted in their future careers and research groups! In LSAC was a very nourishing, supportive, and challenging scientific environment, where Enrique taught us to find cogent explanations for complex problems and taught us to excel. But perhaps more importantly, our stay in the group was one where we forged strong kinships, both personal and professional, that have endured over the years.

For those of us now leading our own research groups, it was not until we began to advise our own students that we truly realized all of the things Enrique constantly did to enrich and nourish his group members, both as researchers and as people. That is not to say we were oblivious, in real time, of his dedication to his research group and his mentees. His remarkable ability to schedule and hold weekly one-hour 1-on-1 meetings with every postdoc and graduate student where he was fully engaged on experimental and mechanistic minutia, even when fueled only on bananas, was enough of an example of his commitment. In these meetings, we strove to have new data, new insights, or new ideas to try to take advantage of his wealth of knowledge. The inherently applied nature of catalysis was always present but never at the expense of fundamental scientific understanding, as we were reminded when Enrique would invariably ask questions about "how the molecule" behaves. Curiosity in the form of questioning was encouraged, not just from Enrique but from the whole group. We could ask questions to our heart's content and discuss or debate points, ask for references to read, follow up, and ask more questions, and there was a perpetual opportunity to learn. This curiosity often meant that a "normal" group meeting presentation prepared you more than a conference talk or interview. It also flowed out of our group meeting conference room into smaller conference and office rooms, in the laboratory, and even in hallways at conferences after leaving the group and across generations of the group. All of this evolved naturally from the mode of inquiry Enrique trained his mentees to take.

11. CONCLUSION

Enrique has performed field-defining work in C_1 chemistry, including Fischer−Tropsch synthesis and other routes for methane conversion, starting from his work at Exxon and prevailing throughout his academic career. In particular, his establishing the relationship between kinetics and transport, as well as primary and secondary reactions within FTS, created an experimental basis for the fundamental understanding of the reaction mechanisms that would follow. At Berkeley, his work on FTS established that CO activation occurs through H_2- and H_2O-assisted mechanisms (as opposed to direct dissociation into C* and O*) on surfaces covered by dense CO*-adlayers that accelerate reaction rates. These conclusions represent scientific themes recurring throughout his work on how reaction mechanisms and kinetics are influenced by crowded surfaces and condensed phases that often prevail during realistic working conditions of catalysis and how strong bonds in molecules are activated (including NO-assisted O_2 dissociation on WO_3−CeO_2, H_2-assisted NO dissociation on Pt, CO-assisted O_2 dissociation on Pt, and H_2O-assisted O_2 dissociation on Au). Similarly, during studies of methane reforming (dry or steam) and catalytic combustion, his work showed that CH_4 activation can occur with the assistance of O* adatoms at high coverages (set by reaction conditions and oxidant) on Group VIII metal catalysts.

Understanding the importance of the crowded nature of metal surfaces during catalysis, his later work examined alkane hydrogenolysis at conditions (high H_2:alkane ratios) that lead to H* as the sole MASI, thus avoiding the "zoo" of surface species present at lower H_2 pressures that had plagued earlier interpretations of kinetic data. Through a combination of kinetic studies and DFT calculations, this uncovered fundamental knowledge of how branching, chain length, and the cyclic versus acyclic nature of the alkane, as well as how metal identity and particle size, influence hydrogenolysis rate and selectivity as a function of H_2 pressure and temperature. This work exemplifies another recurring scientific approach from Enrique's work, inherited from the approach espoused and practiced by Boudart, to measure reaction kinetics on supported and bulk heterogeneous catalysis over widely varying reactant pressures (even orders-of-magnitude, when warranted) to study the kinetics of surface reactions under well-defined regimes of surface coverage. This work also provides an example of the studies that Enrique began to perform in the latter stages of his academic career, to combine insights from both experiment and DFT to provide molecular-level descriptions of the reaction chemistry.

Enrique has also had a history of characterizing active sites on materials with poorly defined surfaces and determining the kinetics of complex reaction networks. His group has characterized active sites for alkane and alkanol oxidations on supported oxides through careful variations in loading to relate observed kinetics to catalyst properties. Eschewing the typical approach of making model substrates, his work demonstrated how well-controlled reaction studies can shed light on the structure and reactivity of active sites that exist on materials that lack long-range order and have a polydisperse local atomic structure. For metal-zeolites, his group showed the nature of MoO_x precursors that lead to MoC_x active sites in Mo-MFI catalysts for methane DHA, as well as the Cu dimers responsible for NO reduction and oxidation during its decomposition on Cu-MFI catalysts. His work even showed NO oxidation in zeolite voids devoid of any active sites—a gas phase reaction accelerated by confinement effects—and the relevance detailing gas-phase reactions in studies of the impact of H_2O on methane OCM.

A complementary focus on more well-defined heterogeneous catalysts allowed Enrique to develop precise experimental and theoretical assessments of the catalytic reactivity and selectivity and the structure and function of active sites. Thermochemical cycles involving hydrogen addition to surface oxygens and C—H bond dissociation energies of the reacting alkanes and alkanols were developed for redox reactions on supported POM clusters. In later years, this platform was utilized to understand surface reoxidation mechanisms, which are often kinetically invisible and otherwise ignored in the literature. Similar efforts were also performed for acid—base reactions through kinetic studies on POMs of varying acid strength (defined by DPE, as calculated by theoretical methods), which demonstrated how rate constants exponentially decrease with increasing DPE (weaker acids) with slopes (sensitivities) that depend on the difference in charge between transition states and kinetically relevant precursors and the extent of charge (de)localization within those moieties. Partway through his career at Berkeley, Enrique established and grew a significant research effort in zeolite materials, which allowed him to broaden structure—function relationships in acid—base catalysis to account for the effects of DPE by studying silica-based microporous materials substituted with distinct heteroatoms (Al, Fe, Ga, and B).

Furthermore, by comparing and contrasting the kinetic behavior of microporous zeolites with environments that confine active sites and transition states to that of unconfined aluminosilicates and POMs, his work was able to decouple the separate influences of acid strength and confinement on reactivity. This work established relationships between confinement effects and the difference in size between transition states and their relevant precursors as well as the size and shape of the zeolite topology. Through studies of MOR zeolites with proton distributions between smaller 8-MR side pockets and larger 12-MR channels, his work showed how 8-MR side-pockets could preferentially stabilize transition states for DME carbonylation and protolytic alkane activation, respectively, due to enthalpic and entropic driving forces. One major consequence of these findings is that observed catalytic reactivity may be dominated by contributions of only a portion of the acid sites contained within the zeolite but not due to steric restrictions, thereby extending conceptually the more well-established mechanisms by which transition state selectivity occurs. This work was later extended to encompass and unify the behavior of several other hydrocarbon and oxygenate reactions (including methanol dehydration and homologation, alkene hydrogenation, dimerization, alkylation, isomerization, β-scission, and aldol and Prins condensation reactions) where rate constants measured on a series of zeolite frameworks exhibit maximum values when the container size is similar to that of the transition state. Increasing van der Waals contacts was shown to eventually destabilize the transition state energy, as enthalpic penalties to undergo accommodating distortions dominate. These same environments, and more importantly their implications on the egress of products via diffusion, have additional roles in dictating selectivities.

The learnings from Enrique Iglesia's research are evident in his publications and patents that encompass a robust approach to understanding molecular reactivity at surfaces, implemented without compromising relevance. They are also evident in his dedication to the many students and postdocs that he has mentored over the years. In addition to his approach to research in surface catalysis (the "method behind the madness"), inherited from his training with Michel Boudart, an important part of Enrique's research success derived from the choice of research problems he decided to address. He chose to study catalytic reactions and materials that were technologically relevant and often occurred in complex environments and under realistic conditions, which served as fertile areas where new and impactful insights could be made. This intense focus and constancy of purpose allowed Enrique to resist the temptations of chasing research topics that fell into and out of fashion with the vagaries of funding climates and economic forces and allowed him to become an exceptional leader in science and of scientists.

■ ASSOCIATED CONTENT

Supporting Information

The Supporting Information is available free of charge at https://pubs.acs.org/doi/10.1021/acscatal.4c02557.

Personal account of Enrique Iglesia's career at the Exxon Corporate Research Laboratories authored by Stuart L. Soled (PDF)

■ AUTHOR INFORMATION

Corresponding Authors

Rajamani Gounder — *Charles D. Davidson School of Chemical Engineering, Purdue University, West Lafayette, Indiana 47907, United States*; orcid.org/0000-0003-1347-534X; Email: rgounder@purdue.edu

Beata A. Kilos — *Core R&D, The Dow Chemical Company, Midland, Michigan 48674, United States*; Email: bakilos@dow.com

Authors

David G. Barton − *Core R&D, The Dow Chemical Company, Midland, Michigan 48674, United States*

Aditya Bhan − *Department of Chemical Engineering and Materials Science, University of Minnesota Twin Cities, Minneapolis, Minnesota 55455, United States;* orcid.org/0000-0002-6069-7626

Prashant Deshlahra − *Department of Chemical and Biological Engineering, Tufts University, Medford, Massachusetts 02155, United States;* orcid.org/0000-0002-1063-4379

David Hibbitts − *Department of Chemical Engineering, University of Florida, Gainesville, Florida 32611, United States;* orcid.org/0000-0001-8606-7000

Gina Noh − *Department of Chemical Engineering, The Pennsylvania State University, University Park, Pennsylvania 16802, United States*

Justin M. Notestein − *Chemical & Biological Engineering, Northwestern University, Evanston, Illinois 60208, United States;* orcid.org/0000-0003-1780-7356

Michele L. Sarazen − *Department of Chemical and Biological Engineering, Princeton University, Princeton, New Jersey 08544, United States*

Stuart L. Soled − *ExxonMobil Engineering and Technology Company, Annandale, New Jersey 08801, United States*

Complete contact information is available at:
https://pubs.acs.org/10.1021/acscatal.4c02557

Author Contributions

The manuscript was written through contributions of all authors.

Notes

The authors declare no competing financial interest.

ACKNOWLEDGMENTS

On behalf of all members of the Laboratory for the Science and Applications of Catalysis (LSAC), we acknowledge the professional and personal support and mentoring we have received from Enrique Iglesia during our time at LSAC and beyond. Along with the collaborators mentioned throughout this article, we also acknowledge Avelino Corma and Johannes Lercher, for their long-term friendship with Enrique and many LSAC group members. Finally, we thank all members of Enrique's biological family, including his wife Terry, his children Daniel, Christina, and Elizabeth, and his grandchildren Julian, Ava, Sebastian, Jacob, Grace and Sienna, for their support of Enrique and his research career that enabled him to be an exceptional mentor for his academic family.

REFERENCES

(1) Iglesia, E. A farewell (of sorts). *J. Catal.* **2010**, *269*, 254.

(2) Domush, H.: Oral history interview with Enrique Iglesia. *Science History Institute*, 2014; https://digital.sciencehistory.org/works/nd33tov (accessed May 29, 2024).

(3) Iglesia, E.; Boudart, M. Decomposition of of formic-acid and copper, nickel, and copper-nickel alloys. 1. Preparation and characterization of catalysts. *J. Catal.* **1983**, *81*, 204−213.

(4) Iglesia, E.; Boudart, M. Decomposition of of formic-acid and copper, nickel, and copper-nickel alloys. 2. Catalytic and temperature-programmed decomposition of formic-acid on Cu SiO_2, Cu Al_2O_3 and Cu powder. *J. Catal.* **1983**, *81*, 214−223.

(5) Iglesia, E.; Boudart, M. Decomposition of of formic-acid and copper, nickel, and copper-nickel alloys. 3. Catalytic decomposition on nickel and copper-nickel alloys. *J. Catal.* **1983**, *81*, 224−238.

(6) Iglesia, E.; Boudart, M. Decomposition of of formic-acid and copper, nickel, and copper-nickel alloys. 4. Temperature-programmed decomposition of bulk nickel formate and of formic-acid preadsorbed on nickel powder. *J. Catal.* **1984**, *88*, 325−332.

(7) Iglesia, E.; Boudart, M. Unimolecular and bimolecular formic-acid decomposition on copper. *J. Phys. Chem.* **1986**, *90*, 5272−5274.

(8) Iglesia, E.; Boudart, M. Structure-sensitivity and ensemble effects in reactions of strongly adsorbed intermediates - catalytic dehydrogenation and dehydration of formic-acid on nickel. *J. Phys. Chem.* **1991**, *95*, 7011−7016.

(9) Iglesia, E.; Soled, S. L.; Fiato, R. A. Fischer−Tropsch synthesis on cobalt and ruthenium - metal dispersion and support effects on reaction-rate and selectivity. *J. Catal.* **1992**, *137*, 212−224.

(10) Iglesia, E.; Soled, S. L.; Fiato, R. A.; Via, G. H. Bimetallic synergy in cobalt ruthenium Fischer−Tropsch synthesis catalysts. *J. Catal.* **1993**, *143*, 345−368.

(11) Iglesia, E.; Reyes, S. C.; Madon, R. J.; Soled, S. L. Selectivity control and catalyst design in the Fischer−Tropsch synthesis - sites, pellets, and reactors. *Adv. Catal.* **1993**, *39*, 221−302.

(12) Madon, R. J.; Iglesia, E. The importance of olefin readsorption and H_2/CO reactant ratio for hydrocarbon chain growth on ruthenium catalysts. *J. Catal.* **1993**, *139*, 576−590.

(13) Herbolzheimer, E.; Iglesia, E. Slurry bubble column (C-2391). U.S. Patent US5348982A, 1994.

(14) Iglesia, E.; Vroman, H.; Soled, S. L.; Baumgartner, J. E.; Fiato, R. A. Selective catalysts and their preparation for catalytic hydrocarbon synthesis. U.S. Patent US 5036032A, 1991.

(15) Soled, S. L.; Iglesia, E.; Fiato, R. A.; Ansell, G. B. Method for stabilizing titania supported cobalt catalyst and the catalyst for use in Fischer−Tropsch process. U.S. Patent 5169821, 1992.

(16) Fiato, R. A.; Iglesia, E.; Soled, S. L. Cobalt-ruthenium catalysts for Fischer−Tropsch synthesis. AU Patent AU595967B2, 1989.

(17) Iglesia, E.; Soled, S. L.; Fiato, R. A. SiO_2-promoted cobalt catalyst on a support of TiO_2 for converting synthesis gas to heavy hydrocarbons. U.S. Patent US4960801A, 1989.

(18) Reyes, S. C.; Iglesia, E.: Simulation Techniques for the Characterization of Structural and Transport Properties of Catalyst Pellets. In *Computer Aided Design of Catalysts*; Becker, R. E.; Pereira, C. J., Eds.; Marcel Dekker: New York, 1993; p 89.

(19) Madon, R. J.; Iglesia, E. Hydrogen and CO intrapellet diffusion effects in ruthenium-catalyzed hydrocarbon synthesis. *J. Catal.* **1994**, *149*, 428−437.

(20) Iglesia, E.; Soled, S. L.; Baumgartner, J. E.; Reyes, S. C. Synthesis and catalytic properties of eggshell cobalt catalysts for the Fischer-Trospch synthesis. *Top. Catal.* **1995**, *2*, 17−27.

(21) Iglesia, E.; Soled, S. L.; Baumgartner, J. E.; Reyes, S. C. Synthesis and catalytic properties of eggshell cobalt catalysts for the Fischer-Trospch synthesis. *J. Catal.* **1995**, *153*, 108−122.

(22) Krishnamoorthy, S.; Tu, M.; Ojeda, M. P.; Pinna, D.; Iglesia, E. An investigation of the effects of water on rate and selectivity for the Fischer−Tropsch synthesis on cobalt-based catalysts. *J. Catal.* **2002**, *211*, 422−433.

(23) Hibbitts, D. D.; Loveless, B. T.; Neurock, M.; Iglesia, E. Mechanistic Role of Water on the Rate and Selectivity of Fischer−Tropsch Synthesis on Ruthenium Catalysts. *Angew. Chem., Int. Ed.* **2013**, *52*, 12273−12278.

(24) Soled, S. L.; Iglesia, E.; Miseo, S.; Derites, B. A.; Fiato, R. A. Selective synthesis of alpha-olefins on Fe-Zn Fischer−Tropsch catalysts. *Top. Catal.* **1995**, *2*, 193−205.

(25) Ojeda, M.; Li, A. W.; Nabar, R.; Nilekar, A. U.; Mavrikakis, M.; Iglesia, E. Kinetically Relevant Steps and H_2/D_2 Isotope Effects in Fischer−Tropsch Synthesis on Fe and Co Catalysts. *J. Phys. Chem. C* **2010**, *114*, 19761−19770.

(26) Ojeda, M.; Nabar, R.; Nilekar, A. U.; Ishikawa, A.; Mavrikakis, M.; Iglesia, E. CO activation pathways and the mechanism of Fischer−Tropsch synthesis. *J. Catal.* **2010**, *272*, 287−297.

(27) Reyes, S. C.; Duran, M. A.; Iglesia, E. Structural Models of Porous Networks and the Optimization of Catalytic Rates and Selectivity. *Proc. XIII Iberoamerican Symp. Catal.* **1993**, *2*, 705−710.

(28) Iglesia, E.; Baumgartner, J. E.; Ribeiro, F. H.; Boudart, M. Bifunctional reactions of alkanes on tungsten carbides modified by chemisorbed oxygen. *J. Catal.* **1991**, *131*, 523−544.

(29) Reyes, S. C.; Iglesia, E.; Kelkar, C. P. Kinetic-transport models of bimodal reaction sequences. 1. Homogeneous and heterogeneous pathways in oxidative coupling of methane. *Chem. Eng. Sci.* **1993**, *48*, 2643−2661.

(30) Iglesia, E.; Barton, D. G.; Biscardi, J. A.; Gines, M. J. L.; Soled, S. L. Bifunctional pathways in catalysis by solid acids and bases. *Catal. Today* **1997**, *38*, 339−360.

(31) Barton, D. G.; Soled, S. L.; Iglesia, E. Solid acid catalysts based on supported tungsten oxides. *Top. Catal.* **1998**, *6*, 87−99.

(32) Baertsch, C. D.; Komala, K. T.; Chua, Y. H.; Iglesia, E. Genesis of Bronsted acid sites during dehydration of 2-butanol on tungsten oxide catalysts. *J. Catal.* **2002**, *205*, 44−57.

(33) Baertsch, C. D.; Soled, S. L.; Iglesia, E. Isotopic and chemical titration of acid sites in tungsten oxide domains supported on zirconia. *J. Phys. Chem. B* **2001**, *105*, 1320−1330.

(34) Iglesia, E.; Barton, D. G.; Soled, S. L.; Miseo, S.; Baumgartner, J. E.; Gates, W. E.; Fuentes, G. A.; Meitzner, G. D. Selective isomerization of alkanes on supported tungsten oxide acids. *Studies in Surface Science and Catalysis* **1996**, *101*, 533−542.

(35) Wang, L. S.; Tao, L. X.; Xie, M. S.; Xu, G. F.; Huang, J. S.; Xu, Y. D. Dehydrogenation and aromatization of methane under nonoxidizing conditions. *Catal. Lett.* **1993**, *21*, 35−41.

(36) Borry, R. W.; Kim, Y. H.; Huffsmith, A.; Reimer, J. A.; Iglesia, E. Structure and density of Mo and acid sites in Mo-exchanged H-ZSM5 catalysts for nonoxidative methane conversion. *J. Phys. Chem. B* **1999**, *103*, 5787−5796.

(37) Kim, Y. H.; Borry, R. W.; Iglesia, E. Genesis of methane activation sites in Mo-exchanged H-ZSM-5 catalysts. *Microporous Mesoporous Mater.* **2000**, *35−36*, 495−509.

(38) Ding, W. P.; Li, S. Z.; Meitzner, G. D.; Iglesia, E. Methane conversion to aromatics on Mo/H-ZSM5: Structure of molybdenum species in working catalysts. *J. Phys. Chem. B* **2001**, *105*, 506−513.

(39) Ding, W. P.; Meitzner, G. D.; Marler, D. O.; Iglesia, E. Synthesis, structural characterization, and catalytic properties of tungsten-exchanged H-ZSM5. *J. Phys. Chem. B* **2001**, *105*, 3928−3936.

(40) Liu, Z.; Nutt, M. A.; Iglesia, E. The effects of CO_2, CO and H_2 co-reactants on methane reactions catalyzed by Mo/H-ZSM-5. *Catal. Lett.* **2002**, *81*, 271−279.

(41) Lacheen, H. S.; Iglesia, E. Stability, structure, and oxidation state of Mo/H-ZSM-5 catalysts during reactions of CH_4 and CH_4-CO_2 mixtures. *J. Catal.* **2005**, *230*, 173−185.

(42) Lacheen, H. S.; Iglesia, E. Isothermal activation of $Mo_2O_5^{2+}$-ZSM-5 precursors during methane reactions:: effects of reaction products on structural evolution and catalytic properties. *Phys. Chem. Chem. Phys.* **2005**, *7*, 538−547.

(43) Lacheen, H. S.; Cordeiro, P. J.; Iglesia, E. Structure and catalytic function of Re-oxo species grafted onto H-MFI zeolite by sublimation of Re_2O_7. *J. Am. Chem. Soc.* **2006**, *128*, 15082−15083.

(44) Lacheen, H. S.; Iglesia, E. Synthesis, structure, and catalytic reactivity of isolated V^{5+}-oxo species prepared by sublimation of $VOCl_3$ onto H-ZSM5. *J. Phys. Chem. B* **2006**, *110*, 5462−5472.

(45) Rostrupnielsen, J. R.; Hansen, J. H. B. CO_2-reforming of methane over transition-metals. *J. Catal.* **1993**, *144*, 38−49.

(46) Wei, J. M.; Iglesia, E. Isotopic and kinetic assessment of the mechanism of methane reforming and decomposition reactions on supported iridium catalysts. *Phys. Chem. Chem. Phys.* **2004**, *6*, 3754−3759.

(47) Wei, J. M.; Iglesia, E. Structural requirements and reaction pathways in methane activation and chemical conversion catalyzed by rhodium. *J. Catal.* **2004**, *225*, 116−127.

(48) Wei, J. M.; Iglesia, E. Isotopic and kinetic assessment of the mechanism of reactions of CH4 with CO2 or H2O to form synthesis gas and carbon on nickel catalysts. *J. Catal.* **2004**, *224*, 370−383.

(49) Wei, J. M.; Iglesia, E. Reaction pathways and site requirements for the activation and chemical conversion of methane on Ru-based catalysts. *J. Phys. Chem. B* **2004**, *108*, 7253−7262.

(50) Wei, J. M.; Iglesia, E. Mechanism and site requirements for activation and chemical conversion of methane on supported Pt clusters and turnover rate comparisons among noble metals. *J. Phys. Chem. B* **2004**, *108*, 4094−4103.

(51) Wei, J. M.; Iglesia, E. Structural and mechanistic requirements for methane activation and chemical conversion on supported iridium clusters. *Angew. Chem., Int. Ed.* **2004**, *43*, 3685−3688.

(52) Chin, Y. H.; Buda, C.; Neurock, M.; Iglesia, E. Reactivity of Chemisorbed Oxygen Atoms and Their Catalytic Consequences during CH_4-O_2 Catalysis on Supported Pt Clusters. *J. Am. Chem. Soc.* **2011**, *133*, 15958−15978.

(53) Chin, Y. H.; Buda, C.; Neurock, M.; Iglesia, E. Selectivity of chemisorbed oxygen in C-H bond activation and CO oxidation and kinetic consequences for CH_4-O_2 catalysis on Pt and Rh clusters. *J. Catal.* **2011**, *283*, 10−24.

(54) Chin, Y. H.; Buda, C.; Neurock, M.; Iglesia, E. Consequences of Metal-Oxide Interconversion for C-H Bond Activation during CH4 Reactions on Pd Catalysts. *J. Am. Chem. Soc.* **2013**, *135*, 15425−15442.

(55) Chin, Y. H.; García-Diéguez, M.; Iglesia, E. Dynamics and Thermodynamics of Pd-PdO Phase Transitions: Effects of Pd Cluster Size and Kinetic Implications for Catalytic Methane Combustion. *J. Phys. Chem. C* **2016**, *120*, 1446−1460.

(56) Chin, Y. H.; Iglesia, E. Elementary Steps, the Role of Chemisorbed Oxygen, and the Effects of Cluster Size in Catalytic CH_4-O_2 Reactions on Palladium. *J. Phys. Chem. C* **2011**, *115*, 17845−17855.

(57) Weiss, B. M.; Iglesia, E. NO Oxidation Catalysis on Pt Clusters: Elementary Steps, Structural Requirements, and Synergistic Effects of NO2 Adsorption Sites. *J. Phys. Chem. C* **2009**, *113*, 13331−13340.

(58) Weiss, B. M.; Iglesia, E. Mechanism and site requirements for NO oxidation on Pd catalysts. *J. Catal.* **2010**, *272*, 74−81.

(59) Takanabe, K.; Iglesia, E. Rate and selectivity enhancements mediated by OH radicals in the oxidative coupling of methane catalyzed by $Mn/Na_2WO_4/SiO_2$. *Angew. Chem., Int. Ed.* **2008**, *47*, 7689−7693.

(60) Takanabe, K.; Iglesia, E. Mechanistic Aspects and Reaction Pathways for Oxidative Coupling of Methane on $Mn/Na_2WO_4/SiO_2$ Catalysts. *J. Phys. Chem. C* **2009**, *113*, 10131−10145.

(61) Flaherty, D. W.; Hibbitts, D. D.; Gürbüz, E. I.; Iglesia, E. Theoretical and kinetic assessment of the mechanism of ethane hydrogenolysis on metal surfaces saturated with chemisorbed hydrogen. *J. Catal.* **2014**, *311*, 350−356.

(62) Flaherty, D. W.; Hibbitts, D. D.; Iglesia, E. Metal-Catalyzed C-C Bond Cleavage in Alkanes: Effects of Methyl Substitution on Transition-State Structures and Stability. *J. Am. Chem. Soc.* **2014**, *136*, 9664−9676.

(63) Flaherty, D. W.; Iglesia, E. Transition-State Enthalpy and Entropy Effects on Reactivity and Selectivity in Hydrogenolysis of *n*-Alkanes. *J. Am. Chem. Soc.* **2013**, *135*, 18586−18599.

(64) Flaherty, D. W.; Uzun, A.; Iglesia, E. Catalytic Ring Opening of Cycloalkanes on Ir Clusters: Alkyl Substitution Effects on the Structure and Stability of C-C Bond Cleavage Transition States. *J. Phys. Chem. C* **2015**, *119*, 2597−2613.

(65) Hibbitts, D. D.; Flaherty, D. W.; Iglesia, E. Effects of Chain Length on the Mechanism and Rates of Metal-Catalyzed Hydrogenolysis of *n*-Alkanes. *J. Phys. Chem. C* **2016**, *120*, 8125−8138.

(66) Hibbitts, D. D.; Flaherty, D. W.; Iglesia, E. Role of Branching on the Rate and Mechanism of C-C Cleavage in Alkanes on Metal Surfaces. *ACS Catal.* **2016**, *6*, 469−482.

(67) Gürbüz, E. I.; Hibbitts, D. D.; Iglesia, E. Kinetic and Mechanistic Assessment of Alkanol/Alkanal Decarbonylation and Deoxygenation Pathways on Metal Catalysts. *J. Am. Chem. Soc.* **2015**, *137*, 11984−11995.

(68) Da Costa, P.; Modén, B.; Meitzner, G. D.; Lee, D. K.; Iglesia, E. Spectroscopic and chemical characterization of active and inactive Cu

species in NO decomposition catalysts based on Cu-ZSM5. *Phys. Chem. Chem. Phys.* **2002**, *4*, 4590−4601.

(69) Modén, B.; Da Costa, P.; Lee, D. K.; Iglesia, E. Transient studies of oxygen removal pathways and catalytic redox cycles during NO decomposition on Cu-ZSM5. *J. Phys. Chem. B* **2002**, *106*, 9633−9641.

(70) Modén, B.; Da Costa, P.; Fonfé, B.; Lee, D. K.; Iglesia, E. Kinetics and mechanism of steady-state catalytic NO decomposition reactions on Cu-ZSM5. *J. Catal.* **2002**, *209*, 75−86.

(71) Weiss, B. M.; Caldwell, K. B.; Iglesia, E. NOx Interactions with Dispersed BaO: Adsorption Kinetics, Chemisorbed Species, and Effects of Oxidation Catalyst Sites. *J. Phys. Chem. C* **2011**, *115*, 6561−6570.

(72) Weiss, B. M.; Artioli, N.; Iglesia, E. Catalytic NO Oxidation Pathways and Redox Cycles on Dispersed Oxides of Rhodium and Cobalt. *ChemCatChem.* **2012**, *4*, 1397−1404.

(73) Iwasaki, M.; Iglesia, E. Mechanistic assessments of NO oxidation turnover rates and active site densities on WO_3-promoted CeO_2 catalysts. *J. Catal.* **2016**, *342*, 84−97.

(74) Artioli, N.; Lobo, R. F.; Iglesia, E. Catalysis by Confinement: Enthalpic Stabilization of NO Oxidation Transition States by Micropororous and Mesoporous Siliceous Materials. *J. Phys. Chem. C* **2013**, *117*, 20666−20674.

(75) Maestri, M.; Iglesia, E. First-principles theoretical assessment of catalysis by confinement: NO-O_2 reactions within voids of molecular dimensions in siliceous crystalline frameworks. *Phys. Chem. Chem. Phys.* **2018**, *20*, 15725−15735.

(76) Hibbitts, D. D.; Jiménez, R.; Yoshimura, M.; Weiss, B.; Iglesia, E. Catalytic NO activation and NO-H_2 reaction pathways. *J. Catal.* **2014**, *319*, 95−109.

(77) Hu, W. S.; Noh, G.; Iglesia, E. Consequences of metal-acid site proximity for alkane isomerization and beta-scission mediated by bifunctional catalytic cascades. *J. Catal.* **2023**, *425*, 125−142.

(78) Fischer, A. F.; Iglesia, E. The nature of ″hydrogen spillover″: Site proximity effects and gaseous intermediates in hydrogenation reactions mediated by inhibitor-scavenging mechanisms. *J. Catal.* **2023**, *420*, 68−88.

(79) Argyle, M. D.; Chen, K. D.; Iglesia, E.; Bell, A. T. In situ UV-visible spectroscopic measurements of kinetic parameters and active sites for catalytic oxidation of alkanes on vanadium oxides. *J. Phys. Chem. B* **2005**, *109*, 2414−2420.

(80) Zalc, J. M.; Green, W. H.; Iglesia, E. NO_x-mediated homogeneous pathways for the synthesis of formaldehyde from CH_4-O_2 mixtures. *Ind. Eng. Chem. Res.* **2006**, *45*, 2677−2688.

(81) Chen, K. D.; Xie, S. B.; Bell, A. T.; Iglesia, E. Alkali effects on molybdenum oxide catalysts for the oxidative dehydrogenation of propane. *J. Catal.* **2000**, *195*, 244−252.

(82) Xie, S. B.; Chen, K. D.; Bell, A. T.; Iglesia, E. Structural characterization of molybdenum oxide supported on zirconia. *J. Phys. Chem. B* **2000**, *104*, 10059−10068.

(83) Chen, K. D.; Xie, S. B.; Iglesia, E.; Bell, A. T. Structure and properties of zirconia-supported molybdenum oxide catalysts for oxidative dehydrogenation of propane. *J. Catal.* **2000**, *189*, 421−430.

(84) Chen, K. D.; Iglesia, E.; Bell, A. T. Isotopic tracer studies of reaction pathways for propane oxidative dehydrogenation on molybdenum oxide catalysts. *J. Phys. Chem. B* **2001**, *105*, 646−653.

(85) Chen, K.; Xie, S.; Bell, A. T.; Iglesia, E. Structure and properties of oxidative dehydrogenation catalysts based on MoO_3/Al_2O_3. *J. Catal.* **2001**, *198*, 232−242.

(86) Liu, H. C.; Cheung, P.; Iglesia, E. Structure and support effects on the selective oxidation of dimethyl ether to formaldehyde catalyzed by MoO_x domains. *J. Catal.* **2003**, *217*, 222−232.

(87) Liu, H. C.; Cheung, P.; Iglesia, E. Zirconia-supported MoO_x, catalysts for the selective oxidation of dimethyl ether to formaldehyde:: Structure, redox properties, and reaction pathways. *J. Phys. Chem. B* **2003**, *107*, 4118−4127.

(88) Liu, H. C.; Cheung, P.; Iglesia, E. Effects of Al_2O_3 support modifications on MoO_x and VO_x catalysts for dimethyl ether oxidation to formaldehyde. *Phys. Chem. Chem. Phys.* **2003**, *5*, 3795−3800.

(89) Cheung, P.; Liu, H. C.; Iglesia, E. Kinetics and mechanism of dimethyl ether oxidation to formaldehyde on supported molybdenum oxide domains. *J. Phys. Chem. B* **2004**, *108*, 18650−18658.

(90) Khodakov, A.; Yang, J.; Su, S.; Iglesia, E.; Bell, A. T. Structure and properties of vanadium oxide zirconia catalysts for propane oxidative dehydrogenation. *J. Catal.* **1998**, *177*, 343−351.

(91) Khodakov, A.; Olthof, B.; Bell, A. T.; Iglesia, E. Structure and catalytic properties of supported vanadium oxides: Support effects on oxidative dehydrogenation reactions. *J. Catal.* **1999**, *181*, 205−216.

(92) Chen, K. D.; Khodakov, A.; Yang, J.; Bell, A. T.; Iglesia, E. Isotopic tracer and kinetic studies of oxidative dehydrogenation pathways on vanadium oxide catalysts. *J. Catal.* **1999**, *186*, 325−333.

(93) Xie, S. B.; Iglesia, E.; Bell, A. T. Effects of hydration and dehydration on the structure of silica-supported vanadia species. *Langmuir* **2000**, *16*, 7162−7167.

(94) Olthof, B.; Khodakov, A.; Bell, A. T.; Iglesia, E. Effects of support composition and pretreatment conditions on the structure of vanadia dispersed on SiO_2, Al_2O_3, TiO_2, ZrO_2, and HfO_2. *J. Phys. Chem. B* **2000**, *104*, 1516−1528.

(95) Chen, K. D.; Iglesia, E.; Bell, A. T. Kinetic isotopic effects in oxidative dehydrogenation of propane on vanadium oxide catalysts. *J. Catal.* **2000**, *192*, 197−203.

(96) Argyle, M. D.; Chen, K. D.; Bell, A. T.; Iglesia, E. Ethane oxidative dehydrogenation pathways on vanadium oxide catalysts. *J. Phys. Chem. B* **2002**, *106*, 5421−5427.

(97) Argyle, M. D.; Chen, K. D.; Bell, A. T.; Iglesia, E. Effect of catalyst structure on oxidative dehydrogenation of ethane and propane on alumina-supported vanadia. *J. Catal.* **2002**, *208*, 139−149.

(98) Argyle, M. D.; Chen, K. D.; Resini, C.; Krebs, C.; Bell, A. T.; Iglesia, E. Extent of reduction of vanadium oxides during catalytic oxidation of alkanes measured by in-situ UV-visible spectroscopy. *J. Phys. Chem. B* **2004**, *108*, 2345−2353.

(99) Dai, H. X.; Bell, A. T.; Iglesia, E. Effects of molybdena on the catalytic properties of vanadia domains supported on alumina for oxidative dehydrogenation of propane. *J. Catal.* **2004**, *221*, 491−499.

(100) Yang, S. W.; Iglesia, E.; Bell, A. T. Oxidative dehydrogenation of propane over $V_2O_5/MoO_3/Al_2O_3$ and $V_2O_5/Cr_2O_3/Al_2O_3$: Structural characterization and catalytic function. *J. Phys. Chem. B* **2005**, *109*, 8987−9000.

(101) Kilos, B.; Bell, A. T.; Iglesia, E. Mechanism and Site Requirements for Ethanol Oxidation on Vanadium Oxide Domains. *J. Phys. Chem. C* **2009**, *113*, 2830−2836.

(102) Li, X. B.; Iglesia, E. Synergistic effects of TiO_2 and palladium-based cocatalysts on the selective oxidation of ethene to acetic acid on Mo-V-Nb oxide domains. *Angew. Chem., Int. Ed.* **2007**, *46*, 8649−8652.

(103) Li, X. B.; Iglesia, E. Selective catalytic oxidation of ethanol to acetic acid on dispersed Mo-V-Nb mixed oxides. *Chem.—Eur. J.* **2007**, *13*, 9324−9330.

(104) Li, X. B.; Iglesia, E. Kinetics and mechanism of ethane oxidation to acetic acid on catalysts based on Mo-V-Nb oxides. *J. Phys. Chem. C* **2008**, *112*, 15001−15008.

(105) Li, X. B.; Iglesia, E. Support and promoter effects in the selective oxidation of ethane to acetic acid catalyzed by Mo-V-Nb oxides. *Appl. Catal., A* **2008**, *334*, 339−347.

(106) Waku, T.; Argyle, M. D.; Bell, A. T.; Iglesia, E. Effects of O_2 concentration on the rate and selectivity in oxidative dehydrogenation of ethane catalyzed by vanadium oxide: Implications for O_2 staging and membrane reactors. *Ind. Eng. Chem. Res.* **2003**, *42*, 5462−5466.

(107) Rulkens, R.; Male, J. L.; Terry, K. W.; Olthof, B.; Khodakov, A.; Bell, A. T.; Iglesia, E.; Tilley, T. D. Vanadyl *tert*-butoxy orthosilicate, OV OSi(O^{t}Bu)$_3$ $_3$: A model for isolated vanadlyl sites on silica and a precursor to vanadia-silica xerogels. *Chem. Mater.* **1999**, *11*, 2966−2973.

(108) Notestein, J. M.; Andrini, L. R.; Kalchenko, V. I.; Requejo, F. G.; Katz, A.; Iglesia, E. Structural assessment and catalytic

consequences of the oxygen coordination environment in grafted Ti-calixarenes. *J. Am. Chem. Soc.* **2007**, *129*, 1122−1131.

(109) Liu, H. C.; Iglesia, E. Effects of support on bifunctional methanol oxidation pathways catalyzed by polyoxometallate Keggin clusters. *J. Catal.* **2004**, *223*, 161−169.

(110) Macht, J.; Iglesia, E. Structure and function of oxide nanostructures: catalytic consequences of size and composition. *Phys. Chem. Chem. Phys.* **2008**, *10*, 5331−5343.

(111) Kwon, S.; Deshlahra, P.; Iglesia, E. Dioxygen activation routes in Mars-van Krevelen redox cycles catalyzed by metal oxides. *J. Catal.* **2018**, *364*, 228−247.

(112) Kwon, S.; Deshlahra, P.; Iglesia, E. Reactivity and selectivity descriptors of dioxygen activation routes on metal oxides. *J. Catal.* **2019**, *377*, 692−710.

(113) Chen, K. D.; Bell, A. T.; Iglesia, E. The relationship between the electronic and redox properties of dispersed metal oxides and their turnover rates in oxidative dehydrogenation reactions. *J. Catal.* **2002**, *209*, 35−42.

(114) Zboray, M.; Bell, A. T.; Iglesia, E. Role of C-H Bond Strength in the Rate and Selectivity of Oxidative Dehydrogenation of Alkanes. *J. Phys. Chem. C* **2009**, *113*, 12380−12386.

(115) Deshlahra, P.; Iglesia, E. Reactivity and Selectivity Descriptors for the Activation of C-H Bonds in Hydrocarbons and Oxygenates on Metal Oxides. *J. Phys. Chem. C* **2016**, *120*, 16741−16760.

(116) Modén, B.; Oliviero, L.; Dakka, J.; Santiesteban, J. G.; Iglesia, E. Structural and functional characterization of redox Mn and Co sites in AlPO materials and their role in alkane oxidation catalysis. *J. Phys. Chem. B* **2004**, *108*, 5552−5563.

(117) Modén, B.; Zhan, B. Z.; Dakka, J.; Santiesteban, J. G.; Iglesia, E. Kinetics and mechanism of cyclohexane oxidation on MnAPO-5 catalysts. *J. Catal.* **2006**, *239*, 390−401.

(118) Modén, B.; Zhan, B. Z.; Dakka, J.; Santiesteban, J. G.; Iglesia, E. Reactant selectivity and regiospecificity in the catalytic oxidation of alkanes on metal-substituted aluminophosphates. *J. Phys. Chem. C* **2007**, *111*, 1402−1411.

(119) Zhan, B. Z.; Modén, B.; Dakka, J.; Santiesteban, J. G.; Iglesia, E. Catalytic oxidation of *n*-hexane on Mn-exchanged zeolites:: Turnover rates, regioselectivity, and spatial constraints. *J. Catal.* **2007**, *245*, 316−325.

(120) Thomas, J. M.; Raja, R.; Sankar, G.; Bell, R. G. Molecular-sieve catalysts for the selective oxidation of linear alkanes by molecular oxygen. *Nature* **1999**, *398*, 227−230.

(121) Iglesia, E.; Ribeiro, F. H.; Boudart, M.; Baumgartner, J. E. Tungsten carbides modified by chemisorbed oxygen - a new class of bifunctional catalysts. *Catal. Today* **1992**, *15*, 455−458.

(122) Iglesia, E.; Ribeiro, F. H.; Boudart, M.; Baumgartner, J. E. Synthesis, characterization, and caatalytic properties of clean and oxygen-modified tungsten carbides. *Catal. Today* **1992**, *15*, 307−337.

(123) Ribeiro, F. H.; Betta, R. A. D.; Boudart, M.; Baumgartner, J.; Iglesia, E. Reactions of neopentane, methylcyclogexane, and 3,3-dimethylpentane on tungsten carbides - the effect of surface oxygen on reaction pathways. *J. Catal.* **1991**, *130*, 86−105.

(124) Ribeiro, F. H.; Boudart, M.; Dallabetta, R. A.; Iglesia, E. Catalytic reactions of normal-alkanes on beta-W_2C and WC - the effect of surface oxygen on reaction pathways. *J. Catal.* **1991**, *130*, 498−513.

(125) Iglesia, E.; Soled, S. L.; Kramer, G. M. Isomerization of alkanes on sulfated zirconia - promotion by Pt and by adamantyl hydride transfer species. *J. Catal.* **1993**, *144*, 238−253.

(126) Soled, S. L.; Iglesia, E.; Kramer, G. M. Modification of isomerization activity and selectivity over sulfacted zirconia catalysts; Elsevier Science Publ B V: Amsterdam, 1994; Vol. *90*.

(127) Hilmen, A. M.; Xu, M. T.; Gines, M. J. L.; Iglesia, E. Synthesis of higher alcohols on copper catalysts supported on alkali-promoted basic oxides. *Appl. Catal., A* **1998**, *169*, 355−372.

(128) Xu, M. T.; Iglesia, E. Carbon-carbon bond formation pathways in CO hydrogenation to higher alcohols. *J. Catal.* **1999**, *188*, 125−131.

(129) Wang, S.; Goulas, K.; Iglesia, E. Condensation and esterification reactions of alkanals, alkanones, and alkanols on TiO_2: Elementary steps, site requirements, and synergistic effects of bifunctional strategies. *J. Catal.* **2016**, *340*, 302−320.

(130) Wang, S.; Iglesia, E. Substituent Effects and Molecular Descriptors of Reactivity in Condensation and Esterification Reactions of Oxygenates on Acid-Base Pairs at TiO_2 and ZrO_2 Surfaces. *J. Phys. Chem. C* **2016**, *120*, 21589−21616.

(131) Wang, S.; Iglesia, E. Entropy-Driven High Reactivity of Formaldehyde in Nucleophilic Attack by Enolates on Oxide Surfaces. *J. Am. Chem. Soc.* **2018**, *140*, 775−782.

(132) Kwon, S.; Lin, T. C.; Iglesia, E. Formic Acid Dehydration Rates and Elementary Steps on Lewis Acid-Base Site Pairs at Anatase and Rutile TiO_2 Surfaces. *J. Phys. Chem. C* **2020**, *124*, 20161−20174.

(133) Kwon, S.; Lin, T. C.; Iglesia, E. Elementary steps and site requirements in formic acid dehydration reactions on anatase and rutile TiO_2 surfaces. *J. Catal.* **2020**, *383*, 60−76.

(134) Barton, D. G.; Shtein, M.; Wilson, R. D.; Soled, S. L.; Iglesia, E. Structure and electronic properties of solid acids based on tungsten oxide nanostructures. *J. Phys. Chem. B* **1999**, *103*, 630−640.

(135) Wilson, R. D.; Barton, D. G.; Baertsch, C. D.; Iglesia, E. Reaction and deactivation pathways in xylene isomerization on zirconia modified by tungsten oxide. *J. Catal.* **2000**, *194*, 175−187.

(136) Macht, J.; Baertsch, C. D.; May-Lozano, M.; Soled, S. L.; Wang, Y.; Iglesia, E. Support effects on Bronsted acid site densities and alcohol dehydration turnover rates on tungsten oxide domains. *J. Catal.* **2004**, *227*, 479−491.

(137) Deshlahra, P.; Carr, R. T.; Chai, S. H.; Iglesia, E. Mechanistic Details and Reactivity Descriptors in Oxidation and Acid Catalysis of Methanol. *ACS Catal.* **2015**, *5*, 666−682.

(138) Liu, H. C.; Bayat, N.; Iglesia, E. Site titration with organic bases during catalysis: Selectivity modifier and structural probe in methanol oxidation on Keggin clusters. *Angew. Chem., Int. Ed.* **2003**, *42*, 5072−5075.

(139) Liu, H. C.; Iglesia, E. Selective one-step synthesis of dimethoxymethane via methanol or dimethyl ether oxidation on $H_{3+n}V_nMO_{12-n}PO_{40}$ Keggin structures. *J. Phys. Chem. B* **2003**, *107*, 10840−10847.

(140) Macht, J.; Janik, M. J.; Neurock, M.; Iglesia, E. Catalytic consequences of composition in polyoxometalate clusters with keggin structure. *Angew. Chem., Int. Ed.* **2007**, *46*, 7864−7868.

(141) Macht, J.; Janik, M. J.; Neurock, M.; Iglesia, E. Mechanistic consequences of composition in acid catalysis by polyoxometalate Keggin clusters. *J. Am. Chem. Soc.* **2008**, *130*, 10369−10379.

(142) Janik, M. J.; Macht, J.; Iglesia, E.; Neurock, M. Correlating Acid Properties and Catalytic Function: A First-Principles Analysis of Alcohol Dehydration Pathways on Polyoxometalates. *J. Phys. Chem. C* **2009**, *113*, 1872−1885.

(143) Carr, R. T.; Neurock, M.; Iglesia, E. Catalytic consequences of acid strength in the conversion of methanol to dimethyl ether. *J. Catal.* **2011**, *278*, 78−93.

(144) Macht, J.; Carr, R. T.; Iglesia, E. Functional assessment of the strength of solid acid catalysts. *J. Catal.* **2009**, *264*, 54−66.

(145) Macht, J.; Carr, R. T.; Iglesia, E. Consequences of Acid Strength for Isomerization and Elimination Catalysis on Solid Acids. *J. Am. Chem. Soc.* **2009**, *131*, 6554−6565.

(146) Knaeble, W.; Carr, R. T.; Iglesia, E. Mechanistic interpretation of the effects of acid strength on alkane isomerization turnover rates and selectivity. *J. Catal.* **2014**, *319*, 283−296.

(147) Knaeble, W.; Iglesia, E. Acid strength and metal-acid proximity effects on methylcyclohexane ring contraction turnover rates and selectivities. *J. Catal.* **2016**, *344*, 817−830.

(148) Deshlahra, P.; Iglesia, E. Reactivity descriptors in acid catalysis: acid strength, proton affinity and host-guest interactions. *Chem. Commun.* **2020**, *56*, 7371−7398.

(149) Wang, S.; Iglesia, E. Mechanism of Isobutanal-Isobutene Prins Condensation Reactions on Solid Bronsted Acids. *ACS Catal.* **2016**, *6*, 7664−7684.

(150) Deshlahra, P.; Carr, R. T.; Iglesia, E. Ionic and Covalent Stabilization of Intermediates and Transition States in Catalysis by Solid Acids. *J. Am. Chem. Soc.* **2014**, *136*, 15229−15247.

(151) Deshlahra, P.; Iglesia, E. Toward More Complete Descriptors of Reactivity in Catalysis by Solid Acids. *ACS Catal.* **2016**, *6*, 5386−5392.

(152) Jones, A. J.; Iglesia, E. The Strength of Bronsted Acid Sites in Microporous Aluminosilicates. *ACS Catal.* **2015**, *5*, 5741−5755.

(153) Jones, A. J.; Carr, R. T.; Zones, S. I.; Iglesia, E. Acid strength and solvation in catalysis by MFI zeolites and effects of the identity, concentration and location of framework heteroatoms. *J. Catal.* **2014**, *312*, 58−68.

(154) Sarazen, M. L.; Doskocil, E.; Iglesia, E. Catalysis on solid acids: Mechanism and catalyst descriptors in oligomerization reactions of light alkenes. *J. Catal.* **2016**, *344*, 553−569.

(155) Noh, G.; Zones, S. I.; Iglesia, E. Consequences of Acid Strength and Diffusional Constraints for Alkane Isomerization and β-Scission Turnover Rates and Selectivities on Bifunctional Metal-Acid Catalysts. *J. Phys. Chem. C* **2018**, *122*, 25475−25497.

(156) Herrmann, S.; Iglesia, E. Elementary steps in acetone condensation reactions catalyzed by aluminosilicates with diverse void structures. *J. Catal.* **2017**, *346*, 134−153.

(157) Hermann, S. T.: Elementary Steps in Aldol Condensation on Solid Acids: Insights from Experiments and Theory. Ph.D. Thesis, University of California, Berkeley, 2016.

(158) Bhan, A.; Allian, A. D.; Sunley, G. J.; Law, D. J.; Iglesia, E. Specificity of sites within eight-membered ring zeolite channels for carbonylation of methyls to acetyls. *J. Am. Chem. Soc.* **2007**, *129*, 4919−4924.

(159) Cheung, P.; Bhan, A.; Sunley, G. J.; Law, D. J.; Iglesia, E. Site requirements and elementary steps in dimethyl ether carbonylation catalyzed by acidic zeolites. *J. Catal.* **2007**, *245*, 110−123.

(160) Neurock, M. Engineering Molecular Transformations for Sustainable Energy Conversion. *Ind. Eng. Chem. Res.* **2010**, *49*, 10183−10199.

(161) Gounder, R.; Iglesia, E. Catalytic Consequences of Spatial Constraints and Acid Site Location for Monomolecular Alkane Activation on Zeolites. *J. Am. Chem. Soc.* **2009**, *131*, 1958−1971.

(162) Gounder, R.; Iglesia, E. Effects of Partial Confinement on the Specificity of Monomolecular Alkane Reactions for Acid Sites in Side Pockets of Mordenite. *Angew. Chem., Int. Ed.* **2010**, *49*, 808−811.

(163) Gounder, R.; Iglesia, E. Catalytic Alkylation Routes via Carbonium-Ion-Like Transition States on Acidic Zeolites. *ChemCatChem.* **2011**, *3*, 1134−1138.

(164) Gounder, R.; Iglesia, E. Catalytic hydrogenation of alkenes on acidic zeolites: Mechanistic connections to monomolecular alkane dehydrogenation reactions. *J. Catal.* **2011**, *277*, 36−45.

(165) Gounder, R.; Iglesia, E. The Roles of Entropy and Enthalpy in Stabilizing Ion-Pairs at Transition States in Zeolite Acid Catalysis. *Acc. Chem. Res.* **2012**, *45*, 229−238.

(166) Gounder, R.; Iglesia, E. The catalytic diversity of zeolites: confinement and solvation effects within voids of molecular dimensions. *Chem. Commun.* **2013**, *49*, 3491−3509.

(167) Gounder, R.; Jones, A. J.; Carr, R. T.; Iglesia, E. Solvation and acid strength effects on catalysis by faujasite zeolites. *J. Catal.* **2012**, *286*, 214−223.

(168) Kester, P. M.; Iglesia, E.; Gounder, R. Parallel Alkane Dehydrogenation Routes on Bronsted Acid and Reaction-Derived Carbonaceous Active Sites in Zeolites. *J. Phys. Chem. C* **2020**, *124*, 15839−15855.

(169) Wang, S.; Agirrezabal-Telleria, I.; Bhan, A.; Simonetti, D.; Takanabe, K.; Iglesia, E. Catalytic routes to fuels from C_1 and oxygenate molecules. *Faraday Discuss.* **2017**, *197*, 9−39.

(170) Hazari, N.; Iglesia, E.; Labinger, J. A.; Simonetti, D. A. Selective Homogeneous and Heterogeneous Catalytic Conversion of Methanol/Dimethyl Ether to Triptane. *Acc. Chem. Res.* **2012**, *45*, 653−662.

(171) Ahn, J. H.; Temel, B.; Iglesia, E. Selective Homologation Routes to 2,2,3-Trimethylbutane on Solid Acids. *Angew. Chem., Int. Ed.* **2009**, *48*, 3814−3816.

(172) Simonetti, D. A.; Carr, R. T.; Iglesia, E. Acid strength and solvation effects on methylation, hydride transfer, and isomerization rates during catalytic homologation of C_1 species. *J. Catal.* **2012**, *285*, 19−30.

(173) Simonetti, D. A.; Ahn, J. H.; Iglesia, E. Mechanistic details of acid-catalyzed reactions and their role in the selective synthesis of triptane and isobutane from dimethyl ether. *J. Catal.* **2011**, *277*, 173−195.

(174) Simonetti, D. A.; Ahn, J. H.; Iglesia, E. Catalytic Co-Homologation of Alkanes and Dimethyl Ether and Promotion by Adamantane as a Hydride Transfer Co-Catalyst. *ChemCatChem.* **2011**, *3*, 704−718.

(175) Sarazen, M. L.; Iglesia, E. Experimental and theoretical assessment of the mechanism of hydrogen transfer in alkane-alkene coupling on solid acids. *J. Catal.* **2017**, *354*, 287−298.

(176) Jones, A. J.; Zones, S. I.; Iglesia, E. Implications of Transition State Confinement within Small Voids for Acid Catalysis. *J. Phys. Chem. C* **2014**, *118*, 17787−17800.

(177) Biscardi, J. A.; Iglesia, E. Isotopic tracer studies of propane reactions on H-ZSM5 zeolite. *J. Phys. Chem. B* **1998**, *102*, 9284−9289.

(178) Sarazen, M. L.; Doskocil, E.; Iglesia, E. Effects of Void Environment and Acid Strength on Alkene Oligomerization Selectivity. *ACS Catal.* **2016**, *6*, 7059−7070.

(179) Sarazen, M. L.; Iglesia, E. Stability of bound species during alkene reactions on solid acids. *Proc. Natl. Acad. Sci. U.S.A.* **2017**, *114*, E3900−E3908.

(180) Sarazen, M. L.; Iglesia, E. Effects of Charge, Size, and Shape of Transition States, Bound Intermediates, and Confining Voids in Reactions of Alkenes on Solid Acids. *ChemCatChem.* **2018**, *10*, 4028−4037.

(181) Noh, G.; Zones, S. I.; Iglesia, E. Isomer sieving and the selective formation of terminal methyl isomers in reactions of linear alkanes on one-dimensional zeolites. *J. Catal.* **2019**, *377*, 255−270.

(182) Noh, G.; Shi, Z. C.; Zones, S. I.; Iglesia, E. Isomerization and β-scission reactions of alkanes on bifunctional metal acid catalysts: Consequences of confinement and diffusional constraints on reactivity and selectivity. *J. Catal.* **2018**, *368*, 389−410.

(183) Reyes, S. C.; Sinfelt, J. H.; DeMartin, G. J.; Ernst, R. H.; Iglesia, E. Frequency modulation methods for diffusion and adsorption measurements in porous solids. *J. Phys. Chem. B* **1997**, *101*, 614−622.

(184) Zalc, J. M.; Reyes, S. C.; Iglesia, E. Monte-Carlo simulations of surface and gas phase diffusion in complex porous structures. *Chem. Eng. Sci.* **2003**, *58*, 4605−4617.

(185) Zalc, J. M.; Reyes, S. C.; Iglesia, E. The effects of diffusion mechanism and void structure on transport rates and tortuosity factors in complex porous structures. *Chem. Eng. Sci.* **2004**, *59*, 2947−2960.

(186) Reyes, S. C.; Iglesia, E. Effective diffusivities in catalyst pellets - new model porous structures and transport simulation techniques. *J. Catal.* **1991**, *129*, 457−472.

(187) Iglesia, E. Design, synthesis, and use of cobalt-based Fischer−Tropsch synthesis catalysts. *Appl. Catal., A* **1997**, *161*, 59−78.

(188) Choi, M.; Wu, Z. J.; Iglesia, E. Mercaptosilane-Assisted Synthesis of Metal Clusters within Zeolites and Catalytic Consequences of Encapsulation. *J. Am. Chem. Soc.* **2010**, *132*, 9129−9137.

(189) Goel, S.; Wu, Z. J.; Zones, S. I.; Iglesia, E. Synthesis and Catalytic Properties of Metal Clusters Encapsulated within Small-Pore (SOD, GIS, ANA) Zeolites. *J. Am. Chem. Soc.* **2012**, *134*, 17688−17695.

(190) Goel, S.; Zones, S. I.; Iglesia, E. Encapsulation of Metal Clusters within MFI via Interzeolite Transformations and Direct Hydrothermal Syntheses and Catalytic Consequences of Their Confinement. *J. Am. Chem. Soc.* **2014**, *136*, 15280−15290.

(191) Wu, Z. J.; Goel, S.; Choi, M.; Iglesia, E. Hydrothermal synthesis of LTA-encapsulated metal clusters and consequences for

catalyst stability, reactivity, and selectivity. *J. Catal.* **2014**, *311*, 458−468.

(192) Otto, T.; Zhou, X. Y.; Zones, S. I.; Iglesia, E. Synthesis, characterization, and function of Au nanoparticles within TS-1 zeotypes as catalysts for alkene epoxidation using O_2/H_2O reactants. *J. Catal.* **2022**, *410*, 206−220.

(193) Otto, T.; Zones, S. I.; Iglesia, E. Challenges and strategies in the encapsulation and stabilization of monodisperse Au clusters within zeolites. *J. Catal.* **2016**, *339*, 195−208.

(194) Otto, T.; Ramallo-López, J. M.; Giovanetti, L. J.; Requejo, F. G.; Zones, S. I.; Iglesia, E. Synthesis of stable monodisperse AuPd, AuPt, and PdPt bimetallic clusters encapsulated within LTA-zeolites. *J. Catal.* **2016**, *342*, 125−137.

(195) Otto, T.; Zones, S. I.; Hong, Y. C.; Iglesia, E. Synthesis of highly dispersed cobalt oxide clusters encapsulated within LTA zeolites. *J. Catal.* **2017**, *356*, 173−185.

(196) Otto, T.; Zones, S. I.; Iglesia, E. Synthetic strategies for the encapsulation of nanoparticles of Ni, Co, and Fe oxides within crystalline microporous aluminosilicates. *Microporous Mesoporous Mater.* **2018**, *270*, 10−23.

(197) Iglesia, E.; Baumgartner, J. E. Hydrogen-transfer and activation of propane and methane on ZSM5-based catalysts. *Catal. Lett.* **1993**, *21*, 55−70.

(198) Iglesia, E.; Baumgartner, J. E.; Meitzner, G. D. The role of surface fugacities and hydrogen desorption sites in catalytic reactions of alkanes. *Stud. Surf. Sci. Catal.* **1993**, *75*, 2353−2357.

(199) Iglesia, E.; Baumgartner, J. E.; Price, G. L. Kinetic coupling and hydrogen surface fugacities in heterogeneous catalysis. 1. Alkane reactions on Te-NaX, H-ZSM5, and Ga/H-ZSM5. *J. Catal.* **1992**, *134*, 549−571.

(200) Biscardi, J. A.; Meitzner, G. D.; Iglesia, E. Structure and density of active Zn species in Zn/H-ZSM5 propane aromatization catalysts. *J. Catal.* **1998**, *179*, 192−202.

(201) Meitzner, G. D.; Iglesia, E.; Baumgartner, J. E.; Huang, E. S. The chemical-state of gallium in working alkane dehydrocyclodimerization catalysts - insitu gallium K-edge X-ray absorption-spectroscopy. *J. Catal.* **1993**, *140*, 209−225.

(202) Biscardi, J. A.; Iglesia, E. Non-oxidative reactions of propane on Zn/Na-ZSM5. *Phys. Chem. Chem. Phys.* **1999**, *1*, 5753−5759.

(203) Biscardi, J. A.; Iglesia, E. Reaction pathways and rate-determining steps in reactions of alkanes on H-ZSM5 and Zn/H-ZSM5 catalysts. *J. Catal.* **1999**, *182*, 117−128.

(204) Yu, S. Y.; Biscardi, J. A.; Iglesia, E. Kinetic relevance of hydrogen desorption steps and virtual pressures on catalytic surfaces during reactions of light alkanes. *J. Phys. Chem. B* **2002**, *106*, 9642−9648.

(205) Biscardi, J. A.; Iglesia, E. Structure and function of metal cations in light alkane reactions catalyzed by modified H-ZSM5. *Catal. Today* **1996**, *31*, 207−231.

(206) Agirrezabal-Telleria, I.; Iglesia, E. Stabilization of active, selective, and regenerable Ni-based dimerization catalysts by condensation of ethene withinordered mesopores. *J. Catal.* **2017**, *352*, 505−514.

(207) Jaegers, N. R.; Iglesia, E. Theoretical Assessment of the Mechanism and Active Sites in Alkene Dimerization on Ni Monomers Grafted onto Aluminosilicates: (Ni-OH) plus Centers and C-C Coupling Mediated by Lewis Acid-Base Pairs. *J. Am. Chem. Soc.* **2023**, *145*, 6349−6361.

(208) Agirrezabal-Telleria, I.; Iglesia, E. Mechanistic insights and consequences of intrapore liquids in ethene, propene, and butene dimerization on isolated Ni^{2+} sites grafted within aluminosilicate mesopores. *J. Catal.* **2020**, *389*, 690−705.

(209) Iglesia, E.; Hibbitts, D. The Fischer−Tropsch synthesis: A few enduring mechanistic conundrums revisited. *J. Catal.* **2022**, *405*, 614−625.

(210) Loveless, B. T.; Buda, C.; Neurock, M.; Iglesia, E. CO Chemisorption and Dissociation at High Coverages during CO Hydrogenation on Ru Catalysts. *J. Am. Chem. Soc.* **2013**, *135*, 6107−6121.

(211) Hibbitts, D.; Iglesia, E. Prevalence of Bimolecular Routes in the Activation of Diatomic Molecules with Strong Chemical Bonds (O_2, NO, CO, N_2) on Catalytic Surfaces. *Acc. Chem. Res.* **2015**, *48*, 1254−1262.

(212) Liu, J. W.; Hibbitts, D.; Iglesia, E. Dense CO Adlayers as Enablers of CO Hydrogenation Turnovers on Ru Surfaces. *J. Am. Chem. Soc.* **2017**, *139*, 11789−11802.

(213) Hibbitts, D.; Dybeck, E.; Lawlor, T.; Neurock, M.; Iglesia, E. Preferential activation of CO near hydrocarbon chains during Fischer−Tropsch synthesis on Ru. *J. Catal.* **2016**, *337*, 91−101.

(214) C.J, K. Water addition for increased CO/H_2 hydrocarbon synthesis activity over catalysts comprising cobalt, ruthenium and mixtures thereof which may include a promoter metal. U.S. Patent US5227407A, 1992.

(215) Dalai, A. K.; Davis, B. H. Fischer−Tropsch synthesis: A review of water effects on the performances of unsupported and supported Co catalysts. *Appl. Catal., A* **2008**, *348*, 1−15.

(216) Yates, I. C.; Satterfield, C. N. Intrinsic kinetics of the Fischer−Tropsch synthesis on a cobalt catalyst. *Energy Fuels* **1991**, *5*, 168−173.

(217) Ojeda, M.; Zhan, B. Z.; Iglesia, E. Mechanistic interpretation of CO oxidation turnover rates on supported Au clusters. *J. Catal.* **2012**, *285*, 92−102.

(218) Zope, B. N.; Hibbitts, D. D.; Neurock, M.; Davis, R. J. Reactivity of the Gold/Water Interface During Selective Oxidation Catalysis. *Science* **2010**, *330*, 74−78.

(219) Brady, R. C.; Pettit, R. Reactions of diazomethane on transition-metal surfaces and their relationship to the mechanism of the Fischer−Tropsch reaction. *J. Am. Chem. Soc.* **1980**, *102*, 6181−6182.

(220) Mims, C. A.; McCandlish, L. E. Evidence for rapid chain growth in the Fischer−Tropsch synthesis over iron and cobalt catalysts. *J. Phys. Chem.* **1987**, *91*, 929−937.

(221) Hibbitts, D. D.; Loveless, B. T.; Neurock, M.; Iglesia, E. Effects of water on the mechanism of Fischer−Tropsch synthesis on Ru catalysts. *Abstracts of Papers of the American Chemical Society* **2014**, *248*, 1.

(222) Dixit, R. S.; Tavlarides, L. L. Kinetics of the Fischer−Tropsch synthesis. *Industrial & Engineering Chemistry Process Design and Development* **1983**, *22*, 1−9.

(223) Allian, A. D.; Takanabe, K.; Fujdala, K. L.; Hao, X.; Truex, T. J.; Cai, J.; Buda, C.; Neurock, M.; Iglesia, E. Chemisorption of CO and Mechanism of CO Oxidation on Supported Platinum Nanoclusters. *J. Am. Chem. Soc.* **2011**, *133*, 4498−4517.

(224) Frost, A. A.; Pearson, R. G. *Kinetics and Mechanism*; Wiley: New York, 1961.

(225) Eckert, C. A.; Boudart, M. On the use of fugacities in gas kinetics. *Chem. Eng. Sci.* **1963**, *18*, 144−147.

(226) Madon, R. J.; Iglesia, E. Catalytic reaction rates in thermodynamically non-ideal systems. *J. Mol. Catal. A: Chem.* **2000**, *163*, 189−204.